Final Technical Report

Submitted to

Department of Energy, NETL

In fulfillment of requirement under project

Distributed Fiber Optic Gas Sensing for Harsh Environment

Award Number: DE-FC26-05NT42438

This report covers work done from 07/25/05 to 03/14/08

==========

Submitted to:	Submitted by:
Dr. Susan Maley	Dr. Juntao Wu
Program Manager	Principal Investigator
NETL/DoE	GE Global Research
3610 Collins Ferry Road, P.O. Box 880	One Research Circle, K1-3C28
Morgantown, WV 26507-0880	Niskayuna, NY 12309
Tel: (304) 285-1321	Tel: (518) 387-7804
Email: Susan.Maley@netl.doe.gov	Email: juntao.wu@ge.com

==========

Submittal date: June 12th, 2008

DISCLAIMER

ABSTRACT

This report summarizes work to develop a novel distributed fiber-optic micro-sensor that is capable of detecting common fossil fuel gases in harsh environments. During the 32-month research and development (R&D) program, GE Global Research successfully synthesized sensing materials using two techniques: sol-gel based fiber surface coating and magnetron sputtering based fiber micro-sensor integration. Palladium nanocrystalline embedded silica matrix material (nc-Pd/Silica), nanocrystalline palladium oxides (nc-PdO_x) and palladium alloy (nc-PdAuNi), and nanocrystalline tungsten (nc-WO_x) sensing materials were identified to have high sensitivity and selectivity to hydrogen; while the palladium doped and un-doped nanocrystalline tin oxide (nc-$PdSnO_2$ and nc-SnO_2) materials were verified to have high sensitivity and selectivity to carbon monoxide. The fiber micro-sensor comprises an apodized long-period grating in a single-mode fiber, and the fiber grating cladding surface was functionalized by above sensing materials with a typical thickness ranging from a few tens of nanometers to a few hundred nanometers. GE found that the morphologies of such sensing nano-materials are either nanoparticle film or nanoporous film with a typical size distribution from 5-10 nanometers. nc-PdO_x and alloy sensing materials were found to be highly sensitive to hydrogen gas within the temperature range from ambient to 150^{o}C, while nc-Pd/Silica and nc-WO_x sensing materials were found to be suitable to be operated from 150^{o}C to 500°C for hydrogen gas detection. The palladium doped and un-doped nc-SnO_2 materials also demonstrated sensitivity to carbon monoxide gas at approximately 500°C.

The prototyped fiber gas sensing system developed in this R&D program is based on wavelength-division-multiplexing technology in which each fiber sensor is identified according to its transmission spectra features within the guiding mode and cladding modes. The interaction between the sensing material and fossil fuel gas results in a refractive index change and optical absorption in the sensing layer. This induces mode coupling strength and boundary conditions changes and thereby shifts the central wavelengths of the guiding mode and cladding modes propagation. GE's experiments demonstrated that such an interaction between the fossil fuel gas and sensing material not only shifts the central wavelengths of the guide mode and cladding modes propagation, but also alters their power loss characteristics. The integrated fiber gas sensing system includes multiple fiber gas sensors, fiber Bragg grating-based temperature sensors, fiber optical interrogator, and signal processing software.

TABLE OF CONTENTS

LIST OF FIGURES

LIST OF TABLES

ACKNOWLEDGEMENTS

The author would like to thank Dr. Susan Maley, the NETL/DoE program manager, for her overall technical guidance and support. I am also very thankful to the management team at GE Global Research, both for their encouragement and supervision, specifically Jeffrey Ashe, David O'Connor, Dr. Matthew Nielsen, Eric Butterfield, John Garrity, Anthony Colucci, David Wardwell, and Kevin McCarthy.

I am very grateful for the enthusiasm shown by the GE Global Research team members and am proud to be one of them. Many thanks to the team members—Dr. Hua Xia, Dr. Kung-li Deng, Ken Bousman, Renato Guida, and Jennifer Zhao—for their hard work and inspiration.

Special thanks go to Professor Stuart Yin and Dr. Chun Zhan, The Pennsylvania State University, for their outstanding work on the development of high temperature LPG sensors. I also wish to thank Professor Mengbing Huang, SUNY Albany, for his support on high concentration syngas test facility.

CHAPTER 1: EXECUTIVE SUMMARY

With the support of the Department of Energy (DOE), GE has pioneered fiber-optic-based fossil fuel gas sensing technology. After a 32-month R&D program, the research team demonstrated the early feasibility of this technology and its potential capability for use in distributed harsh environmental sensing instruments. Work in this project can be summarized as follow:

1. Developed fabrication techniques for high-temperature fiber-grating
2. Designed and integrated sensing material with fiber gratings
3. Simulated and validated fiber gas sensing modulus
4. Designed and fabricated single-point sensing system
5. Designed and fabricated distributed sensing instrumentation

The proof-of-concept demonstration for fiber-optic gas sensing was based on a modified fiber cladding approach that can be used for combustible gas concentration measurements in a harsh environment. The GE team demonstrated a wavelength-division-multiplexing technology based on a fiber-optic gas sensing system, fiber gas sensing device, and nano-material modified fiber-grating cladding based “smart skin” fiber gas sensors. These fiber-grating devices are composed of both short-period Bragg gratings and long-period gratings, fabricated in a fiber core as a sensing module. The introduction of an apodized index grating profile, in which the guided mode energy is effectively coupled into the cladding and radiation modes, has greatly enhanced the sensitivity of the fiber gas sensors. The modified fiber-grating cladding (smart skin) has a nanostructural morphology between 20-100 nm in thickness and was fabricated either with a sol-gel-based dip-coating method or with a magnetron-sputtering deposition method.

Three fiber gas sensing module prototypes were designed and validated. The simplest prototype was a single fiber long-period grating that was functionalized with sensing material around the grating cladding surface. The second prototype was comprised of one fiber Bragg grating for temperature calibration and one functionalized fiber long-period grating for gas sensing. The third prototype had two fiber Bragg gratings with a functionalized fiber long-period grating in the middle.

These integrated fiber gas sensors were interfaced with an optical interrogation unit to measure the corresponding wavelength shift induced by either effective a refractive index variation or optical absorption in the smart skin layer, as well as the boundary condition variation corresponding transmission or reflectance loss. Such boundary condition changes modified the cladding modes coupling to the evanescent field and its distribution in the sensing skin area. The fossil fuel gas or combustible gas, such as hydrogen and carbon monoxide, interacts with the sensing material, such as a palladium-alloy-based nanostructure, and can alter the cladding

propagating properties during the hydrides PdHx formation. The refractive index change and phase transition in the sensing material can be measured by observing the transmission or reflectance spectra of the fiber gas sensor, as characterized by both the central wavelength shift and transmission loss variation. Since a NIST-standard gas cell was integrated with the signal interrogation unit, the accuracy on wavelength shift measurement can be down to ±1 pm and only infrequent calibration is required. The integrated fiber gas sensing system includes multiple fiber gas sensors, fiber-Bragg-grating-based temperature sensors, a fiber-optical interrogator, and signal processing software.

GE's fiber-optic, harsh environment fossil fuel gas sensing method is a cost-effective, versatile, plug-and-play platform that can be used to detect and measure a large number of combustible gases. These gases include hydrogen-rich syngas, hydrogen and carbon monoxide balanced syngas, hydrocarbons, chemical agents, and solvents. The platform can also potentially be used to measure heavy metals, such as mercury, lead, and actinides, by using different functionalized sensing materials integrated with the fiber grating.

The distributed fiber-optic fossil fuel gas sensing instrumentation was designed to be deployed in harsh environmental applications with its plug-and-play fiber gas sensing module. As a result, GE's fiber gas sensing instrument is modular, ruggedized, and field-deployable technology. The unique fiber gas sensing module design and its performance, as demonstrated in this program, highlight a shorter path to build a new sensing method from a matured telecom technology.

GE's fossil fuel gas sensing technology—perhaps more than with any other technology—provides DOE a significant advantage in improving power industrial production efficiency, process control, and optimization. Unlike existing chromatography, mass spectrometers, Raman spectroscopes, and ring-down spectrometer-based offline devices, which are bulky and dedicate, this new fiber sensing device and sensing system can be used in gas turbines, coal boilers, and coal gasification systems, and at exhaust sections and interfaces. The newly-developed fiber-grating-based gas sensor uses also commercially-available grating fabrication technology and integrated sensing material preparation processes (provided by sol-gel and magnetron sputtering technologies), thereby significantly reducing the cost to procure a sensing instrument.

CHAPTER 2: INTRODUCTION

The DOE's National Energy Technology Laboratory (DOE NETL) is the United State's fossil fuel research organization and is leading the effort to develop clean, efficient, and cost-effective technologies for fossil fuels. The ultimate goal of DOE NETL's work is to benefit the public by creating affordable and reliable sources of domestic energy, protecting the environment, fueling economic prosperity, and strengthening energy security in the U.S.

One primary DOE NETL initiative is to bridge the gap between scientific research and commercial fossil energy applications. This is being accomplished by using innovative sensing instruments and control strategies and by fostering the full-scale implementation of new and more efficient power generation technologies. New sensing instruments and technologies, and advanced process control strategies will enable power generation equipment that can be operated in a safe, efficient, and environmentally-sound manner. Existing power plants will also greatly benefit from these efforts. Retrofitting outdated power plants with new instrumentation and controls will result in many high value benefits at comparably low costs.

Research is still needed to bridge the gap between research and commercial technologies in the area of novel, high temperature materials that can be used to fabricate miniaturized in situ sensing devices for various gas species. New sensor materials and micro-sensor devices should be able to withstand high temperatures (>500ºC) and high pressures (200 psi) while maintaining gas-sensing reliability. However, existing sensors that measure common fossil fuel gases (CO, CO_2, HCs, H_2, H_2S, NO_x, etc.) cannot withstand the high-temperature and hostile environments found in today's fossil energy systems. To overcome this issue, GE's program focused primarily on new materials (including material matrices, modified optical fibers, functionalized or doped ceramics, and nano-derived micro structures) and developing fiber-based sensors for targeted fossil fuel gases, particularly those found in gas turbine and coal gasification applications.

Syngas sensing devices and systems that are based on fiber-optic technology offer a feasible path to enable a distributed sensor network for plant-wide monitoring and diagnosis. These light-weight, small-size, all-passive fiber sensors have the potential to measure a large number of data points with minimum intrusion into the gas or heat flow. This makes these

sensors an ideal candidate for collecting valuable data in the integrated gasification combined cycle (IGCC) environment. Also, these sensors allow for multi-parameter sensing, including temperature, strain/stress, vibration, and syngas (H_2, CO), in harsh environments. The fiber-optic sensing technologies have great potential to facilitate future plant-wide control and instrumentation systems for IGCC applications. Specific potential IGCC applications include fouling detection in radiant syngas cooler (RSC) water wall, structure health monitoring, raw syngas composition analysis, and pollutant reduction.

The output of GE's innovative research program is closely related to advanced sensing research for fuel cells, turbines, gasification, and carbon sequestration and supports large initiatives such as the Clean Coal Power Initiative and FutureGen. The Clean Coal Power Initiative's purpose is to demonstrate advanced coal-based power generation technologies. The goal is to accelerate commercial deployment of advanced technologies with improved efficiency or environmental performance relative to the existing fleet of power generation equipment. FutureGen, the Integrated Sequestration and Hydrogen Research Initiative, is a $1 billion government/industry partnership to design, build, and operate a nearly emission-free, coal-fired electric and hydrogen production plant. The 275-megawatt prototype plant will serve as a large-scale engineering laboratory and will be used to test new clean power, carbon capture, and coal-to-hydrogen technologies.

GE's advanced gas sensing technology developed in this program can be used to measure the methane concentration, which is presently measured downstream in an IGCC system, to estimate the gasifier temperature. Methane is formed by decompolization of the fuel as it first enters the hot gasifier. Subsequently, it is both formed and destroyed by other reactions between the gases and solids in the gasifier. The rate and extent to which methane is formed and destroyed can be correlated to the gasifier temperature. The ideal location to measure methane for gasifier temperature is at the outlet of the gasifier. However, existing gas sensing instruments are not capable of measuring gases in such harsh environments. As a result, methane is measured further downstream before entering the gas turbine. The syngas temperature history between gasifier and gas turbine must be taken into account when considering accurate gasifier temperature.

2.1. Fiber-grating-based sensors

The intrinsic and extrinsic wave propagation properties of light in the fiber waveguide have been used for decades for chemical and biochemical sensing applications. This is because the guided wave in a fiber is totally reflected at the core/cladding interface, and at every reflection a small amount of the guide wave field penetrates into the cladding region and effectively excites the evanescent field. In the case of a thin cladding, the evanescent field can reach the outer diameter of the fiber. This results in additional attenuation of the guided wave. Such a wave

propagation property provides reasonable sensitivity to measure chemical and biochemical species. Most chemical and biochemical fiber optic sensors use one of physical mechanisms for detection, including transmittance, reflectance, interference, fluorescence, or absorption variations. Although optical fiber can be used for chemical and biochemical sensing, it does not provide good gas selectivity because the evanescent field is only sensitive to the refractive index variation of the surrounding medium rather than molecular species.

Short-period fiber Bragg gratings (FBG) and fiber long-period gratings (LPG) are simple, intrinsic in-fiber-core sensing elements that can be photo-inscribed into a fiber core and have all of the advantages normally attributed to fiber sensors. These fiber-grating-based devices are easily multiplexed in a serial fashion along a single fiber. The wavelength-division-multiplexing advantage enables fiber-grating-based sensors to be useful for a variety of applications because the fibers with sensor arrays can be either embedded into the material or distributed in a large-scale infrastructure to allow for measurement of parameters such as load, strain, temperature, and vibration. Using these parameters, the health of a structure can be assessed and tracked on a real-time basis.

Short- and long-period fiber gratings have demonstrated their potential as elements that can sense chemical and biochemical species and gases. The advantages of fiber-grating-based fiber-optic sensing systems are their small size, high sensitivity, and multiplexing capability. These sensing systems are highly adaptable for remote, distributed sensing and they are robust to the exposure of hazardous chemicals, radiation, and high temperatures. Meanwhile, fiber-grating-based fiber-optic sensing systems are electrical isolators and chemically inert, thus offering an intrinsic safety feature.

For FBGs, the mode coupling between the forward and backward-guided modes can be functionalized to be a chemical sensing device. Since the guided light in the fiber is totally reflected at the core/cladding interface, a small amount of the light intensity penetrates into the cladding (evanescent field) at every reflection. In the case of a thin cladding, if most of the grating-cladding thickness can be etched away, the evanescent field can reach the outer diameter of the fiber. This is the reason that the cladding of the grating must be partially etched away to provide sensitivity to the outside refractive index variations. The wavelength of interaction depends on the refractive index and thus the concentration of the surrounding medium. Despite its capability as distributed sensing system, such a FGB-based chemical sensor has limitations because the removal (or etching) of the fiber cladding is costly, time consuming to implement, and difficult to handle.

LPGs are an alternative based on forward coupling between the core fundamental mode and cladding modes. A LPG-based sensing element shows a high sensitivity in the transmission dip position shift to the refractive index variations of the medium surrounding the cladding. This enables an LPG to act as a chemical/biochemical or gas sensor and to operate as a stand alone,

remote sensor without having to remove the fiber with the cladding reduced at the sensing position. This sensing system offers good performance and high sensitivity to external chemicals and gases; however, its drawbacks include sensing resolution, accuracy, and distribution capability because of the multiple transmission dips of a LPG element from coupling modes (LP_{01}, LP_{11}, …etc.), which have much wider linewidth (20~60 nm) than a FBG element (~0.2 nm). Moreover, it is difficult to differentiate one chemical or gas from another when their refractive indices are nearly identical because the resulting wavelength shift from two chemicals or gases might be the same.

After several years of development of fiber-grating-based high-temperature sensing device and sensing system at GE Global Research and the Penn State University, this DOE NETL program has provided GE and PennState the opportunity to advance new diagnostics and monitoring/sensing technologies. The progress made in this program has demonstrated fundamental fiber-grating devices that have high thermal survivability and stability, advanced fossil fuel gas sensing prototypes that integrate fundamental long-period grating devices with fuel gas sensitive nanomaterial, and a wavelength-division-multiplexing based sensing instrumentation that includes a plurality of the fiber gratings (short-period Bragg grating and long-period grating), optical circulators, tunable laser source, NIST-calibrated gas cell, Fabry-Perot filter based signal interrogation unit, and associated fiber-grating wavelength shift and power loss detection algorithm and software.

2.2. Smart-skin fiber gas sensor

Although fiber-grating-based devices have shown great success as filters in the telecom industry and the general marketplace, their application for chemical and biochemical sensing is limited. One reason for this is that the fiber-grating element is insensitive to external chemicals, gases, and vapors because the guided waves are mainly confined inside the fiber core and partially in the cladding region, and there is very limited evanescent field distribution from the fiber core to the outside of the fiber cladding surface. In order to use fiber gratings for sensing applications, the grating element must first be functionalized by modifying the fiber structure to enable internal wave and field extension to the grating cladding surface. The grating element must also be modified by adding a chemically-sensitive coating layer around the fiber-grating cladding (i.e., making a "smart skin" surrounding the grating cladding surface).

Obviously, guided wave propagation in a LPG is much easier to couple to the cladding region and the resulting cladding modes can extend their evanescent field from the fiber-grating cladding surfaces to the surrounding environment. Despite the extended evanescent field beyond the cladding surface from a LPG, the detection of a chemical, gas, or vapor requires a reasonable sensitivity and selectivity from such a grating element. Unfortunately, a LPG cladding surface does not provide any sensitivity and selectivity to chemicals and gases. On the other hand, a

uniform LPG may still have a limited evanescent field outside the fiber-grating cladding surface. Modifying a fiber-grating structure is accomplished either by adding apodization on the refractive index modulation profile or by changing the fiber geometry from a cylinder shape to a so-called "D-Type" fiber or a tapered shape.

However, based on the LPG's unique optical properties in response to variations in the surrounding environment, it could be made as a gas sensing device if the fiber-grating surface can be functionalized. One method to functionalize a fiber grating with chemical activity is by coating a thin film around the grating surface. Whenever this thin layer material interacts with a gas, such as natural gas and hydrogen mixed fuel, its absorption or dielectric function are perturbed and the light propagating in the fiber long-period grating will be wavelength shifted and/or attenuated. Functionalizing a fiber-grating cladding surface to have chemical sensitivity and selectivity requires advanced sensing materials and integration processes. Such sensing materials must be reversible to respond to chemicals and gases and the response time should be short enough to satisfy the sensing requirements. They should also be thermally stable at elevated temperatures for environment applications such as are found in gas turbines, coal boilers, or coal gasification power generation plants. With a smart skin surrounding the fiber-grating cladding surface, the sensing material integrated fiber grating is called a "fiber gas sensor" or alternatively a "smart skin fiber gas sensor".

During this program, GE developed fiber-gas sensing prototypes, or smart-skin sensing devices, by combining FBGs and LPGs for differential gas concentration detection. This smart skin interacts with fossil fuel gas to change either its refractive index or its optical absorption property so that the gas sensing can be interrogated by wavelength response and transmission or reflection response. Details are provided in the following chapters.

2.3. Fundamental gas sensing device – fiber long period grating

An LPG, a special form of the conventional Bragg grating, is a periodic modulation of the refractive index along the core of a single-mode optical fiber that is normally used as an in-fiber, low-loss, band rejection filter. The periodicity of a LPG is chosen to couple the fiber guided mode to the forward propagating cladding modes, where it is lost due to absorption and scattering between the cladding/air interface. Coupling from the guided mode to the unguided cladding modes is wavelength dependent; thus, the transmission signature of LP_{01} propagating mode may show a spectrally selective loss variation. The consequence of this refractive index modulation is the coupling of the fundamental mode propagating in the fiber with forward-propagating cladding modes or radiation modes, under the Bragg phase-matching condition:

$$\kappa_0^{(co)} - \kappa_i^{(cl)} = \Delta\kappa = \frac{2\pi}{\Lambda} \qquad (2.1)$$

where $\kappa_0^{(co)}$ and $\kappa_i^{(cl)}$ are the propagation constants of the fundamental mode and the ith cladding mode, respectively, and Λ is the pitch of the grating. The coupling produces series of attenuation bands in the fiber transmission spectrum, since a cladding mode is rapidly attenuated in the fiber, with central wavelengths that are solutions of the following equation

$$\lambda_i = [n_0^{(co)}(\lambda_i) - n_i^{(cl)}(\lambda_i)]\Lambda, \tag{2.2}$$

where $n_0^{(co)}(\lambda_i)$ and $n_i^{(cl)}(\lambda_i)$ are the effective indices of the fundamental mode and the *i*th cladding mode, respectively. In particular, only $n_i^{(cl)}(\lambda_i)$ depends on the refractive index of the external medium. When the external refractive index increases, $n_i^{(cl)}(\lambda_i)$ also increases and a shift in the central wavelengths can be observed.

It is important to note that the cladding modes attenuate rapidly as they propagate along the length of the fiber due to the lossy cladding coating interface and bends in the fiber. Since $\Delta\kappa$ is discrete and a function of wavelength, this coupling to the cladding mode is highly selective and leads to a wavelength-dependent loss. As a result, any modulation of the core and cladding guiding properties modifies the transmission signatures of the LPG. This is the basis by which an LPG can be used as a sensing device with a response to external perturbations such as strain and temperature. Furthermore, since the cladding modes interact with any surrounding medium through its evanescent field, changes in the optical properties or refractive index of the surrounding medium can also be detected. This unique feature is the working principle of most LPG based liquid or gas sensors, and results in being highly sensitive to changes of cladding and/or surrounding refractive indices, as compared with fiber Bragg gratings (FBG).

In this program, GE and the Penn State University developed two kinds of LPG devices. One is based on a thermal arc technique that effectively inscribes strain modulated grating pattern inside the fiber core. The second method uses a high-power pulse laser to inscribe an apodized long period grating that is similar to the Type-II FBG inscription process. The third process uses a femtosecond laser to inscribe a high-temperature grating on a sapphire fiber. These fiber gratings provided the fundamental devices for the development of advanced fossil fuel gas sensors. Details are found in the following chapters.

2.4. Challenges in using a fiber LPG as a gas sensing device

Despite its high sensitivity to an external medium, using a conventional fiber LPG as a fossil fuel gas sensor has several challenges that must be understood, especially when such a fiber gas sensing device will need to work in harsh environments where the temperature could reach 500ºC or beyond.

2.4.1. Thermal sensitivity compensation

If one can assume the difference of the fiber thermo-optic coefficient, $\beta = \frac{\partial n}{n \partial T}$, in fiber core and cladding is negligible, the thermal response of a LPG can be described as:

$$\begin{aligned} \frac{\partial \lambda_i}{\partial T} &= \Lambda\left(n_o^{co}\left(\frac{\partial n_o^{co}}{n_o^{co}\partial T} + \frac{\partial \Lambda}{\Lambda \partial T}\right) - n_i^{cl}\left(\frac{\partial n_i^{cl}}{n_{io}^{cl}\partial T} + \frac{\partial \Lambda}{\Lambda \partial T}\right)\right) \\ &= \Lambda[(n_o^{co} - n_i^{cl})\alpha + (n_o^{co} - n_i^{cl})\beta] \end{aligned} \tag{2.3}$$

where α is the coefficient of fiber thermal expansion and the thermo-optic coefficient β is normally a quadratic function of temperature. In the nominal case, every one degree Fahrenheit could lead to an LP_{01} mode wavelength upwards shift of 50~80 pm, which is about 8-10 times higher than FBG thermal sensitivity. On the other hand, Equation 2.3 ignores the fiber's strain effect or assumes the fiber grating has no length change during gas sensing. As discussed in the following section, the fiber-grating cladding must be functionalized so that an LPG cladding can act as a smart skin. When a sensing material has a different coefficient of thermal expansion, α_{sm}, the thermal axial strain could be written as

$$\Delta\varepsilon(T) = (\alpha_{sm} - \alpha_F)\cdot(T - T_o), \tag{2.4}$$

where α_F is the fiber coefficient of thermal expansion, and T_o is the reference temperature that corresponds to an initial LPG LP_{01} mode central wavelength. This thermal strain could modify the LPG wavelength shift by

$$\Delta\lambda_i(T) = \kappa_\varepsilon \Delta\varepsilon(T) = \kappa_\varepsilon(\alpha_{sm} - \alpha_F)\cdot(T - T_o), \tag{2.5}$$

where κ_ε is the corresponding fiber-grating strain sensitivity factor. We point out that one of the purposes for using thin sensing material in our fiber gas sensing device is to mitigate any lattice expansion from the sensing material induced fiber-grating length change. It becomes obviously that without a temperature, strain, and gas differential measurement, it is challenging to correctly interpret sensing data, especially when such a fiber-gas sensor is used for long-term online monitoring and diagnostics for a power plant, such as a coal boiler, gasifier, or combustor.

In this program, GE developed hybrid FBG/LPG-based gas sensing devices by combining short-period Bragg gratings and long-period gratings to detect differential gas concentrations. One of these prototype sensing devices uses a very thin sensing materia, so the strain effect is negligible. For this device, the LPG is coated with a layer of nanomaterial for gas sensing, and the FBG is uncoated but inscribed adjunct to the LPG. Such a FBG can only detect temperature for the LPG wavelength shift thermal correction. For the other prototype device, both the FBG and LPG were coated with a sensing material. The FBG detected both temperature and thermal strain effect, and the information from the FBG wavelength shift was used to correct the LPG gas sensing observed wavelength shift. The third prototype sensing device was based on two

FBGs with one LPG in the middle. The fiber sensing system was operated in a reflection mode so the reflectance ratio from two FBGs can be correlated with the gas concentration because the light twice passes through the LPG sensing element – the first time when traveling from the first FBG to the second FBG then the second time when it is reflected back to the sensing interrogation unit. In this sensing configuration, thermal drift from the LPG can be corrected.

Thus, the thermal effects must be corrected for a reliable gas sensing application whenever a fiber grating is used in an elevated environment. A combination of LPGs and FBGs in one fiber gas sensing device provides the capability to simultaneously monitor the surrounding chemical gas concentration, operating temperature, and corresponding thermal strain. In return, the measured temperature and strain effects are deducted from the wavelength shift of the LPG based sensing element. Details are provided in the following chapters.

2.4.2. Thermal stability and survivability

Conventional fiber LPGs have a limited operational temperature of about 150ºC because of the temperature-dependent dopant diffusion induced grating fading. Such fiber gratings break down in more elevated temperature environments. Conventional LPGs exhibit poor thermal drifting whenever T>150ºC and the grating can be completely erased in hours by a temperature around 500ºChours. For operation as a harsh environmental gas sensing device or analytical instrument, it requires the fiber LPG's refractive index modulation amplitude to have high thermal stability. Since the fiber material is normally a floppy structure with a random amorphous network of silicon dioxide with different defects, temperature change could modify the material's microstructure and morphology. After inscribing a grating in such a fiber material and annealing it at an elevated temperature, the grating structure that is associated with the material microstructure and effective refractive index in the fiber core can be thermally stabilized. The research in this program targeted toward harsh environments with temperatures at least 500ºC. This is the critical challenge for using an LPG as a basic gas sensor device with high thermal stability and survivability at elevated temperatures. In this program, GE and Penn State developed a high-thermal stabilized fiber LPG as a basic gas sensing device. The thermal-arc-based grating inscription technique demonstrated its thermal survivability and stability. Details are provided in the following chapters.

2.5. Fiber LPG cladding functionalization

As mentioned in the previous section, the fiber-grating cladding has no specific sensitivity toward any chemical or gas. Thus, a fiber LPG cladding must be functionalized to enable selective chemical sensing. One method normally used for aqueous chemical or biochemical detection is to etch away part of the LPG cladding thickness, either removing nearly half of the

cladding to form a "D-type" structure or tapering down the LPG element by different chemical etching processes, to effectively expose the evanescent field to external cladding. The aqueous analyte is detected primarily via refractive index variation. Using this mechanism, it is difficult to distinguish between two chemical species when their refractive indices induce the same amount of LPG LP_{01} mode wavelength shift and transmission loss. Mechanical strength weakness caused by etching away or tapering down the fiber cladding diameter also results in sensor reliability issues, especially for practical harsh environmental installation and chemical sensing. Nevertheless, the above methods to functionalize a fiber LPG for chemical sensing have been successfully demonstrated in many applications, typically for aqueous chemicals and biochemical detection.

Fiber cladding etching or tapering methods cannot be used to functionalize LPG sensors because gases have very small refractive index differences from air. For such gas sensing, two methods can be used to functionalize an LPG. The first method is to coat a thick layer of a chemical active material, such as a thin layer of palladium, on a FBG surface for hydrogen leakage detection, or a polymeric material for humidity detection. For hydrogen detection, hydrogen diffusion inside the palladium will form hydride by lattice expansion, thereby it will introduce mechanical strain on the FBG that can be read by its Bragg resonant wavelength up-shift by $\Delta\lambda_B = 1.22\Delta a / a_o$, where a_o is the lattice constant and Δa is due to the hydride formation induced lattice expansion. This microstrain effect could simply be used to detect leaks without requiring quantitative detection of the hydrogen gas concentration. However, this sensing mechanism will require the sensing film to have bulk-like, or thick film, material properties, so that the wavelength up-shift of the FBG response to hydrogen can be quantitatively controlled. The downside of this technique is that the sensing response time could be too slow because the hydrogen atoms need to diffuse deep into the film. Meanwhile, the recovery time could be too slow because the hydrogen atoms also require a long time for outward diffusion. For polymeric material functionalized fiber-grating sensing devices, there is a tradeoff between the thickness of the coating material, the material expansion induced microstrain, and the response and recovery times.

In this program, GE developed two fiber-grating cladding functionalization processes. The first method is to apodize the grating structure to effectively shed more guide mode energy to the cladding/air interface with refractive index modulation to have Gaussian/cosine apodized, or blazed, or titled profile. The second method is to coat ultra-thin nanocrystalline layer around the fiber-grating cladding that has specific sensitivity to one of fossil fuel gas such as hydrogen, carbon monoxide etc. The interaction of such a nanomaterial with a target gas mainly induces a variation of the refractive index in the sensing material so that the boundary condition in-between the cladding and sensing material is changed and can be detected by cladding modes or radiation modes. Details are found in the following chapters.

2.6. Sensing material integrated fiber LPG gas sensor

When a gas sensitive material is integrated around a fiber grating, the theoretical understanding of a real gas-sensing device can be explored based on a three-layered structure. The interaction of such a nanomaterial with a target gas mainly induces a variation of the refractive index in the sensing material so that the boundary condition between the cladding and the sensing material is changed and it can be detected by cladding modes or radiation modes. Such a sensing device has been modeled as follows.

The wavelength response of the LPG can be quantitatively analyzed by a three-layer model that includes a core, an LPG written in the core, a cladding, and surrounding medium, as shown in Figure 2.1. In this case, the effective refractive index of the core n_{eff_co} can be calculated based on the following dispersion relationship:

$$V\sqrt{1-b}\,\frac{J_1(V\sqrt{1-b})}{J_0(V\sqrt{1-b})} = V\sqrt{b}\,\frac{K_1(V\sqrt{b})}{K_0(V\sqrt{b})}, \tag{2.6}$$

where J_m (m = 0, 1) is a Bessel function of the first kind, K_m (m = 0, 1) is a modified Bessel function of the second kind, $V = 2\pi a_1/\lambda\sqrt{n_1^2 - n_2^2}$ is the normalized frequency of the fiber at a wavelength λ, $b = (n_{eff\_co}^2 - n_2^2)/(n_1^2 - n_2^2)$ is the normalized refractive index of the core, and the rest of the parameters are as defined in Figure 2.1.

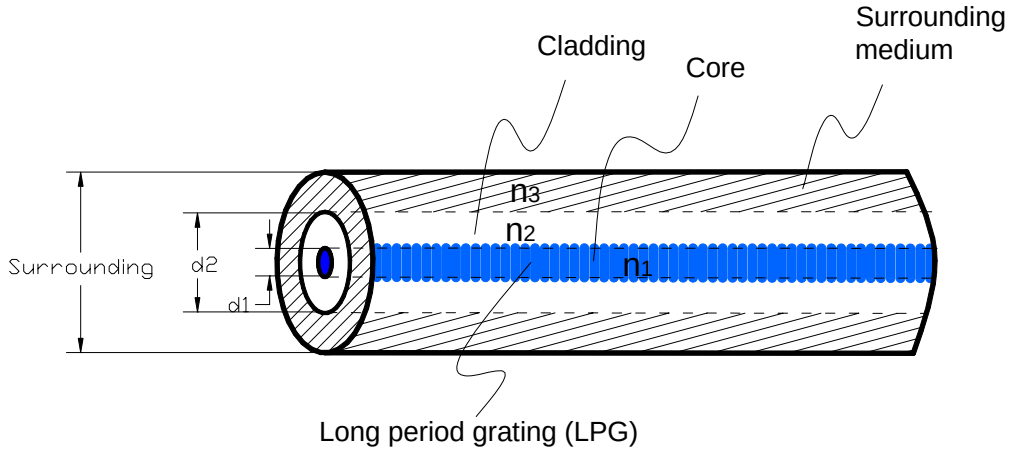

Figure 2.1 A schematic diagram of the three-layer model.

n_1 – refractive index of core, $d_1 = 2a_1$ - diameter of the core

n_2 – refractive index of cladding, $d_2 = 2a_2$ – diameter of the cladding

n_3 – refractive index of the surrounding medium

The cladding modes are calculated in following the three-layer model. The dispersion relationship for a cladding mode with azimuthal dependence $\exp(\pm il\phi)$ becomes

$$\zeta = \zeta', \tag{2.7}$$

where

$$\zeta = \frac{1}{\sigma_2}\frac{u_2\left(JK + \frac{\sigma_1\sigma_2 u_{21}u_{32}}{{n_2}^2 a_1 a_2}\right)p_l(a_2) - Kq_l(a_2) + Jr_l(a_2) - \frac{1}{u_2}s_l(a_2)}{-u_2\left(\frac{u_{32}}{{n_2}^2 a_2}J - \frac{u_{21}}{{n_1}^2 a_1}K\right)p_l(a_2) + \frac{u_{32}}{{n_1}^2 a_2}q_l(a_2) + \frac{u_{21}}{{n_1}^2 a_1}r_l(a_2)}, \tag{2.8}$$

(2.8)

$$\zeta' = \sigma_1\frac{u_2\left(\frac{u_{32}}{a_2}J - \frac{{n_3}^2 u_{21}}{{n_2}^2 a_1}K\right)p_l(a_2) - \frac{u_{32}}{a_2}q_l(a_2) - \frac{u_{21}}{a_1}r_l(a_2)}{u_2\left(\frac{{n_3}^2}{{n_1}^2}JK + \frac{\sigma_1\sigma_2 u_{21}u_{32}}{{n_1}^2 a_1 a_2}\right)p_l(a_2) - \frac{{n_3}^2}{{n_1}^2}Kq_l(a_2) + Jr_l(a_2) - \frac{{n_2}^2}{{n_1}^2 u_2}s_l(a_2)}. \tag{2.9}$$

(2.9)

Note that following definitions are used in Eqs. (2.8) and (2.9)

$$\begin{aligned}
\sigma_1 &\equiv i\ln_{eff-cl}/Z_0, \\
\sigma_2 &\equiv i\ln_{eff-cl}Z_0, \\
u_{21} &\equiv \frac{1}{{u_2}^2} - \frac{1}{{u_1}^2}, \\
u_{32} &\equiv \frac{1}{{w_3}^2} + \frac{1}{{u_2}^2},
\end{aligned} \tag{2.10}$$

where l is the azimuthal number, Z_0 is the vacuum impedance.

$$\begin{aligned}
{u_j}^2 &\equiv (2\pi/\lambda)^2({n_j}^2 - {n_{eff-cl}}^2), \qquad [j \in (1,2)] \\
{w_3}^2 &\equiv (2\pi/\lambda)^2({n_{eff-cl}}^2 - {n_3}^2), \\
J &\equiv \frac{J_l'(u_1a_1)}{u_1J_l(u_1a_1)}, \\
K &\equiv \frac{K_l'(w_3a_2)}{w_3K_l(w_3a_2)},
\end{aligned} \tag{2.11}$$

$$
\begin{aligned}
P_l(r) &\equiv J_l(u_2 r)N_l(u_2 a_1) - J_l(u_2 a_1)N_l(u_2 r),\\
q_l(r) &\equiv J_l(u_2 r)N_l'(u_2 a_1) - J_l'(u_2 a_1)N_l(u_2 r),\\
r_l(r) &\equiv J_l'(u_2 r)N_l(u_2 a_1) - J_l(u_2 a_1)N_l'(u_2 r),\\
s_l(r) &\equiv J_l'(u_2 r)N_l'(u_2 a_1) - J_l'(u_2 a_1)N_l'(u_2 r).
\end{aligned}
\tag{2.12}
$$

Based on Equations (2.8)-(2.12), the effective refractive index of cladding n_{eff-cl} is calculated. These formulas are the basis for the gas sensing response calculation and prediction.

2.7. Gas active sensing materials

This program aims to bridge the gap between basic science and applied research as it relates to fossil energy applications. Conventional and currently-available sensors that are used to measure common fossil fuel gases (CO, CO_2, HCs, H_2, H_2S, NO_x, etc.) cannot withstand the high temperature and hostile environments found in fossil energy-based power generation systems. One critical challenge is that these sensing devices must be able to detect various fossil fuel gases under high temperature (>500ºC), high pressure (200 psi) conditions. The sensing materials used for these devices are not only required to withstand high temperatures, they also need to have sensitivity for fossil fuel gases. These new materials include material matrices, modified optical fibers, functionalized or doped ceramics, and nano-derived microstructures, such that the bulk properties of the material can be utilized in miniaturized devices with gas sensing characteristics at high temperatures and for various gas species. The development of fiber-based sensors modified for gas sensing is a specific area of interest.

GE successfully synthesized sensing materials with both a sol-gel-based fiber surface coating method and magnetron sputtering based fiber gas sensor integration techniques. Palladium nanocrystalline embedded silica matrix material (nc-Pd/Silica), nanocrystalline palladium oxides (nc-PdO_x) and alloy (nc-PdAuNi), and nanocrystalline tungsten (nc-WOx) sensing materials were identified to have high sensitivity and selectivity to H; while the palladium doped and un-doped nanocrystalline tin oxide (nc-$PdSnO_2$ and nc-SnO_2) materials were verified to have high sensitivity and selectivity to CO. The fiber gas sensor is comprised of both FBGs and LPGs; and the fiber-grating cladding surface was functionalized using above sensing material with a typical thickness from a few tens of nanometers to a few hundred nanometers. We have found that the morphologies of such sensing nano-materials are either nanoparticle film or nanoporous film with a typical size distribution from 5-10 nanometers. nc-PdOx and nc-PdAuNi sensing materials exhibit high sensitivity to hydrogen gas from ambient to 150ºC, while (nc-Pd/Silica) and nanoparticle tungsten (nc-WOx) sensing materials are suitable for hydrogen gas detection at temperature ranging from 150ºC to 500ºC. The palladium doped and un-doped nanocrystalline tin oxide (nc-$PdSnO_2$ and nc-SnO_2) materials also demonstrated sensitivity to carbon monoxide gas around 500ºC. Details are found in the following chapters.

CHAPTER 3: FIBER SENSOR DEVELOPMENT

3.1 Electric arc technique fabricated fiber optic gratings
3.2 Femtosecond laser technique fabricated Sapphire fiber gratings
3.3 Sensor performance enhancement through mode control
3.4 A new grating fabrication technique based on refractive element
3.5 Fabricating the grating in sapphire fibers with cladding
3.6 Grating survival capability at ultra-high temperature
3.7 Feasibility demonstration of a sapphire fiber Bragg grating

Fiber grating elements are the fundamental devices for our fiber gas sensors. Conventional fiber gratings, such as Bragg gratings and long-period gratings, are inscribed onto a photosensitive fiber. The fiber core is doped with germanium (Ge) or co-doped with boron, fluorine, phosphor, and erbium, which consequently leads to the formation of intra-band impurity energy levels in the silicon dioxide fiber material band-gap. The dopants distributed in these impurity bands will be thermally excited to the conduction band and consequently induce thermal-degradation of the effective refractive index modulation by the thermo-optical effect. Such thermal instability normally limits the conventional fiber LPG sensor to operations below 200ºC - the periodic refractive index modulation structure in the fiber will be quickly erased at an elevated temperature such as 500ºC.

Fossil fuel gas detection requires that fiber sensors survive harsh environments of at least 500ºC. Although Bragg gratings with high thermal stability have been demonstrated, e.g., fiber pretreated with heat, or fibers with special composition, the stability of UV-induced LPGs at high temperatures may not be so straightforward. In fact, the considerable decrease of the refractive index modulation during the annealing process can be a major practical constraint in such applications. Several non-UV methods to fabricate LPGs have been published. These methods rely on physical deformation of the fiber, diffusion of the core dopants in special nitrogendoped Ge free fibers, or refractive index variation produced by CO lasers, CO lasers, infrared femtosecond laser pulses, ion implantation, or electrical discharges. Fiber LPGs inscribed with periodical local heating of the fiber with CO_2 or CO laser radiation haave demonstrated very high thermal stability.

The following text summarizes how GE approached the technical solutions to develop a high-temperature fiber-grating element as a fundamental device. Two fiber-grating inscription techniques were developed, namely, thermal-arc and pulsed femtosecond laser inscription methods on both silica based fibers and sapphire based fibers. The electric arc method was used to demonstrate its feasibility to fabricate an excellent quality grating by applying lateral stress to a standard telecommunication fiber. We have further demonstrated that the electric arc induced gratings have highly temperature stability at elevated temperature up to 500ºC and beyond.

3.1. Electric arc fabricated fiber optic gratings

The electric arc technique has been used to fabricate fiber LPGs for several years. This grating inscription technique is much simpler than other insprition techniques and does not need expensive laser equipment. Such LPGs can be written in any type of optical fiber, because their characteristics are mainly defined by the intrinsic properties of the silica glass itself. Local heating of the fiber also takes place in the electric arc discharge grating inscription process. Since there is no requirement for the fiber to be photosensitive, its thermal stability can be comparable to silicon-dioxide-based fused silica material. The mode coupling in these gratings can result from the periodical tapering of the fiber diameter, the dopant diffusion, or a change in the glass properties by the fast local heating-cooling process. On the other hand, the fiber cladding can be easily modified to expose more of the evanescent field and thereby obtain a highly-sensitive LPG to be used for fossil fuel gas detection. Figures 3.1(a) and (b) show the picture and corresponding drawing of the electric arc grating fabrication system. The fabrication process consists of positioning an uncoated fiber between the electrodes. During the fabrication of the fiber grating, a standard single mode fiber (SMF-28e) is used and may be doped with GeO_2. A short unjacketed section was placed in two fiber holders. Both ends of the fiber were clamped by the holders and held straight. Two electrodes were mounted in a fixture that was moved by a nano-precision translation stage. The fiber-grating spectrum was monitored while the arc discharge was being produced. The entire fabrication process was fully controlled by a computer with automation program.

Two methods were used to fabricate fiber LPGs by electric arc discharge. The first method creates micro-bends in the fiber by introducing a small lateral displacement at one end of the fiber. The other technique tapers the fiber by attaching a mass to one end. Both methods induced refractive index modulation along with mechanical deformation. Depending on the position of the fiber in the arc flame and the applied stress to the fiber, the induced refractive index profile inside the fiber can be greatly affected, which in turn, affects the coupling constant between core and cladding modes. For our experiment, the fiber sat in V-grooves made on the electrodes fixture. There was no lateral displacement at one end of the fiber, and no additional mass was attached.

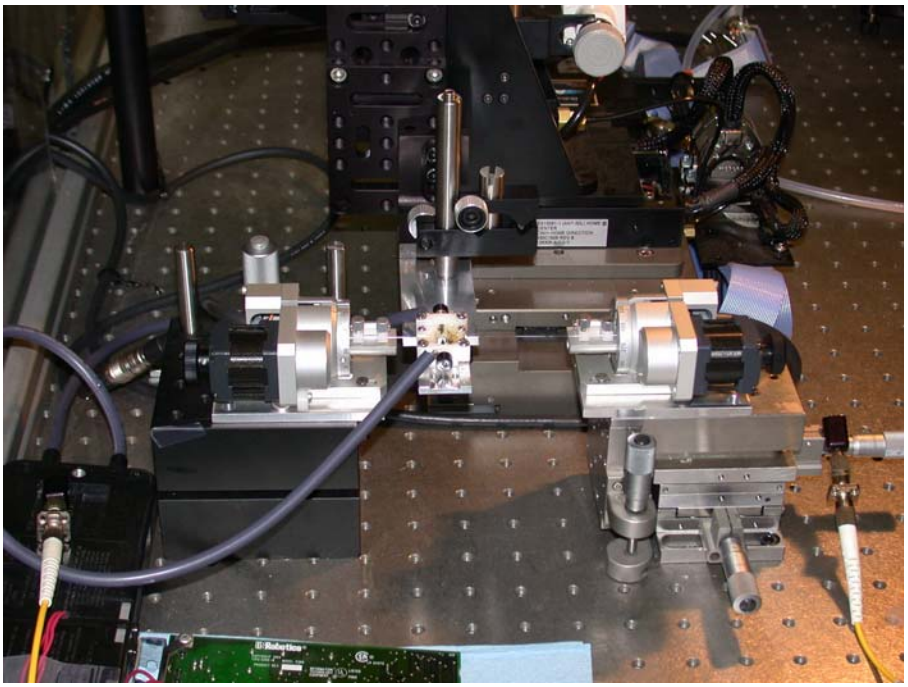

Figure 3.1 (a) Electric arc grating fabrication system with a nano-precision translation stage. The grating spectrum was monitored while the arc discharge was being produced.

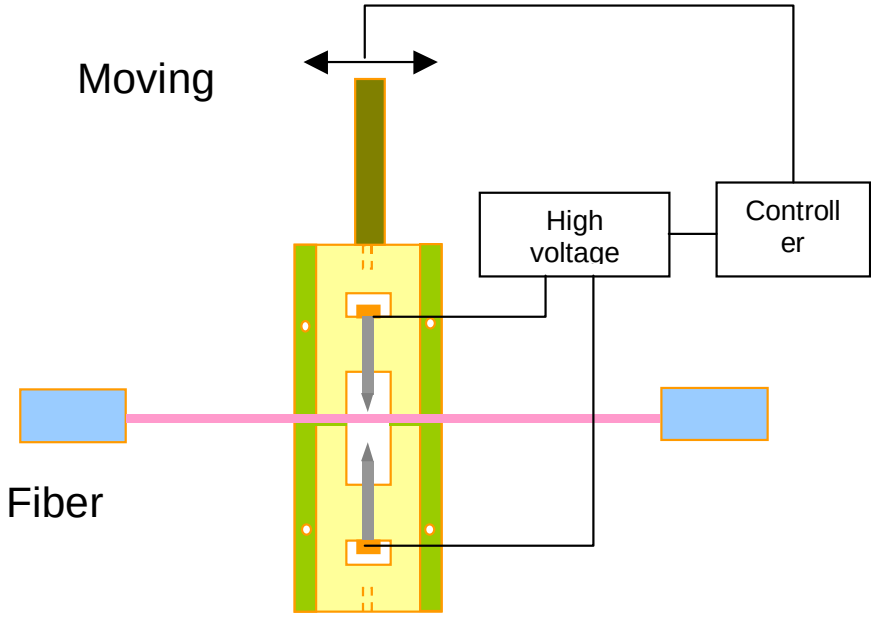

Figure 3.1 (b) The corresponding drawing of electric arc grating fabrication system.

The arc current was ~15mA (RMS) with 20 kHz frequency and the arc duration was changed while keeping arc current constant. The transmission peaks were monitored online and the number of the discharge exposure was control by maintaining a maximum dynamic range of the transmission dip. Usually the discharge exposure would be repeated 10-50 times, giving rise to periodic perturbations along the fiber core. The local temperature of the fiber during the arc exposure was expected to be between 1500-1700ºC. The fiber-grating period, typically 100-600 μm, and grating length of 20-50 mm can be finely controlled by mechanical translation stage.

Figure 3.2 shows the evolution of a short fiber LPG as the number of arc discharges is increased. The arc duration was 357 ms and the period was 500 μm for this grating. The resonant coupling rapidly grew and reached its deepest peak (-30 dB) with 4 grating periods (5 arc discharges). The peak depth was reduced to -13.2 dB with one more arc discharge due to over coupling. The total grating length was 2 mm when it reached the deepest peak. Using the measured peak depths, the number of periods, and the relation $t_{\times,\max} = \sin^2(\kappa L)$, the coupling constant for this mode was estimated to be in the order of 10 cm^{-1}, which is more than ten times larger than the typical coupling constant of LPGs.

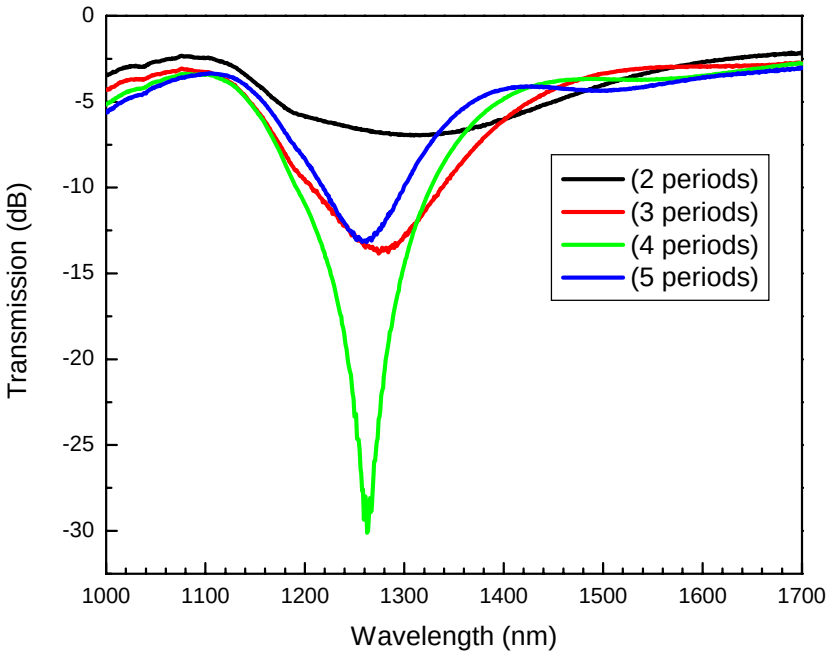

Figure 3.2 Evolution of the short arc-written LPG transmission spectra with increased discharge exposure number.

For this short grating, a mechanical deformation was observed by an optical microscope, as shown in Figure 3.3. The magnitude of the deformation was estimated to be approximately 10μm.

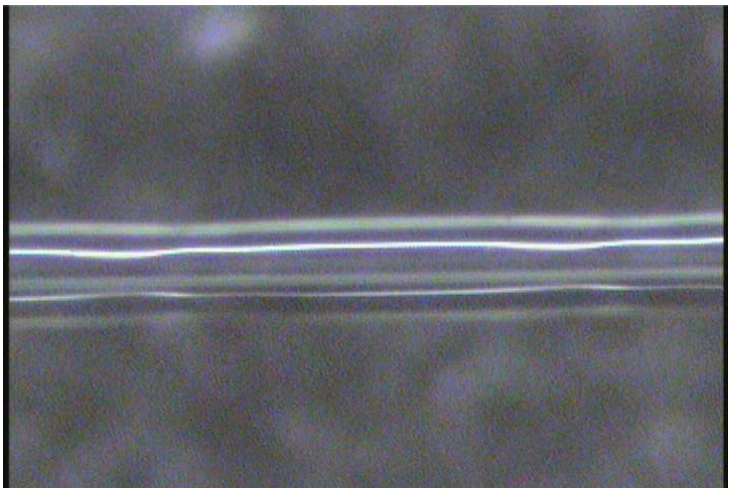

Figure 3.3 Optical microscope image of short arc-written LPG.

Electric arc fabricated fiber gratings in silica fibers were tested at elevated temperatures. The long-term thermal test setup, as shown in Figure 3.4, is comprised of a programmable oven and an optical spectral analyzer. The fiber grating was pre-strained across the oven with quartz tubing. The oven's temperature was maintained by +/1ºC auto pulsed feedback controller.

Figure 3.4 Long-period fiber grating thermal stability tests with an online optical spectral analyzer with a programmable testing oven.

Figure 3.5 shows a typical fiber LPG's transmission spectra measured at 500, 550, 600, 650ºC. There are three cladding modes that can be clearly seen. The first cladding mode is located at about 1420 nm to 1435 nm, the second at about 1480 nm to 1500 nm, and the third at about 1620 nm to 1640 nm. Their wavelength is shifted up at about 53-67 pm/ºC (30-37 pm/ºF). This temperature sensitivity is nearly 60% that of conventional UV-laser inscribed LPGs.

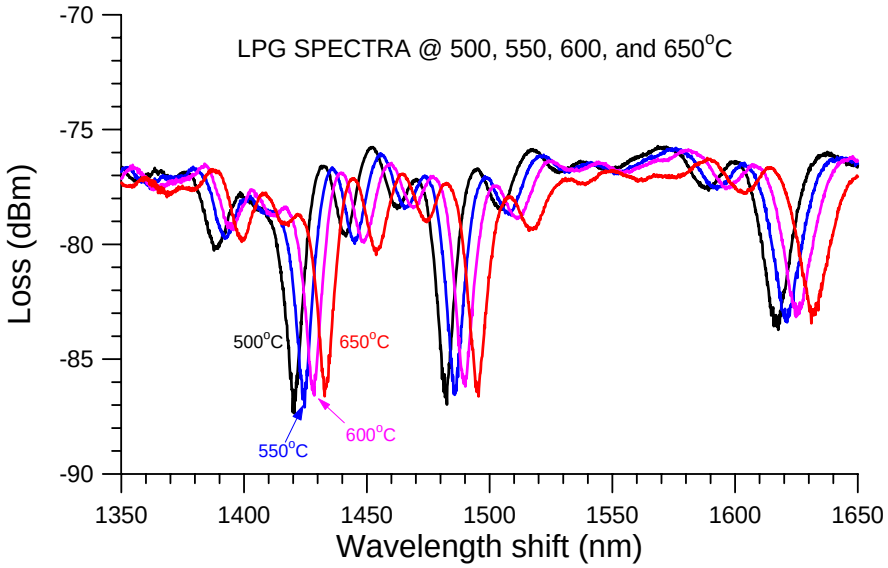

Figure 3.5 Cladding modes transmission spectra measured at 500, 550, 600, and 650°C.

The thermal stability of the electric arc fabricated LPG further was investigated by an isothermal annealing process to see the thermal drifting. Figure 3.6 shows the measured thermal stability from four cladding modes. Except for three modes, one weak mode at 390 nm was also tracked for nearly 200 hours. The measured fiber-grating wavelength drifting rate are -2.9 pm/hr, -6.1pm/hr, -8.1 pm/hr, and -9.3 pm/hr, respectively. Compared with their corresponding temperature sensitivity. The converted thermal drifts are –0.055°C/hr, -0.113°C/hr, -0.140°C/hr, and –0.139°C/hr, respectively. In general, all cladding mode thermal drifting is around about -0.1ºC/hr.

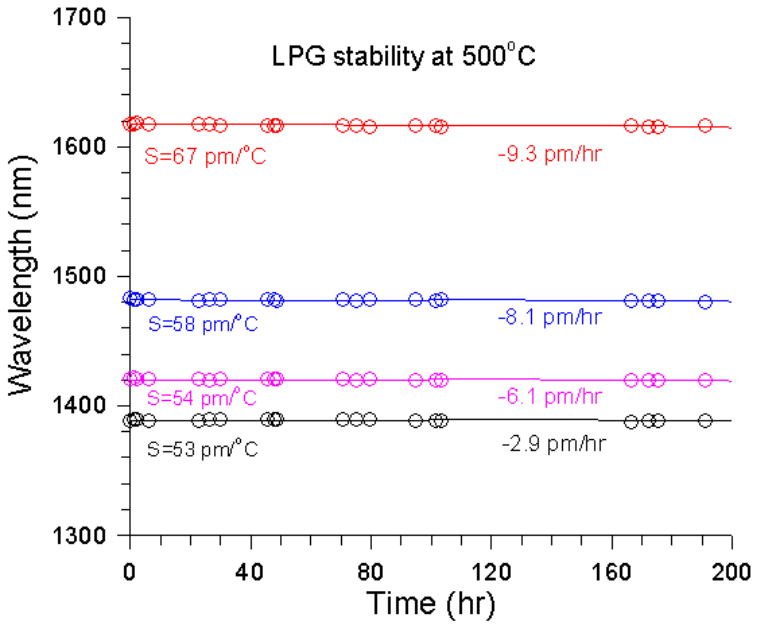

Figure 3.6 Observed cladding modes thermal stability at 500°C from 200 hours isothermal tests.

Figure 3.7 shows the corresponding transmission power loss measured from three cladding modes with wavelengths greater than 1400 nm. There is no obvious drifting during 200 hours of isothermal testing, which is an indication of thermal stability of the refractive index modulation strength at this elevated temperature.

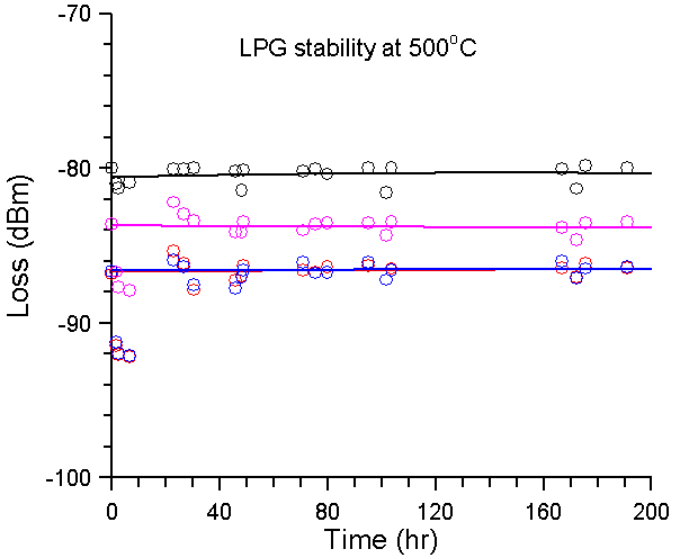

Figure 3.7 Observed cladding modes power loss at 500 °C from a 200 hours isothermal tests.

Figure 3.8 shows the wavelength response to four isothermal test levels of three cladding modes. The data from 500ºC to 600ºC shows nearly negligible wavelength drift. The fiber LPG starts to drift slightly upward at temperature greater than 600ºC. This up-shift feature of the current electric arc fabricated LPG with temperature can be attributed either to a fiber material phase transition from the amorphous structure to the compact structure or to the thermal inscription process induced thermal strain/stress relief process.

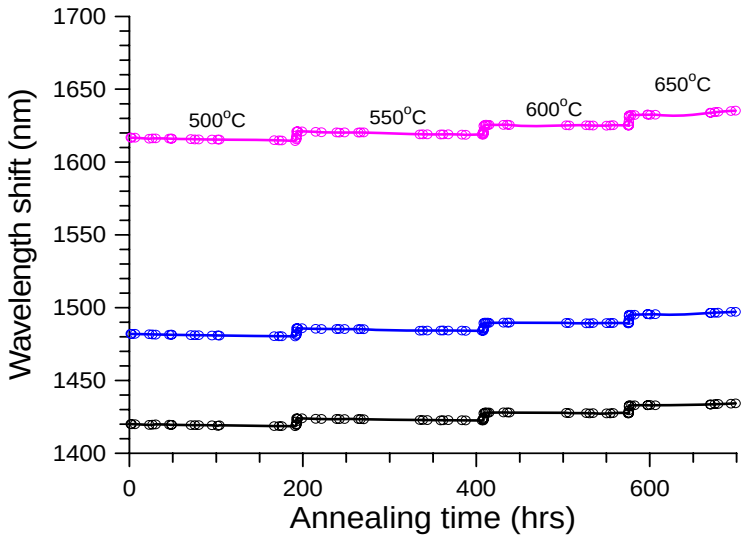

Figure 3.8 Wavelength shift of three cladding modes at isothermal annealing tests from 500, 500, 600, and 650ºC.

From the above laboratory thermal stability test results, it is clear that the fiber LPG fabricated with the electric arc discharge exposure method can effectively inscribe a thermal stabilized LPG element. The short-term isothermal tests have demonstrated its survivability at 500ºC and beyond and without observable grating degradation.

3.2. Femtosecond laser fabricated sapphire fiber grating

To further improve the high temperature capability of fiber grating sensors, Penn State inscribed gratings in sapphire fiber using a femtosecond laser fabrication technique. Fabricating gratings in optical fibers using high power, ultra short (e.g., femtosecond) laser pulses is a very recent approach. There is a lack of systemic study on how fiber gratings are generated in optical fibers via femtosecond illumination. To obtain high-quality gratings, the major efforts have focused on the systemic study on how fiber gratings can be generated in optical fibers via femtosecond illumination. Different exposure times and different system configurations (such as the distance between the fiber and phase mask) have been tried.

Penn State set up a dedicated high-power femtosecond laser system to write gratings in single mode optic fiber, as illustrated in Figure 3.9. The laser system has following parameters:

- Output wavelength: 800 nm
- Energy: ~2 mJ/pulse
- Pulse repetition rate: 1 kHz
- Pulse width ~150 fs

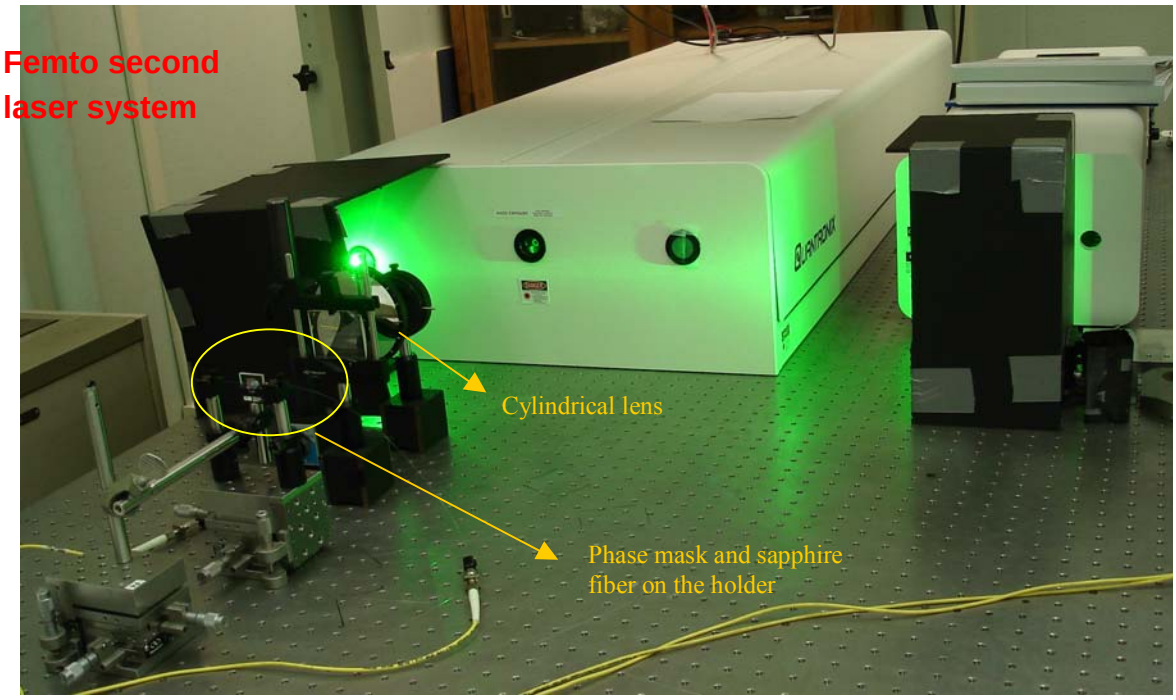

Figure3.9 A high power femtosecond laser system.

The major challenge of writing gratings using ultrashort laser pulses is the short coherent length (< 100 micron) of the laser beam - an almost perfect alignment is needed. After practicing for several weeks, clear gratings were finally inscribed in the optical fibers (including sapphire fiber), as shown in Figure 3.10.

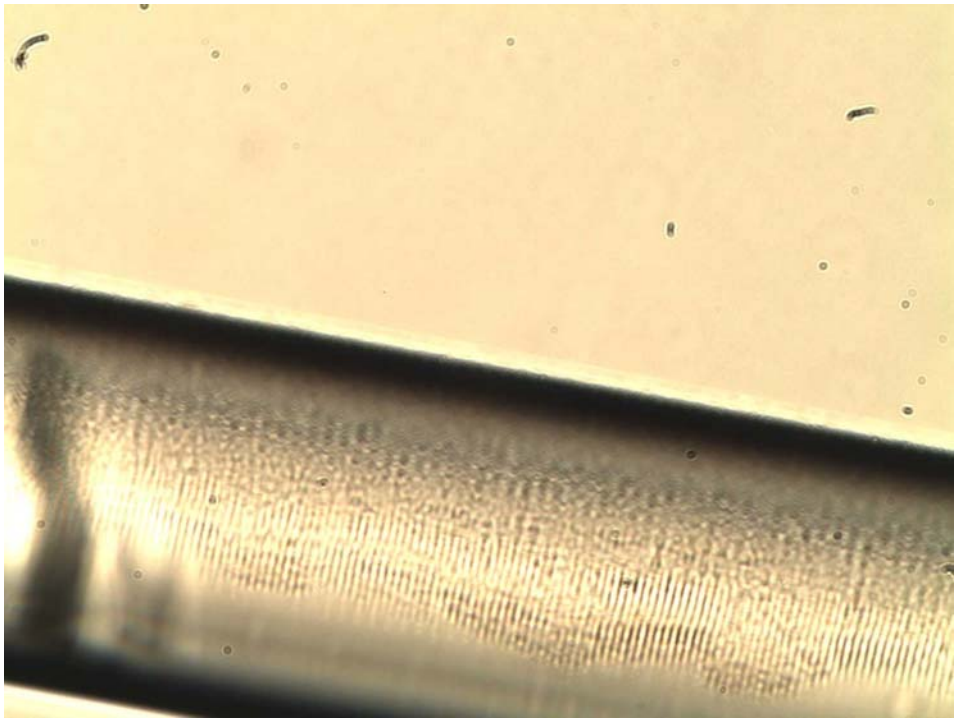

Figure 3.10 Fabricated grating in optical fiber via femtosecond illumination.

Another challenge was encountered since the writing wavelength is at 800 nm – the first order phase mask that has a peak in the near IR region (i.e., 1550 nm) is not achievable. Instead, the fifth order phase mask is used. In order to observe the spectrum for the fifth order phase mask, a very strong grating must be fabricated, which could cause the substantial loss in the fiber.

Base on our observations, the grating fabricated by the femtosecond laser also has a certain loss. In other words, it is not a pure phase grating. This may be the reason why it can be easily seen under the microscope. The loss may be caused by scattering effect.

3.3. Sensor performance enhancement through mode control

It is well known that sapphire fibers are extremely multimodal fibers without cladding. When a light beam is launched into the sapphire fibers with Bragg gratings, besides the coupling between the forward and the backward propagated fundamental (and/or lower order) modes, there are also couplings between the forward fundamental mode and higher-order back propagated guided modes as well as the coupling between the guided modes and radiation modes. Thus, the spectrum of the sapphire fibers is complicated, and includes multiple peaks and the main peak (defined as the one that corresponds to the coupling between the forward and backward propagated fundamental modes) may not be the highest peak. Figure 3.11 shows the experimentally measured results of the spectral response from a grating inscribed in a sapphire fiber. Indeed, the main peak does not have the highest peak. To overcome this, Penn State developed a technique to enhance the main peak. By properly controlling the mode of the sapphire fiber, they were able to enhance the coupling between the forward and the backward propagated fundamental modes and suppress the coupling between the forward propagated fundamental mode and other modes (including the higher order guided modes and the radiation modes). Figure 3.12 shows the experimentally measured spectral response from the same sapphire fiber with the same grating. After mode control, the fundamental mode has the highest peak, which is critical for the development of a reliable harsh environmental sensing system.

Figure 3.11 The spectrum of a Bragg grating fabricated in a sapphire fiber inscribed by ultra-short duration femtosecond pulses without mode control. The peak (corresponding to the coupling between the forward and the back propagated modes) does not have the highest peak.

Figure 3.12 Spectrum of a Bragg grating fabricated in a sapphire fiber inscribed by ultra-short duration femtosecond pulses with mode control. Now, the peak (corresponding to the coupling between the forward and the back propagated modes) indeed has the highest peak.

3.4. A new grating fabrication technique based on refractive element

It is well known that the primary prior state-of-the-art grating fabrication technique uses a phase mask to generate multiple diffracted beams; these beams are then mixed to form the interference patterns to fabricate the gratings in the sapphire fibers. Unfortunately, due to the broadband spectral content of ultra-short femtosecond duration pulses, the diffracted beam has a large angular dispersion (i.e., different wavelength light propagates at different directions), which reduces the visibility of the interference pattern.

To overcome this problem in this research period, Penn State developed a proprietary grating fabrication technique that employs a unique refractive element instead of a phase mask. This new technique eliminates the angular dispersion problem of the phase mask. Figure 3.13 shows the microscopic image of a grating inscribed in a sapphire fiber using this innovative technique.

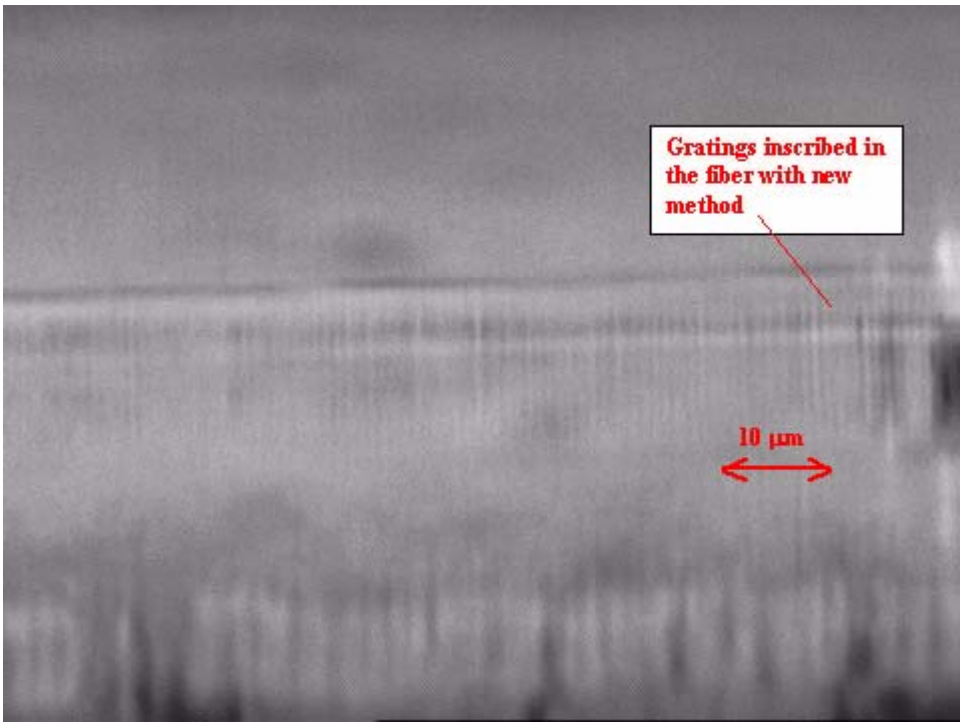

Figure 3.13 Microscopic image of a grating inscribed in a sapphire fiber using a new grating fabrication technique (a refractive element plus an ultra-short femtosecond laser).

3.5. Fabricating the grating in sapphire fibers with cladding

Penn State also performed an initial investigation to fabricate gratings in sapphire fibers with claddings. They are working on a new cost-effective method to synthesize claddings in sapphire fibers. If this new method is feasible, it could enable the fabrication of gratings in sapphire fibers with claddings.

3.6. Grating survival capability at ultra-high temperatures

Penn State tested the survival capability of a grating at very high temperatures. In previous experiments, the highest temperature achieved was approximately 1500ºC. During this program, the grating inscribed in the sapphire fiber was inserted in a furnace at 1650ºC for ten hours. The grating patterns before and after baking at 1650ºC were compared under the microscope. There is no noticeable change after the baking. Thus, at least, the gratings fabricated in sapphire fiber can survive temperature of 1650ºC for a reasonably long time.

3.7. Feasibility demonstration of a sapphire fiber Bragg grating

GE also focused on different high-temperature fiber grating fabrication techniques, including the development of a sapphire fiber Bragg grating fabrication method. Figure 3.14 shows a microscopic image from a sapphire fiber Bragg grating surface. The periodic light contrast indicates a modulation pattern has formed after femtosecond laser inscription. The grating length is about 3 mm, total fiber length is about 250 mm, and the sapphire fiber diameter is about 250 μm. Figure 3.15 shows the sapphire fiber Bragg grating is sealed in quartz tubing as a package. With a multimode silica fiber connection, it can be directly connected to an optical spectral analyzer for sensor performance evaluation.

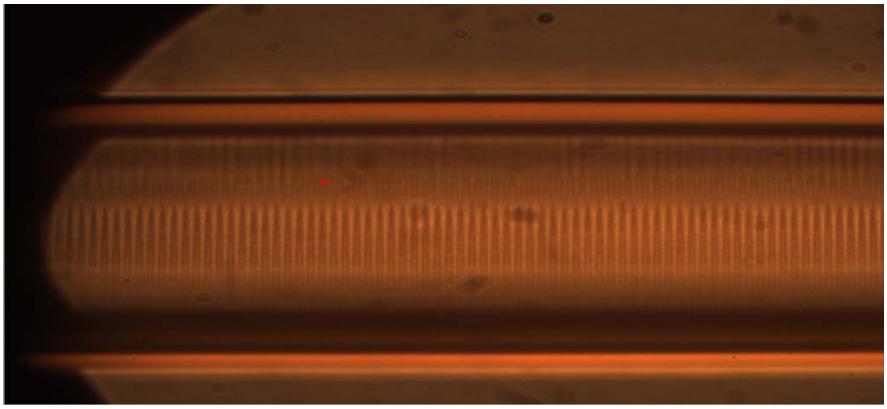

Figure 3.14 Microscopic image from a sapphire fiber Bragg grating temperature sensor prototype, where the femtosecond laser pulse produced periodic modulation.

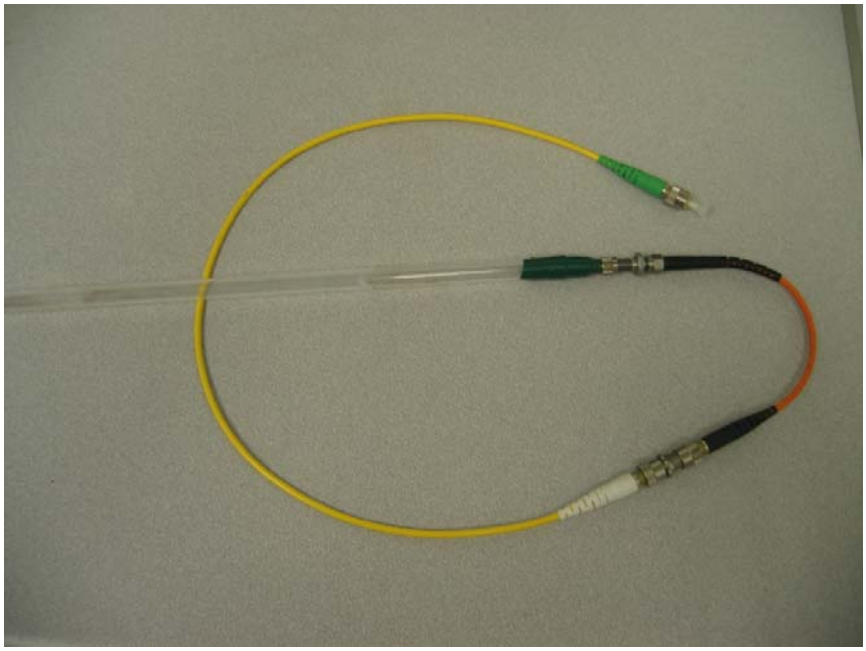

Figure 3.15 Prototype of a sapphire fiber Bragg grating temperature sensor that is packaged by a quartz tubing with a multimode silica fiber connection for sensor performance evaluation.

The periodic modulation seen from the sapphire fiber surface could be attributed to a fiber material density modulation induced by the high-power femtosecond laser pulse exposure process. The femtosecond laser pulse may introduce nanovoids in the exposure area, so that an effective refractive index modulation is formed by periodic modulated nanovoids/uniform crystalline.

The prototype was further evaluated in a laboratory environment where the oven temperature was controlled and the spectra from the sapphire fiber sensor was analyzed via an optical interrogator. Figure 3.16 shows the measured Bragg resonant spectra from the sapphire fiber sensor prototype. The packaged prototype was inserted into a programmable oven with a K-type thermocouple as feedback control. The observed dynamic range of the Bragg peak was about 5 dB. Since it is a multimode fiber sensor, the Bragg resonant peak is actually an envelope of different high-order modes.

Only three modes can be easily identified from the data shown in Figure 3.16. A peak-tracking algorithm has been developed for tracking the different small peaks. Figure 3.17 shows the wavelength plotted as a function of the oven temperatures. The temperature sensitivity of the sapphire fiber Bragg grating sensor is close to 18.5 pm/ºC. This sensitivity is relatively higher than conventional silica fiber Bragg grating sensors, which are about 10 to 14pm/ºC.

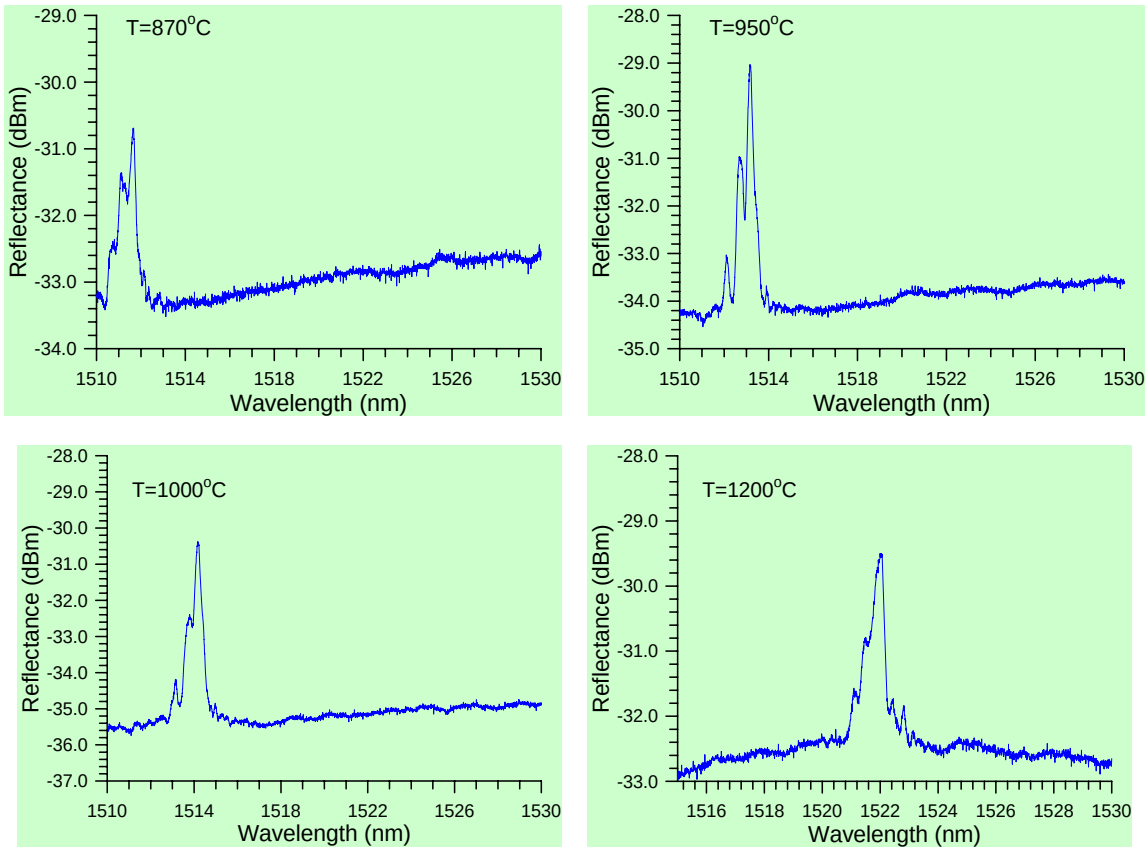

Figure 3.16 Sapphire fiber Bragg grating temperature sensor reflected power loss spectra at several elevated temperatures.

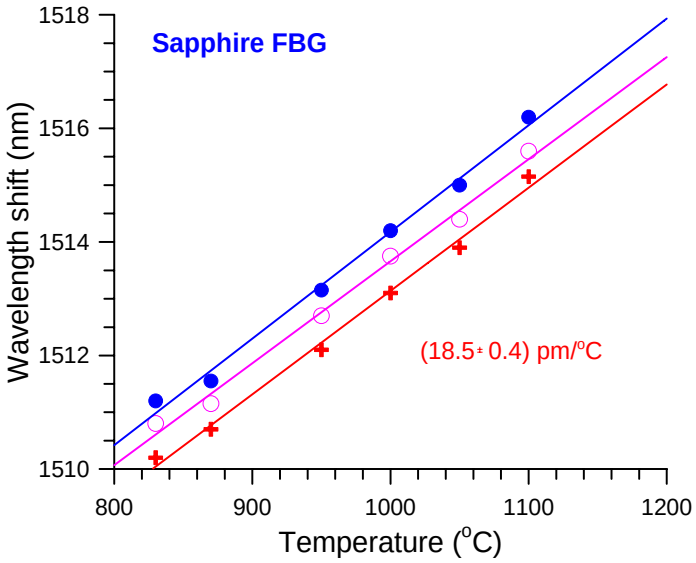

Figure 3.17 Temperature sensitivity from sapphire fiber Bragg grating sensor.

Further evaluation at isothermal status was also conducted for thermal stability and reliability performance. Figure 3.18 shows the thermal stability of the three peak wavelengths at 1065ºC for nearly 6.5 hours. Generally, the sapphire sensor performance was demonstrated to be more stable than silica based fiber Bragg grating sensors at temperature greater than 1000ºC.

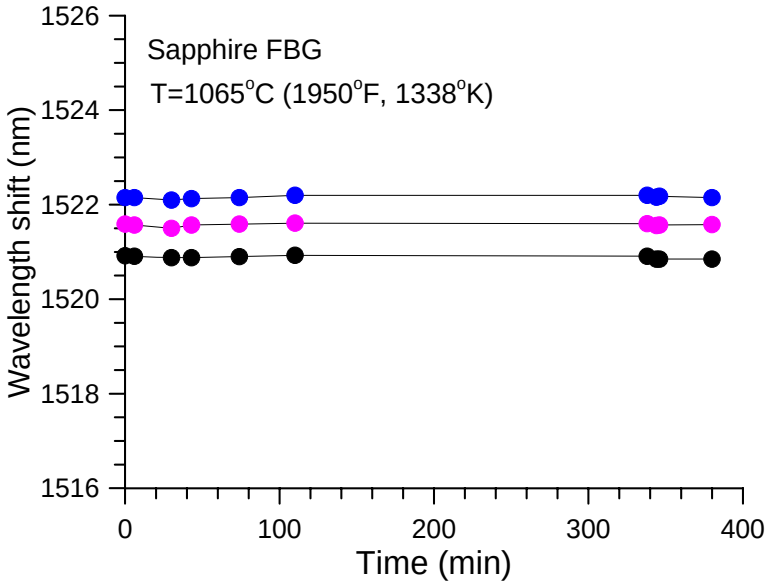

Figure 3.18 Sapphire fiber Bragg grating sensor thermal stability measured at 1065ºC for ~6.5 hours.

Summary: This chapter presented the fiber grating fabrication methods used to inscribe the high-temperature fiber grating elements. We have had great success fabricating micro-sensors using electric arc and femtosecond laser technologies, and our laboratory validation verified these fiber gratings have acceptable thermal stability at 500°C for the electric arc discharge technique and 1600°C for the femtosecond laser technology. A third fiber grating fabrication method, not discussed in this chapter, is based on a commercially-available phase mask technology. These fiber grating fabrication technologies have provided the fundamentals for the fiber gas sensor development during this program.

CHAPTER 4: SENSING MATERIAL DEVELOPMENT

4.1. Colloid sol-gel process for active fiber cladding materials
4.2. Sensing film thickness control
4.3. Surface morphology
4.4. Sensing material down-selecting
4.5. Sol-gel process development for H_2 sensing
4.6. Sol-Gel Process Development for CO sensing
4.7. Sputtering thin film deposition
4.8. X-ray photon spectroscopy analysis of the sputtered sensing film (WOx)

This report has previously discussed that high-temperature fiber gratings can be used as a fundamental element or carrier to prepare a fiber gas sensor. Although a fiber grating can be used for temperature sensing, it does not provide selective combustible gas, syngas, or chemical sensing capability. A fiber LPG can be fabricated with apodized refractive index modulation, though even including the blazed profile, its sensitivity still is in the refractive index response. For all combustible gases, their refractive index is nearly similar to air and it is difficult to detect any low gas concentration directly from a fiber-grating element.

The practical technical solution, as was developed in this program, is to use a combustible gas active material as a thin layer that surrounds a fiber-grating cladding to form so-called “smart skin”. These sensing materials included colloid sol-gel processed silica-based sensing materials and sputtering produced metal oxide alloys. These materials were evaluated using reflectance based optical measurement, x-ray diffraction, an atomic force microscope, and an x-ray photon spectroscope. Experiments demonstrated that the microstructure of these materials strongly depends upon the material preparation processes and their post-thermal treatment. The morphology of these materials could be amorphous film, clusters, nano-particles, nanoporous, and polycrystalline structures. The laboratory evaluation results will be discussed in the following sections.

4.1. Colloid sol-gel process for active fiber cladding materials

The sol-gel process is a versatile method to prepare ceramic and glass materials. Generally, the sol-gel process consists of the transition of a solution-based system from a liquid “sol” (colloidal) into a solid “gel” phase. By using the sol-gel process, ceramic and glass materials can be fabricated in a wide variety of forms, such as ultra-fine or spherical shaped powders, thin film coatings, ceramic fibers, microporous inorganic membranes, monolithic ceramics and glasses, or

extremely porous aerogel materials. An overview of the sol-gel process is presented graphically in Figure 4.1.

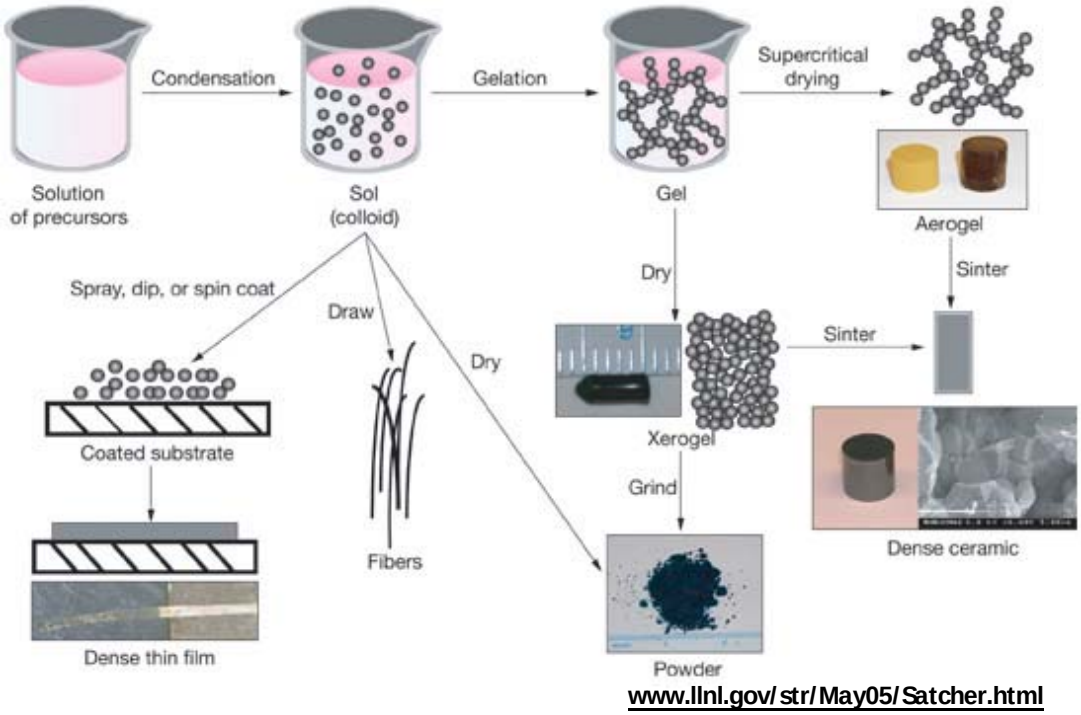

Figure 4.1. Colloid (sol-gel) process.

The starting materials to prepare sols are typically inorganic metal salts or metal organic compounds (e.g., metal alkoxides). The precursor is subjected to hydrolytic and polymerization conditions to form a colloidal suspension, or a sol. Subsequent applications of the sol allow for the preparation of ceramic materials in different forms. For example, thin films are prepared on a substrate by spin coating or dip coating. Alternately, when the prepared sol is cast into a mold, a wet gel will form. Subsequent drying and heat-treatment steps can convert the gel into dense ceramic or glass articles.

In the preparation of a stable and sensitive fiber-optic based sensor system for in situ detection of trace quantities of environmental analytes, we explored the use of an innovative hybrid sol-gel system. This system will provide the sensing capabilities for syngas by using SnO_2/Pd composites while allowing for material compatibility to the fiber optic substrate. GE's current sol-gel process is being used to fabricate test samples and modified fiber cladding. GE's sol-gel process is summarized as the following:

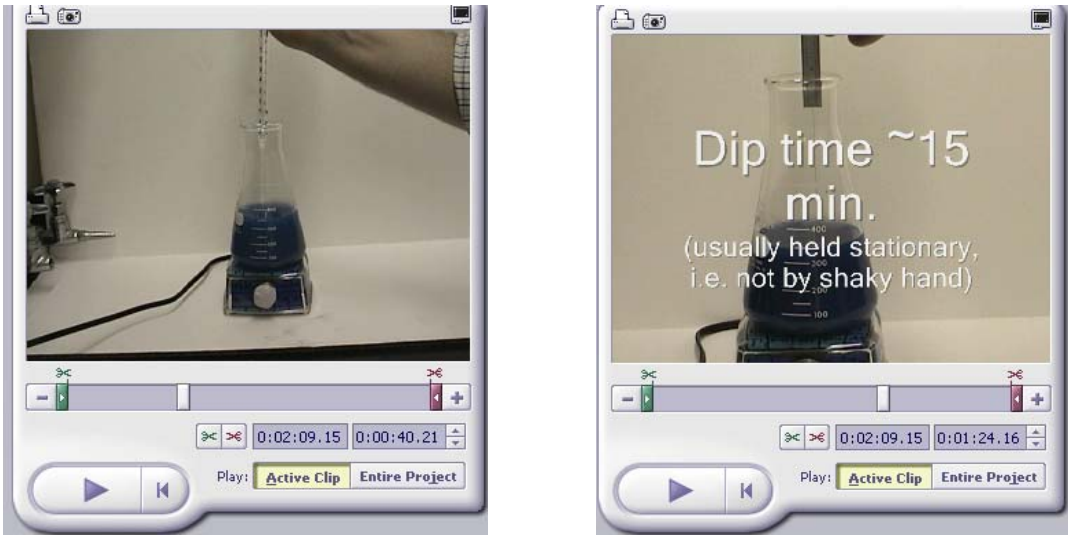

Figure 4.2. Illustrate sol preparation and thin-film deposition on fiber surface. Solution is dyed for contrast.

Figure 4.3. Illustration of high-temperature conversion process.

Using the sol-gel method, tin dioxide and palladium was incorporated into a silicon dioxide matrix under acid conditions. A thin film of the resultant sol material was then either spun coated onto glass and/or silicon substrates or alternately dip coated onto standard fiber optic fibers, as shown in Figure 4.2. The samples were then dried and fired at elevated temperatures to complete the densification to a glassy film, as illustrated in Figure 4.3. Several fiber samples were successfully made based this process, as shown in Figure 4.4. A sample was prepared through

this process to have final layer with 10%Pd/90%SiO_2. From our previous film test, this layer will respond to H_2 at high temperatures. A second sample was prepared with 15%SnO_2/5%Pd/80%SiO_2, suitable to respond to CO at higher temperatures. Microscopic pictures of both samples are shown in Figure 4.4. A blank fiber is also shown for comparison. The final thickness of the sol-gel modified layers is around 1-2 μm. With LPG devices, these layers are sufficiently thin to allow the tail end of surface evanescent wave for interaction.

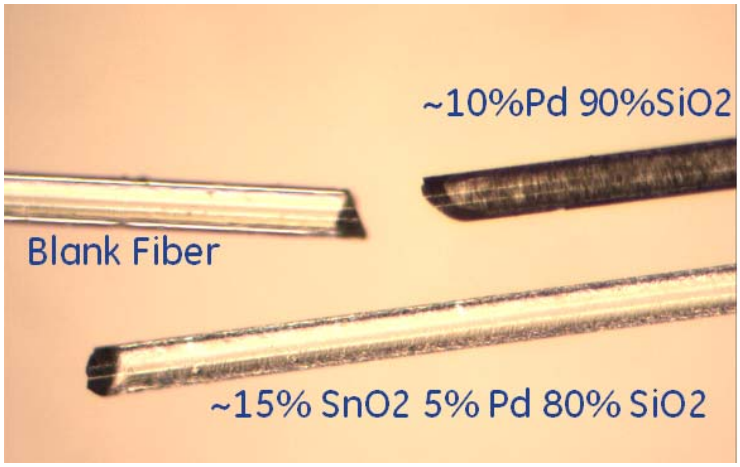

Figure 4.4. Sol-gel sensing film on fused silica fibers.

4.2. Sensing film thickness control

The thickness of the prepared films will have an effect upon the sensing delay due to analyte diffusion time increasing for thicker films. Hence a degree of control over the film thickness is required. The simplest means to attain this control in spin coating to vary the spin coating rate, which increases the lateral force that spreads the film across the substrate. As expected, the rate of spin coating provides control of the film thickness. By operating at spin coating speeds of greater than 2000 rpm, the film thickness for the Pd doped films can be kept at approximately 1 micron in thickness. This trend carries over to the samples doped with higher percentages of sensing moieties. In order to achieve this same degree of control using a dip coating method, which is the method of choice for coating fiber samples using a reel-to-reel dip coater set up, the rate of fiber draw and the coating solution viscosity were varied.

4.3. Surface morphology

In an optical sensing system, a smooth film is of paramount importance to avoid light scattering of incident light issues and a corresponding loss of signal intensity. In GE's spin coating trials, the films formed were uniformly smooth. The infrequent step-like features (see

Figure 4.5) were less than 0.5 micron in the vertical dimension and showed no evidence of crack formation except in the regions where compressive stress cracks were introduced in the SEM sample preparation (see Figure 4.6 and Figure 4.7 for examples of induced cracking regions).

In general, the samples showed homogeneity throughout the films as prepared. SEM-EDS results show no variation across the films, as shown in Figure 4.8. This is advantageous as it maximizes the exposed surface of the sensing moieties.

In samples subjected to thermal cycling during testing, subsequent SEM-EDS showed phase segregation of the palladium dopant into small crystalline structures embedded upon the surface of the film, see Figure 4.9(a-d).

Via this method, GE was able to produce clean thin films with the desired compositions with a thickness between 0.5 μm and 6 μm as determined by SEM cross-sectional analysis. EDS results show a dispersion of the constituent elements as expected.

	1	2	3	Ave	StDev
1K RPM	5.04	5.25	5.88	5.39	0.44
2K RPM	1.155	1.365	1.155	1.23	0.12
4K RPM	1.05	1.155	1.055	1.09	0.06

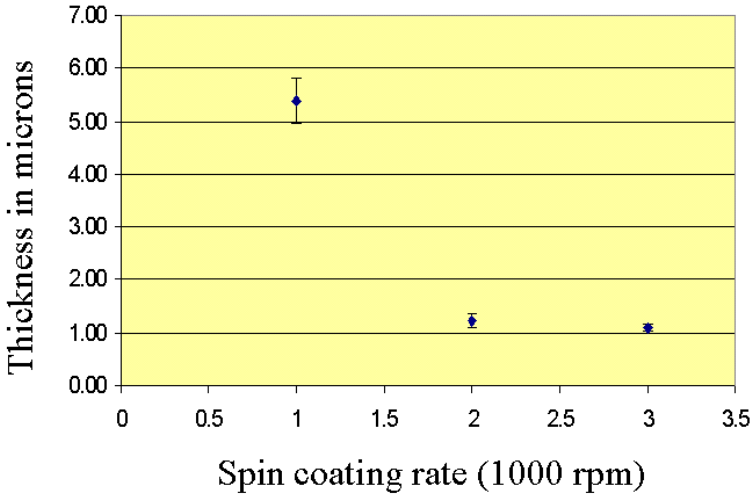

Figure 4.5. 1% Pd doped SiO_2 – Film Thickness

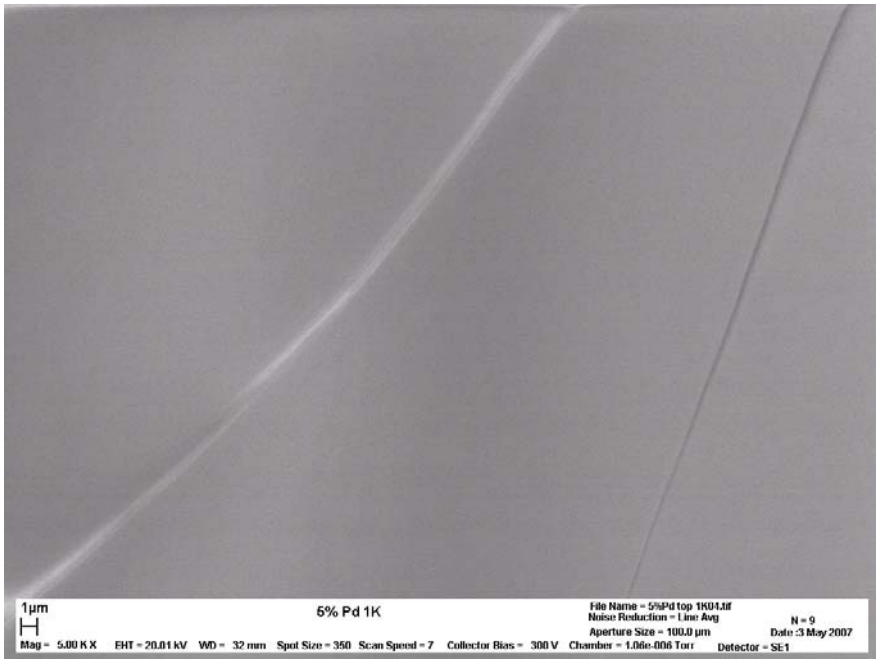

Figure 4.6. SEM image exhibiting typical surface features.

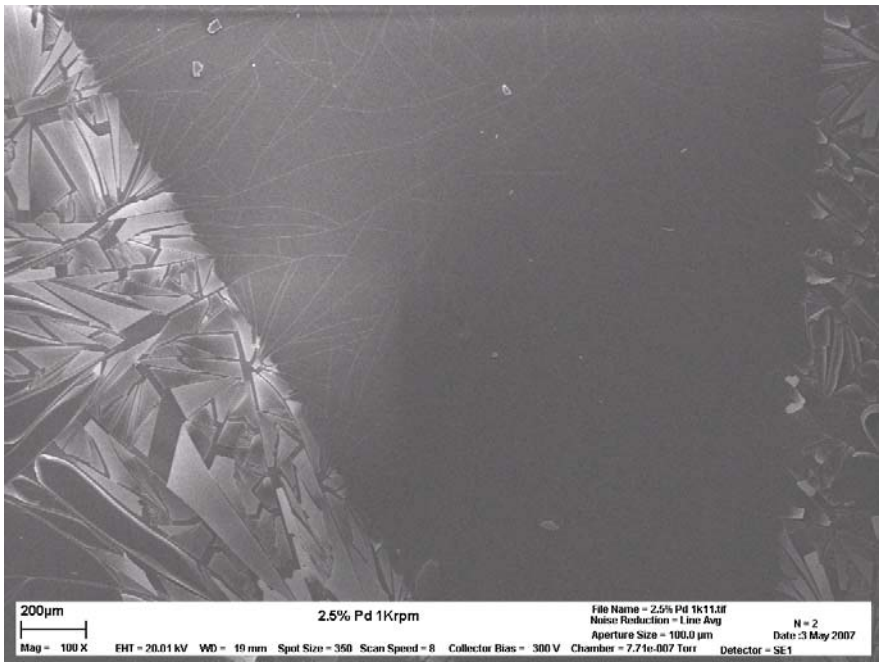

Figure 4.7. SEM image exhibiting SEM-preparation stress induced cracks.

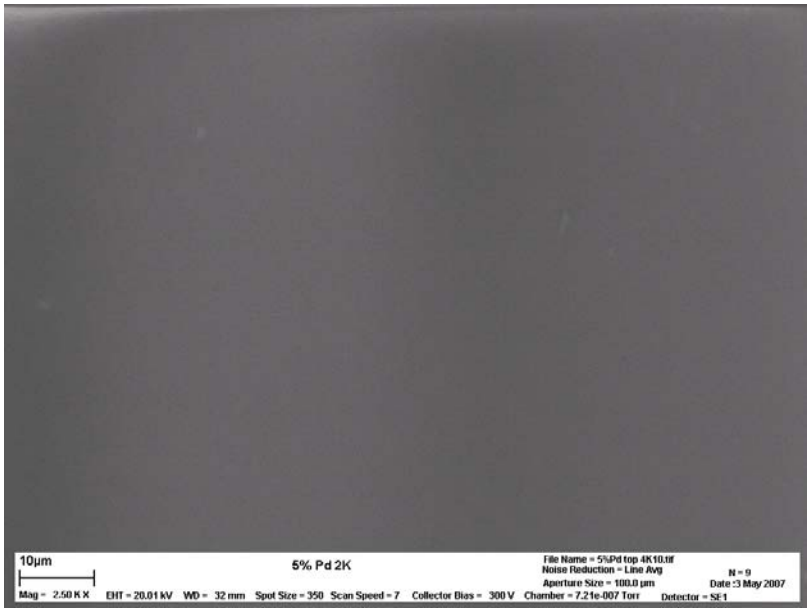

Figure 4.8. Secondary electron image showing homogeneity of the film surface as prepared.

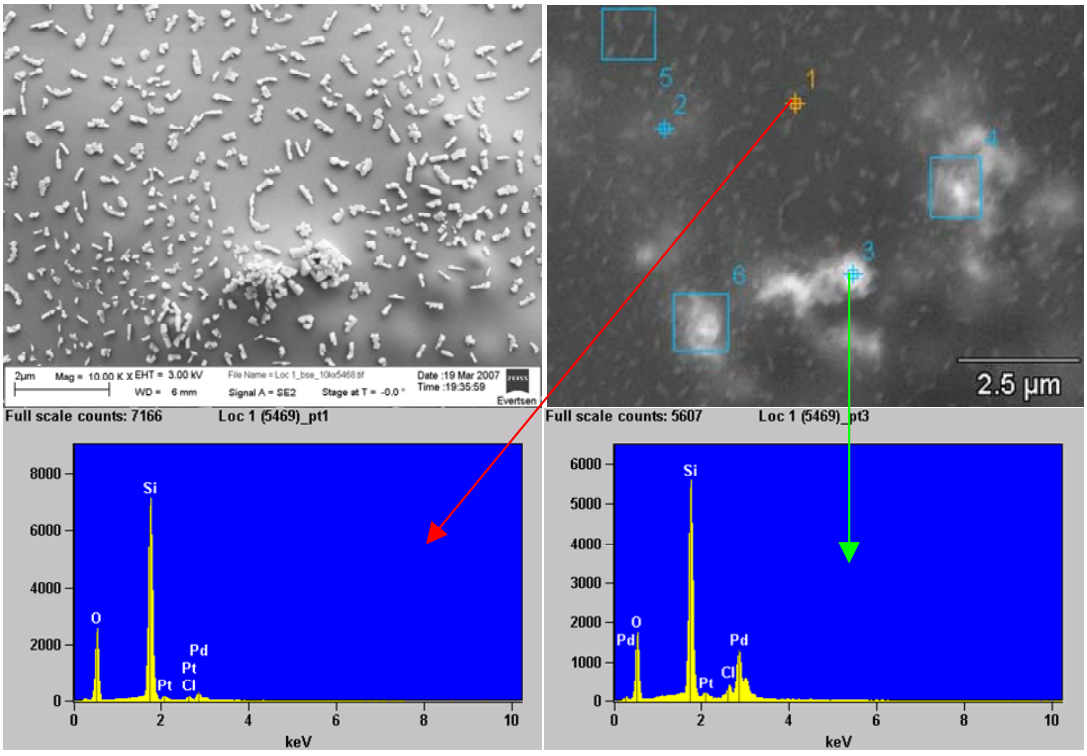

Figure 4.9. (a) Example of phase segregation seen subsequent to thermal cycling. (b) Secondary electron image used for EDS analysis. (c) EDS spectra of non- palladium containing underlying film. (d) EDS spectra of crystalline features observed to contain palladium.

4.4. Sensing material downselection

A sensing material can contain different materials, such as Pd in SiO_2 sol-gel formed matrix for hydrogen sensing. However, an optimization should be conducted to determine the best mixture of different raw materials. The criterion to determine the doping percentage of a catalyst is based on the material response properties to a target combustible gas, such as hydrogen or carbon monoxide. Alternatively, the sensing material should have a proper refractive index so that it is close to the fiber cladding refractive index of ~1.46 for maximum sensitivity. Table 4.1 summarizes the DoE (design of experiment) process GE used to down-select the material set fabricated using the sol-gel process. Detailed test results are included in later sections.

Film	Material	CO sensing			H_2 Sensing		
		Test	**Optical Reflectivity Change**	**High Temperature Test (200, 300, 400, 500°C)**	**Test**	**Optical Reflectivity Change**	**High Temperature Test (200, 300, 400, 500°C)**
AS100 (Sputter)	SiO_2 80% SnO_2 15% (100nm)	Yes	Yes	Yes	Yes	No	Yes
K335-0 (Gel)	Blank TEOS	Yes	No	Yes	Yes	No	Yes
K335-1 (Gel)	TEOS +5% WO_3	Yes	No	Yes	Yes	No	Yes
K335-2 (Gel)	TEOS +5% WO_3	Yes	No	Yes	Yes	No	Yes
K335-3 (Gel)	TEOS +5% WO_3	Yes	No	Yes	Yes	NO	Yes
K335-4 (Gel)	TEOS +5% Pd	Yes	No	Yes	Yes	Yes	Yes
K335-5 (Gel)	TEOS +10.545% Pd	Yes	No	Yes	Yes	Yes	Yes
K335-6 (Gel)	TEOS +10.545% Pd	Yes	No	Yes	Yes	Yes	Yes
K335-7 (Gel)	TEOS +5% Pd	Yes	No	Yes	Yes	Yes	Yes
K335-8 (Gel)	TEOS +5% Pd	Yes	No	Yes	Yes	Yes	Yes
K335-9 (Gel)	TEOS +5% Pd	Yes	No	Yes	Yes	Yes	Yes
K335-10 (Gel)	TEOS +2.5% Pd +2.5%WO_3	Yes	No	Yes	Yes	Best	Yes

Table 4.1. Design of Experiment (DoE) conducted at GE to downselect materials.

4.5. Sol-gel process development for H_2 sensing

Preparation of silica based films:

Pd/SiO_2 nanocomposites were synthesized as follows. Palladium acetylacetonate ($Pd(acac)_2$) was introduced to a 20 ml solution containing reagent grade tetraethoxysilane (TEOS), ethanol (EtOH) and deionized water, with a 0.2 mL nitric acid (HNO_3) added as a catalyst. The TEOS/EtOH/H_2O molar ratio was set at 1:10:15 for all preparations and the mixture was stirred overnight at room temperature using a magnetic stirrer. 200 ml of the slightly viscous yellow sol was then added drop wise to a solvent cleaned (acetone/hexane) glass cover slip on a spin coater operating between 400 and 2000 rpm. The wetted surface was then added to an ambient atmosphere pressure furnace and heated at a rate of 0.5ºC/min to 100ºC and held at temperature for 2 hours to completely evaporate the solvent. The films were then heated at 0.5ºC/minute to 350ºC and held for 10 hours to complete the conversion process. The samples were then cooled to room temperature at 0.5°C/minute.

Analogous preparations were performed to prepared 0.1 wt% atomic Palladium, 0.1 wt% WO_3, 0.1 wt% Pd nanoparticles, mixed 0.1 atomic palladium / 0.1 wt% atomic silver, 0.1 wt% PVP (-25 and –29) coated palladium nanoparticles, 0.1 wt% 1-dodecanethiol modified palladium nanoparticles and 0.1 wt% 11-mercaptoundecanoic acid modified palladium nanoparticles. Control TEOS films were also prepared.

Preparation of silicon oxycarbide based films:

SiO_xC_y nanocomposite films were prepared as follows.0.05 g of 0.1-0.3 μm palladium nanoparticles were added to 5.0 g of Starfire Systems Inc. TR-040-006 silicon oxycarbide solution in hexanes. The resulting solution was sonicated for 1 hour. Subsequently, the sol was spin coated onto a fused quartz plate at 1000 rpm. The wetted surface was added to an ambient atmosphere furnace and heated at a rate of 2.0°C/min to 100°C and held at temperature for 2 hour to fully evaporate any remaining solvent. The films were heated at 2.5°C/minute to 850°C and held for 1 hour to complete the conversion process. The samples were then cooled to room temperature at 0.5°C/minute overnight.

Analogous preparations were concurrently made with WO_3, atomic palladium using palladium acetate as a precursor, 1-dodecanethiol modified palladium nanoparticles, 11-mercaptoundecanoic acid modified palladium nanoparticles, 1-hexanethiol modified palladium nanoparticles, and unfilled SiO_xC_y film controls. A limited test of the viscosity modification ability of 1 wt% ethylene glycol to reduce surface migration was also successfully undertaken using a 0.1 wt% atomic palladium sample.

5% Palladium Doped **Silicon Dioxide:**

0.29 g of palladium acetate ($C_4H_6O_4Pd$) was introduced to a solution containing 20.00 g of reagent grade tetraethoxysilane (TEOS), 22.11 g pharmaceutical grade ethanol (EtOH), and

6.92 g deionized water. 0.5 mL of hydrochloric acid (HCl) was added as a catalyst. The mixture was stirred overnight at room temperature using a magnetic stirrer. 1 mL of the low viscosity orange-red sol was then added drop wise to an ethanol rinsed glass slide on a spin coater operating between 1000 and 4000 rpm. The wetted surface was then introduced to an ambient atmosphere furnace and heated at a rate of 1°C/min to 80°C and held at temperature for 1 hour followed by heating at 1°C/minute to 200°C and held for 2 hours to evaporate the solvent. The films were then heated at 1°C/minute to 430°C and held for 10 hours to complete the conversion process. The samples were cooled to room temperature at ~0.5°C/minute.

Analogous preparations were performed to prepared 1, 2.5 and 10% palladium doping as shown in Table 4.2. Control undoped TEOS films were also prepared.

2.5% Pd doping

TEOS	20.00	g
Ethanol	22.11	g
Water	6.92	g
Pd Acetate	0.14	g
HCl	0.50	mL

5% Pd doping

TEOS	20.00	g
Ethanol	22.11	g
Water	6.92	g
Pd Acetate	0.29	g
HCl	0.50	mL

1.0% Pd doping

TEOS	20.00	g
Ethanol	22.11	g
Water	6.92	g
Pd Acetate	0.06	g
HCl	0.50	mL

10.0% Pd doping

TEOS	20.00	g
Ethanol	22.11	g
Water	6.92	g
Pd Acetate	0.58	g
HCl	0.50	mL

Table 4.2 Palladium doped SiO_2 film formulations

Thin film samples under investigation and evaluation are listed in Table 4.3.

	Film Composition	Spin Coating Rate	Additive Source
K311-1a	0.1 wt% Pd in TEOS	400	Pd(acac)2
K311-1b	0.1 wt% Pd in TEOS	1000	Pd(acac)2
K311-2a	0.1 wt% WO3 in TEOS	400	WO3 powder
K311-2b	0.1 wt% WO3 in TEOS	1000	WO3 powder
K311-3a	0.1 wt% Pd nanoparticles in TEOS	400	Pd nanoparticle
K311-3b	0.1 wt% Pd nanoparticles in TEOS	1000	Pd nanoparticle
K312-1a	0.1 wt% Pd in TEOS	500	Pd(acac)2
K312-1b	0.1 wt% Pd in TEOS	1000	Pd(acac)2
K312-1c	0.1 wt% Pd in TEOS	2000	Pd(acac)2
K312-2a	0.1 wt% WO3 in TEOS	500	WO3 powder
K312-2b	0.1 wt% WO3 in TEOS	1000	WO3 powder
K312-2c	0.1 wt% WO3 in TEOS	2000	WO3 powder
K315-1d	TEOS film control	-	-
K315-1s	TEOS film control	1000	-
K315-2d	0.1 wt% Pd in TEOS	-	Pd(acac)2
K315-2s	0.1 wt% Pd in TEOS	1000	Pd(acac)2
K315-3d	0.1 wt% Pd and 0.1 wt% Ag in TEOS	-	Pd(acac)2/AgNO3
K315-3s	0.1 wt% Pd and 0.1 wt% Ag in TEOS	1000	Pd(acac)2/AgNO3
K315-4d	0.1 wt% WO3 in TEOS	-	WO3 powder
K315-4s	0.1 wt% WO3 in TEOS	1000	WO3 powder
K315-5d	0.1 wt% Pd nanoparticles in TEOS	-	coated Pd(nano) powder
K315-5s	0.1 wt% Pd nanoparticles in TEOS	1000	coated Pd(nano) powder
K319-1	0.1 wt% WO3 in TEOS	1000	WO3 powder
K319-2	0.1 wt% atomic Pd in TEOS	1000	Pd(acac)2
K319-3	0.1 wt% PVP-25 coated Pd nanoparticles in TEOS	1000	coated Pd(nano) powder
K319-4	0.1 wt% PVP-29 coated Pd nanoparticles in TEOS	1000	coated Pd(nano) powder
K319-5	0.25 wt% PVP-25 coated Pd nanoparticles in TEOS	1000	coated Pd(nano) powder
K319-6	0.25 wt% PVP-29 coated Pd nanoparticles in TEOS	1000	coated Pd(nano) powder
K319-7	0.1 wt% 1-DDE coated Pd nanoparticles in TEOS	1000	coated Pd(nano) powder
K319-8	0.1 wt% 11-MUDA coated Pd nanoparticles in TEOS	1000	coated Pd(nano) powder
K319-9	0.1 wt% WO3, 0.1 wt% atomic Pd	1000	WO3 powder, Pd(acac)2
K325-1	0.1 wt% atomic Pd in TR-040-006	1000	Pd acetate
K325-2	0.1 wt% WO3 in TR-040-006	1000	WO3 powder
K325-3	0.1 wt% 1-hexanethiol coated Pd nanoparticles in TR040-006	1000	coated Pd(nano) powder
K325-4	0.1 wt% 11-MUDA coated Pd nanoparticles in TR040-006	1000	coated Pd(nano) powder
K325-5	0.1 wt% 1-DDE coated Pd nanoparticles in TR040-006	1000	coated Pd(nano) powder
K329-1	0.1 wt% atomic Pd in TR-040-006 w/ 1 wt% Ethylene Glycol	1000	Pd(acac)2

Table 4.3 Thin film samples under investigation and evaluation.

4.6. Sol-gel process development for CO sensing

Thin films comprised of silicon dioxide, tin dioxide, and palladium were prepared as follows:

80% Silicon Dioxide**: 15% Tin Dioxide: 5% Palladium**

0.014 g of palladium acetylacetonate ($C_{10}H_{14}O_4Pd$) was introduced to a solution containing 45 mL of deionized water, 45 mL 1-propanol, 30 mL 2-propanol and 0.277 g tetraethoxysilane (TEOS). 15 mL tin tetrachloride was added, which upon immediate hydrolysis released sufficient hydrochloric acid to act as a catalyst. The mixture was stirred overnight at room temperature using a magnetic stirrer. 1 mL of the low viscosity yellow-white sol was then added drop wise to an ethanol rinsed glass slide on a spin coater operating between 1000 and 4000 rpm. The wetted

surface was then introduced to an ambient atmosphere furnace and heated at a rate of 1°C/min to 80°C and held at temperature for 1 hour followed by heating at 1°C/minute to 200°C and being held for 2 hours to evaporate the solvent. The films were then heated at 1°C/minute to 430°C and held for 10 hours to complete the conversion process. The samples were cooled to room temperature at ~0.5°C/minute.

Analogous preparations were undertaken to prepared films with a composition of SiO_2: SnO_2: Pd of 80:10:10, and 80:19:1, as shown in Table 4.4.

Component	Mass(g) precursor	Volume(L)	Moles (target)	
SnCl4	2.251	0.015	0.015	
H2O		0.045		
C3H7OH		0.045		80:15:05
2-C3H7OH		0.03		
TEOS	0.277		0.08	
Pd(acac)2	0.014		0.005	
		Total moles	0.1	

Component	Mass(g) precursor	Volume(L)	Moles (target)	
SnCl4	1.501	0.01	0.01	
H2O		0.045		
C3H7OH		0.045		80:10:10
2-C3H7OH		0.03		
TEOS	0.277		0.08	
Pd(acac)2	0.029		0.01	
		Total moles	0.1	

Component	Mass(g) precursor	Volume(L)	Moles (target)	
SnCl4	2.851	0.019	0.019	
H2O		0.045		
C3H7OH		0.045		80:19:01
2-C3H7OH		0.03		
TEOS	0.277		0.08	
Pd(acac)2	0.003		0.001	
		Total moles	**0.1**	

Table 4.4. SiO_2: SnO_2: Pd film formulations.

A CO gas test was performed on a TEOS-based sensing film made from the sol-gel process on glass substrate over a wide range of temperatures (room temperature to 525°C). First, a blank film with only glass was tested over the temperature range (25~525°C) to baseline the optical absorption probe in the high temp gas chamber. The baseline was used to calibrate any variation in the test condition caused by temperature changes such as mechanical, local temperature, and vibration. With the baseline data, we then test both the alloy-based and sol-gel based films both with similar contents (SiO_2 80% SnO_2 15% 5% Pd) over a wide temperature range (25~525°C). A high-temperature optical probe was used to send and receive optical signals from the film

placed inside the gas chamber. Significant optical absorption was observed with TEOS-based Pd-doped films at elevated temperatures from 280°C ~ 555°C. A high-level summary of the tested samples is shown in Table 4.5.

Film	Material	CO sensing							
		25°C	120°C	170°C	235°C	280°C	355°C	425°C	525°C
Blank film	Glass	No	No	No	No	No	No	No	No
AS100 (Sputtered)	80% SiO_2 +15% SnO_2 +5% Pd (100nm)	Yes	Yes	Yes	No	Good	No	No	No
SnO_2, SiO_2, Pd sol-gel sample	80% SiO_2 +15% SnO_2 +5%Pd	No	No	No	No	Good	Good	Good	Good
K335-0(Gel)	Blank TEOS	No	No	No	No	No	No	No	No
K335-1(Gel)	TEOS +5% WO_3	No	No	No	No	No	No	No	No
K335-2(Gel)	TEOS+5% WO_3	No	No	No	No	No	No	No	No
K335-3(Gel)	TEOS+5% WO_3	No	No	No	No	No	No	No	No
K335-4(Gel)	TEOS+5% Pd	No	No	No	No	No	No	No	No
K335-5(Gel)	TEOS+10.545% Pd	No	No	No	No	No	No	No	No
K335-6(Gel)	TEOS+10.545% Pd	No	No	No	No	No	No	Good	Good
K335-7(Gel)	TEOS+5% Pd	No	No	No	No	No	No	No	No
K335-8(Gel)	TEOS+5% Pd	No	No	No	No	No	No	No	No
K335-9(Gel)	TEOS+5% Pd	No	No	No	No	No	No	No	No
K335-10(Gel)	TEOS+2.5% Pd +2.5%WO_3	No	No	No	No	No	No	No	No

Table 4.5. Summary of CO test over elevated temperatures.

4.7. Sputtering thin film deposition

In additional to the sol-gel process, a sputtering process was also used for nanoparticle sensing film deposition. Since sputtering is a commonly used technique with standard procedures, the detailed process will not be described in this report. Instead, the sensing films fabricated with the deposition system are shown in the following paragraphs.

The Perkin-Elmer model 2400 was used for all sensing material deposition. It uses a cryogenic pump to achieve a base vacuum in the approximately 2 x 10^{-6} range. Two other

identical systems are also available that use turbo-molecular pumps, both of which achieve base vacuum in the 10^{-7} range. The system is energized by RF (radio frequency) generators and DC capability.

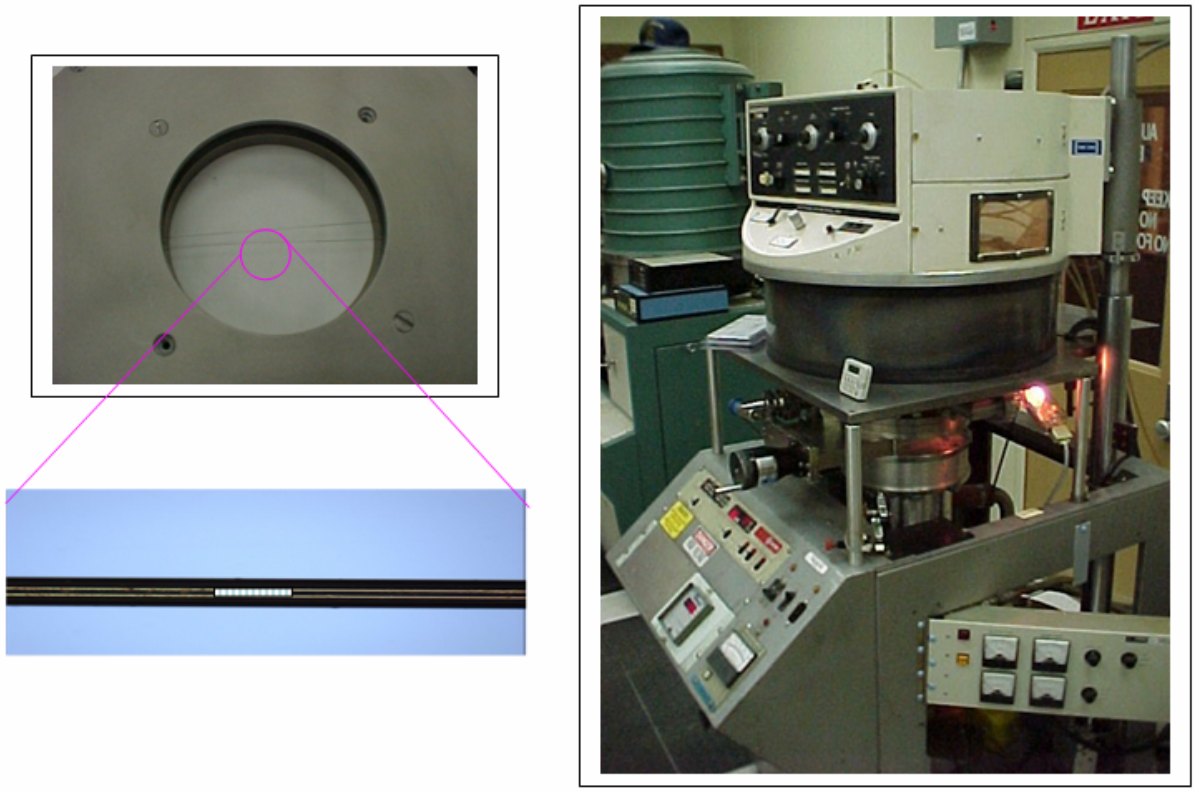

Figure 4.10 Sputtering system and fiber deposition fixture with fiber grating with a 2" wide window for sensing film deposition.

H_2 sensing material structural analysis

Using a pure palladium target in the O_2-riched chamber, the H_2 sensing material was deposited onto both fiber grating and a quartz glass substrate. The following deposition conditions have been used:

- Base vacuum: 1 x 10^{-6} Torr
- 6" 99.999% Pd target run in 18 % O_2 (balance Argon)
- Gas flow of 50-60 sccm
- Run pressure 6-8 mTorr
- Target to substrate distance: 2"
- Forward power of 100 watts (radio frequency)
- Target bias approximately 700 volts with no reflected power
- Rate of deposit around 50 A per minute
- Substrate temperate reached approximately +/-50°C

Figure 4.11 shows the x-ray diffraction spectral data as a function of diffraction angle, 2θ. This result reflects that the sensing material has (111) and (220) textures, and the calculated grain size from the main peak is about 10 nm. Figure 4.12 demonstrates the different hydrogen sensing material nanostructural information. These sensing materials include pure palladium (Pd), $Pd_xAu_{(1-x)}$ alloy, $Pd_xAu_yNi_{(1-x-y)}$ alloy.

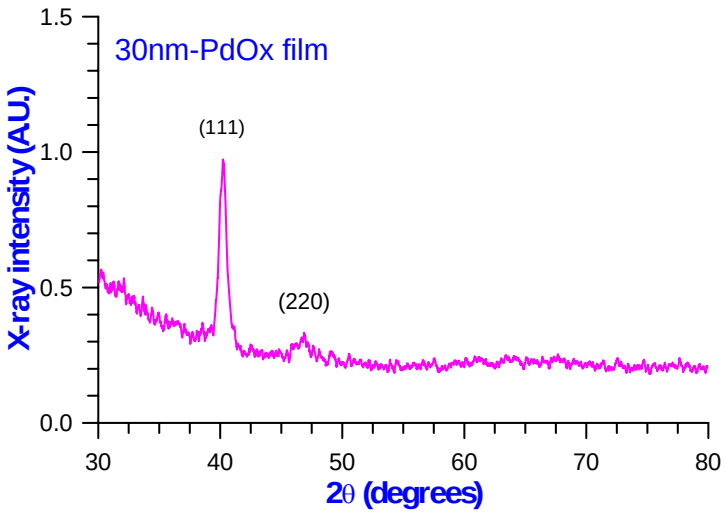

Figure 4.11. X-ray diffraction from a typical PdOx sensing film that is of 30nm thickness.

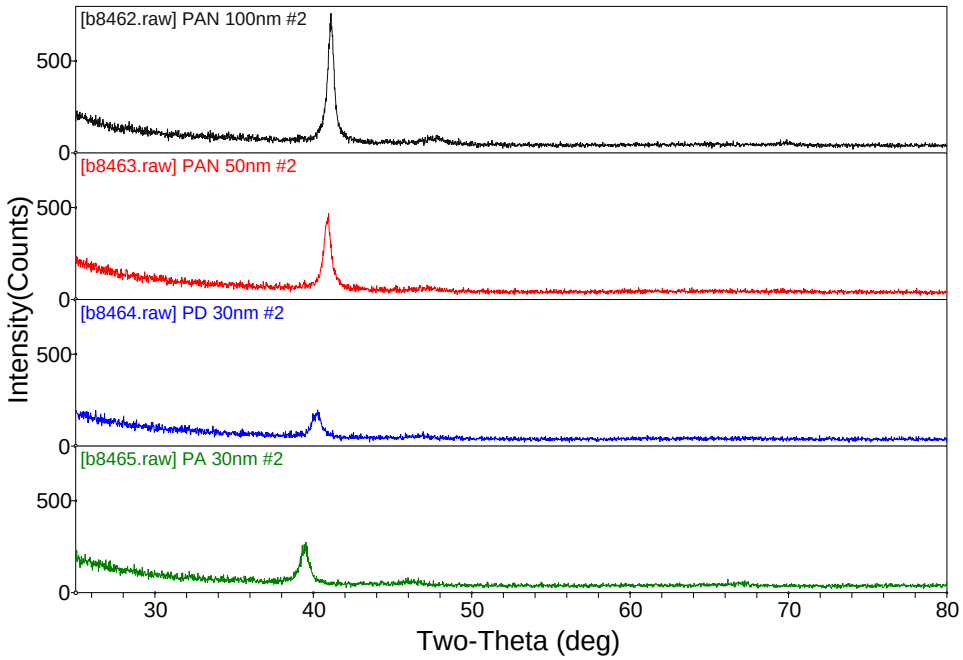

Figure 4.12. X-ray diffraction data from 30nm thick PdAu alloy (dark green), 30nm Pd oxide (blue), 50nm PdAuNi alloy (red), and 100nm PdAuNi alloy (black) hydrogen sensing materials.

CO sensing material structural analysis

Tin oxides based materials are mainly used for carbon monoxide (CO) sensing. Its high-temperature operation is due to its wide band-gap structure. Figures 4.13 and 4.14 are AFM and x-ray diffraction measurements from as-grown SnO_2 film. It is obvious that the as-grown material does not to have large grains and the diffraction peak is mainly dominated by the quartz substrate. The AFM image indicates that the grain size could be about 3.7 nm or less. Meanwhile, both results are consistent that SnO_2 film structure hasn't shown obvious textures.

CO gas sensing is mainly based on palladium doped or undoped tin oxide material. The following deposition conditions were used.

- Base vacuum 4×10^{-7} Torr
- 6" SnO_2 target run in 18 % O_2 (balance Argon)
- Gas flow of 65 sccm
- Run pressure 6 mTorr
- Target to substrate distance = 2"
- Forward power of 200 watts (radio frequency)
- Target bias approximately 730 volts with no reflected power
- Rate of deposit around 50 A per minute
- Substrate temperature reached approximately +/-60^{o}C

Figures 4.13 and 4.14 show AFM and x-ray diffraction measurements from as-grown SnO_2 film. It is obvious that the as-grown material seems not to have large grains and the diffraction peak is mainly dominated by the quartz substrate. The AFM image only indicates that grain size could be about 3.7 nm or less. Meanwhile, both results are consistent that SnO_2 film structure has not shown obvious textures.

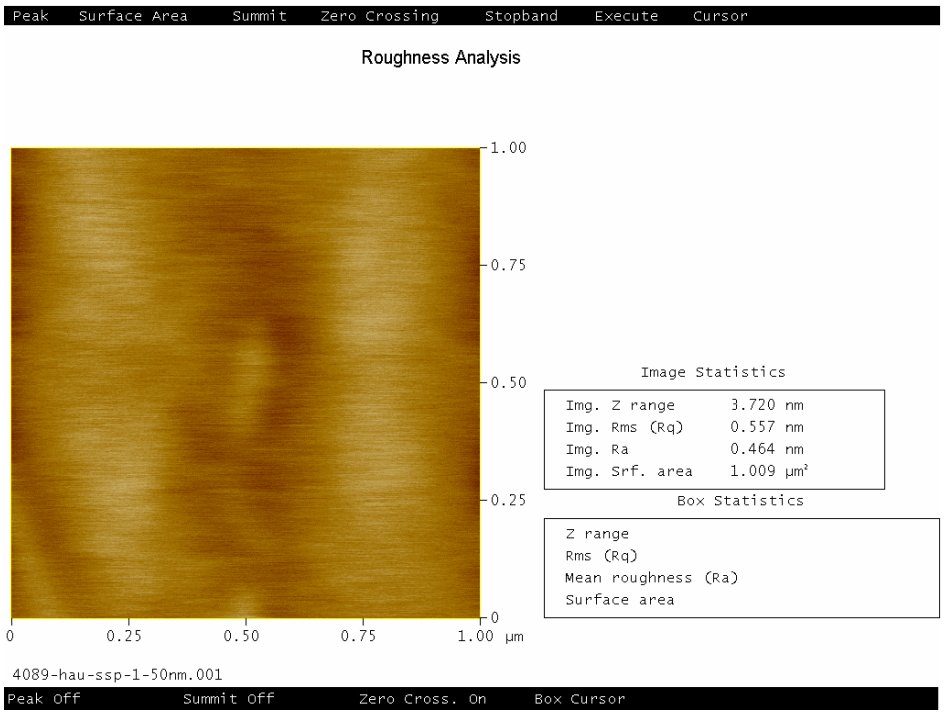

Figure 4.13. AFM image analysis on SnO_2 sensing material structure.

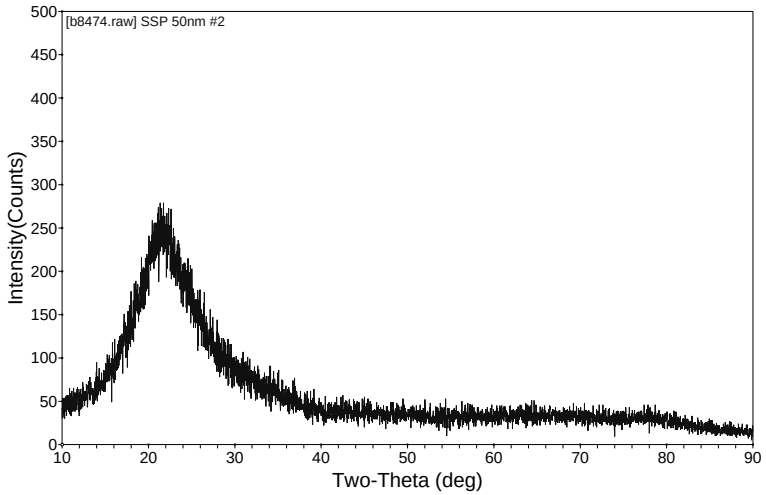

Figure 4.14. X-ray diffraction analysis on CO sensing material structure.

4.8. X-ray Photon Spectroscopy analysis of the sputtered sensing film (WO_3)

X-ray photon spectroscopy (XPS) is mainly dedicated to the identification of chemical composition/bonding on surfaces since it has the sensitivity to detect peak energy shifts due to the chemical bond formation. The XPS measurements were performed on a Kratos Axis Ultra DLD XPS system using a monochromatic Al Kα radiation (1486.6 eV) at 225W. XPS probing depth is typically 0.5-5 nm. The analysis area employed for this study is ~700×300 μm. The samples were analyzed as received. Survey scans were performed to obtain the overall compositions, which are reported in atomic percent, see Table 4.6. The quantitative compositions of the surface species taken from survey scans were determined from the integrated intensities corrected by atomic sensitivity factors provided by the vendor.

High resolution spectra were also collected for chemical bonding information. The binding energy scales of all the core-level spectra were charge-corrected to C(1s) signal for the hydrocarbon at 284.6 eV.

						From O1s Peak-fitting				
	C	N	O	W	O/W ratio (total)	O (W-O)	O (weak)	O (W-O)	O (weak)	O(W-O)/W ratio
Dark/2 u	16.9	1.9	60.9	20.3	3.0	89.3	10.7	54.4	2.7	2.7
Green/3750 A	16.1	2.5	61.7	19.7	3.1	89.2	10.8	55.0	2.8	2.8
Yellow/1350 A, region 1	37.6	1.7	46.5	14.1	3.3	87.0	13.0	40.4	2.9	2.9
Yellow/1350 A, region 2	47.3	2.0	39.6	11.1	3.6					

Table 4.6 Atomic concentrations from survey scans (atom%, the uncertainty is less than 1 atom%).

The yellow film showed much higher hydrocarbon contaminations on the film. The O/W ratios for all three films were close to 3. Representative high resolution scans of the key elements include:

- Chemical bonding information both C1s and O1s showed the presence of weakly adsorbed oxygen species (mainly oxidized HC), which can be due to the air exposure
- The O1s peak position of 530.3-530.6 eV corresponds to W-O bonding.
- The O1s peak shape itself cannot tell if it is associated with WO_3 or WO_2 since they expect to have an approximately same peak position.

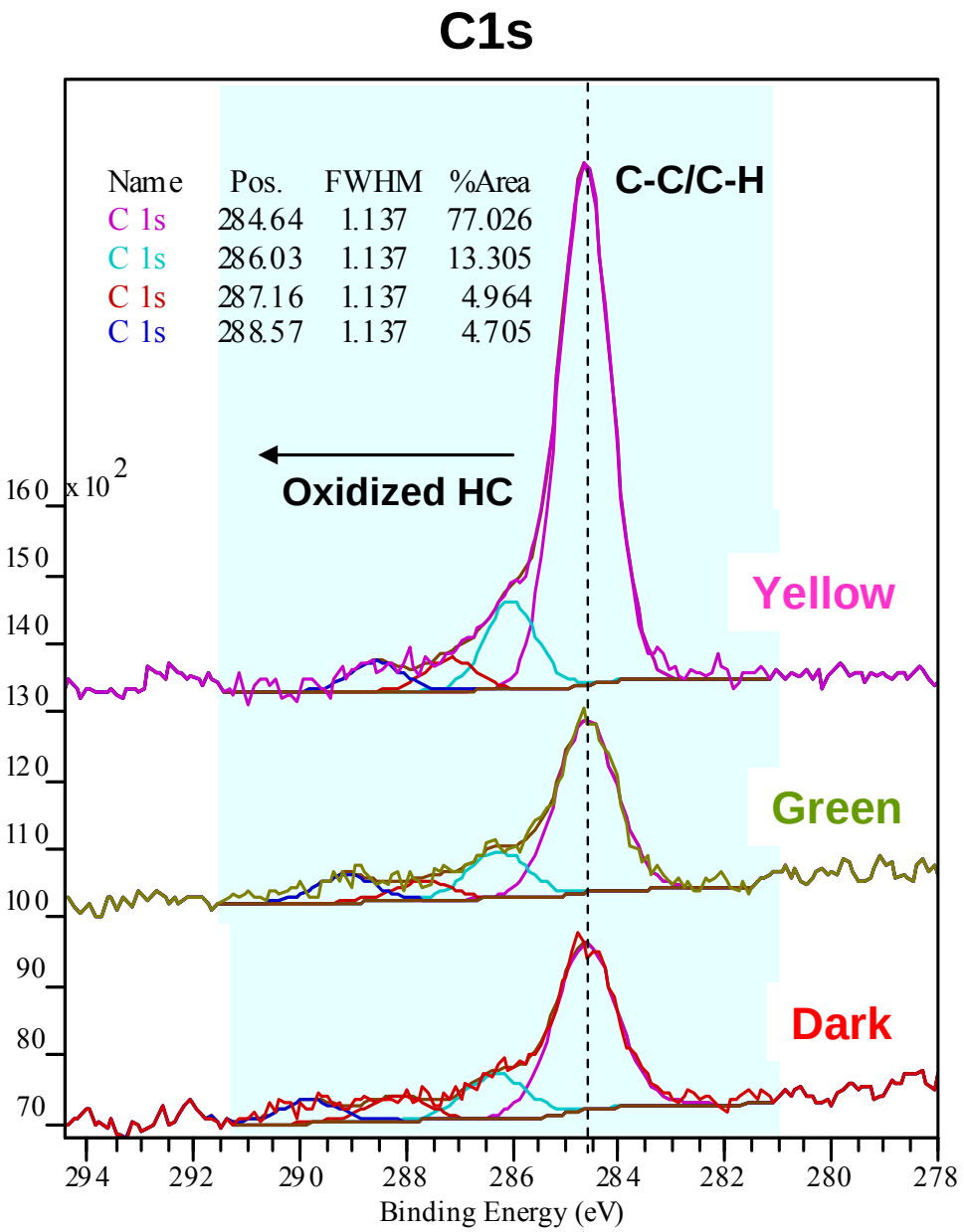

Figure 4.15. X-ray Photon Spectroscopy measurement from a WO_3 sensing material.

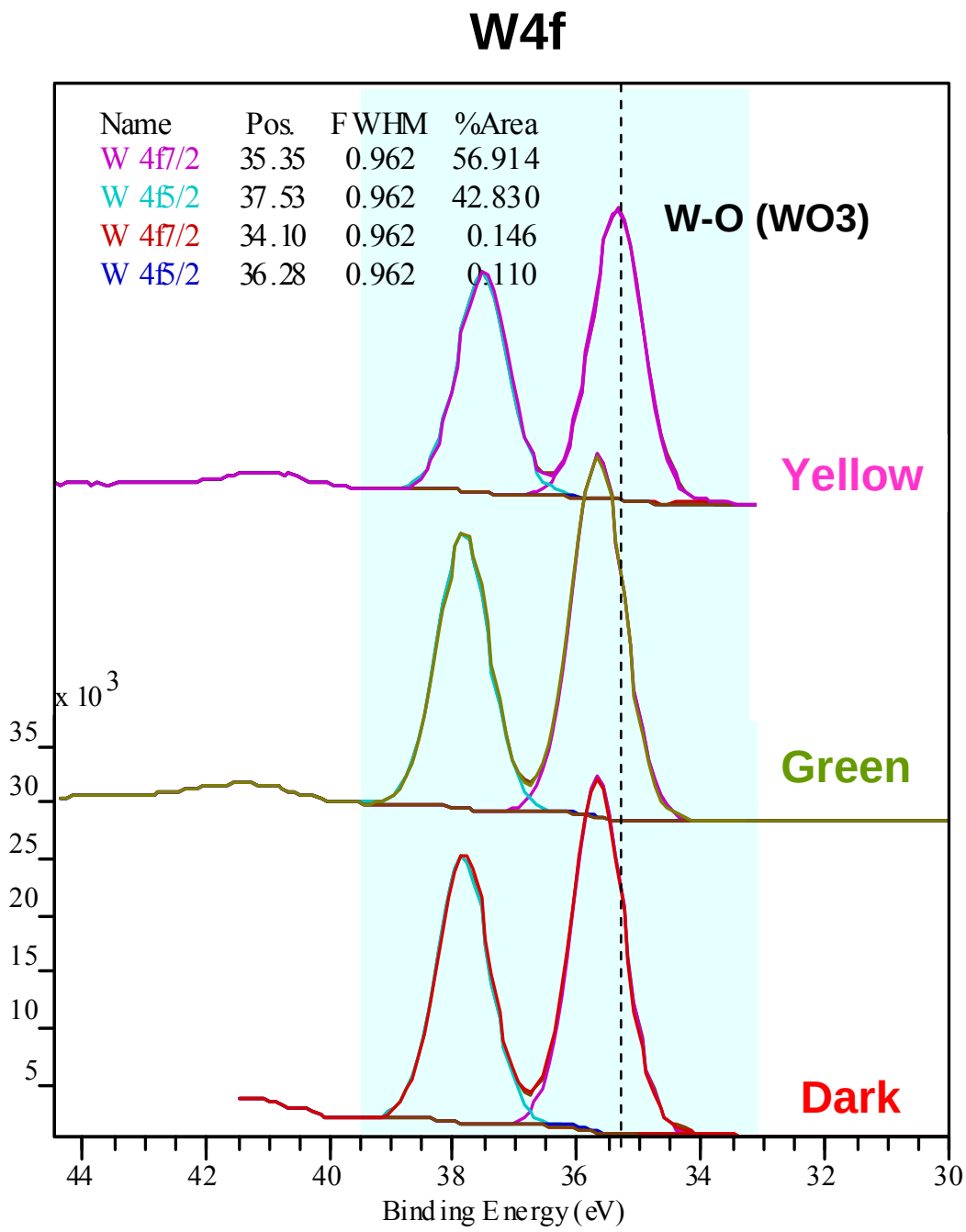

Figure 4.16. X-ray Photon Spectroscopy measurement from a WO_3 sensing material.

The peak position of 35.3-35.6 eV for W4f7/2 line is close to WO_3 species. The slightly peak shift (~0.3 eV) for both O1s and W4f core level lines can be due to the film thickness effect. As a conclusion, all three films showed the WO_3 chemistry.

CHAPTER 5: DISTRIBUTED FIBER GAS SENSING INSTRUMENTATION

The fiber-gas-sensing instrumentation used in this program is based on wavelength-division-multiplexing technology, where the fiber gratings are fundamental sensing elements. Two kinds of fiber gratings were integrated as a fiber gas sensing device or modulus. Fiber Bragg grating (FBG) and fiber long-period grating (LPG) based fiber gas sensors offer a number of unique advantages over alternative fiber gas sensors due to their wavelength-encoded nature. These sensor can be inscribed along a single fiber length, creating quasi-distributed FBG, LPG or FBG/LPG hybrid sensing arrays, which can be multiplexed in the wavelength, frequency, time, and spatial domains.

A number of methods were demonstrated to determine the measurand-induced wavelength shift from both FBG and LPG sensors. These include edge filters, holograms, Fabry-Perot tunable filters, matched receiving gratings, and interferometry. The basic principle of a Fabry-Perot tunable filter demodulation system is to “scan” over the wavelength by changing the spacing of two mirrors. Once the spectral peak from the grating is detected, its wavelength is determined by the spacing of the mirrors. Fabry-Perot tunable filter systems are capable of handling multiple fiber gratings and can operate at a bandwidth of 1000 Hz, which is commercially available from Micron Optics. The second signal interrogation system is an optical spectrum analyzer (OSA), commercially-available from Agilent, with a scanning rate of a few Hz . In addition, fiber gratings can be demodulated by ratiometric approaches involving chirped fiber gratings or Mach-Zehnder/Michelson interferometers.

In general, such demodulation or signal interrogation systems use a broadband source, typically 5–110 nm, to illuminate multiple FBGs, LPGs, or several arrays. The reflected or transmitted signals are interrogated by either flight-of-time or wavelength/frequency methods. Such schemes have been widely investigated and a number of successful field and application trials have been demonstrated. However, fiber-gas sensing instruments are mainly comprised of three critical parts. The first is signal interrogation method, which is either intensity based or

wavelength based. The second part is a sensing device that can be FBG, LPG, or a hybrid-sensing modulus. The third part is the data-acquisition-related software and hardware. Descriptions of each part are given in the following paragraphs, and at the end, a distributed fiber gas sensing instrumentation system is shown.

5.1. Wavelength-division-multiplexing technology based fiber-sensing system

The fiber gas sensing systems, as shown in Figure 5.1, are based on a tunable laser with the range from 1510 nm to 1590 nm. The light is sent to a fiber gas sensor or sensing arrays by an optical coupler. Experimental setups for both the reflection and transmission measurements, where one FBG is for real-time temperature monitoring, the second FBG and one LPG are a

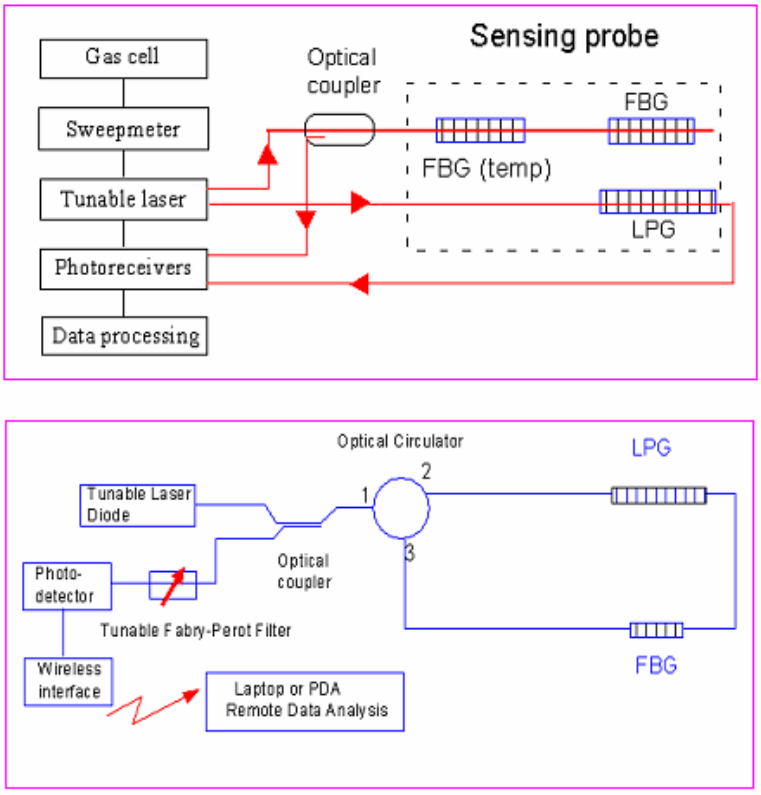

Figure 5.1. Schematic illustrating wavelength-division-multiplexing based fiber gas sensor interrogation technique. The sensing device could be FBGs, LPGs or hybrid FBG/LPG sensing modulus. Left is three grating-based sensing module, right is hybrid FBG/LPG integrated sensing module.

sensing modulus, could be used for simultaneous combustible gas or fossil fuel gas sensing. It should be pointed out that the hybrid sensing modulus provides a greater advantage than a single

LPG sensing device because a hybrid FBG/LPG device could provide strain-free and temperature-corrected gas sensing at elevated temperatures. The sensing probe could be one fiber with several fiber gratings along its axis. It is also feasible to have multiple fibers with one fiber grating for each fiber.

Figure 5.2 illustrates a fiber-grating based signal interrogation system and its software interface. A fiber-optic sensor could be a FBG, LPG, or hybrid FGB/LPG. This instrumentation has been successfully used for harsh environment temperatures and strain sensing at GE Energy for coal gasification and gas turbine exhaust temperature profile mapping. One of the signal demodulation units is an optical interrogator from Micron Optics (model # sm125) that can be operated at either 1Hz or at 5Hz. The other optical interrogator can be used for dynamic sensing with a bandwidth of 250 Hz, 500 Hz, 1000 Hz, and 500 kHz. A fiber laser, with a power of less than 1 mW and a wavelength tunable range from 1510 nm to 1590 nm, was connected to the sensing fiber through fiber-optic coupler. The scanned wavelength, with a rate of 150 nm/s, is precisely calibrated with a gas cell. The system resolution was 0.4 pm for FBG-based sensing and 25 pm for LPG-based sensing. A tracking algorithm for transmission-dip and reflected peak was used to record the time-dependent chemical sensing process. The measured data were analyzed by customized Labview based software interface.

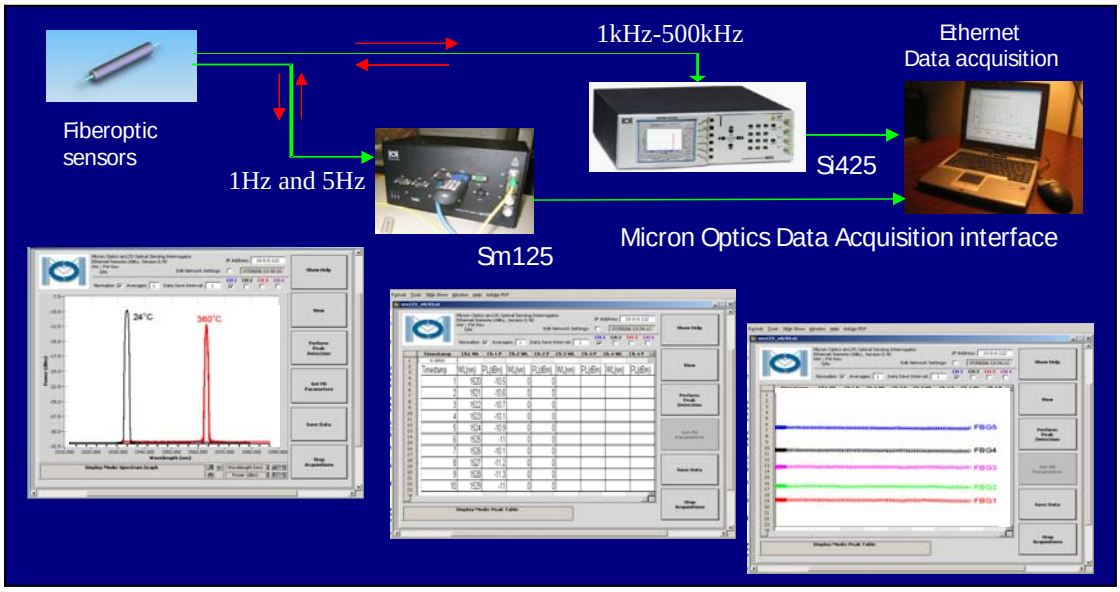

Figure 5.2. Schematic illustrating fiber gas sensor interrogation system used in current program. The fiber sensor could be FBGs, LPGs or hybrid FBG/LPG, and the sensing signal is shown by customized Labview software to detect sensor wavelength and reflectance/transmittance loss simultaneously.

5.2. Fiber gas sensing devices

5.2.1. Two-fiber-gratings-based sensing modulus

A fiber gas sensing system is comprised mainly of a sensing system (described above), fiber gas sensor or sensing modulus, data acquisition hardware, and data analysis software and algorithms. With a gas delivery system, test chamber, chamber temperature heating elements, and controls, the fiber gas sensor can be evaluated either at elevated temperatures or at various gases concentrations.

The fiber sensor can be a single fiber grating, either a FBG or a LPG, or combination of both. As shown in Figure 5.3, a fiber sensing modulus may be comprised of two short-period Bragg gratings or a hybrid FBG and LPG combination. Usually, a FBG is used for temperature measurement so that the thermal effect on the LPG wavelength shift can be corrected. On the other hand, a FBG can also be coated with a sensing material, and the function of the FBG is mainly to correct both the temperature and strain on the LPG wavelength shift. It is possible for a bared fiber Bragg grating to detect aqueous chemicals, however, fiber Bragg gratings normally have no sensitivity to fossil fuel gases because the evanescent field is confined inside the fiber core and cladding interface. Since the forward propagating cladding modes induced evanescent field is located at the cladding/air interface, a LPG shows a certain sensitivity to external mediums, which experience refractive index changes. Such a sensing modulus of two fiber gratings is the fundamental fiber gas sensing element, but it does not provide gas sensitivity using either a FBG or an LPG. This is because the refractive index of any fossil fuel gas is almost 1, very similar to that of air, which makes it difficult to use a bared LPG for gas sensing. Meanwhile, a bared fiber long-period grating has no selectivity to identify chemicals even though it can show strong refractive index variation sensitivity.

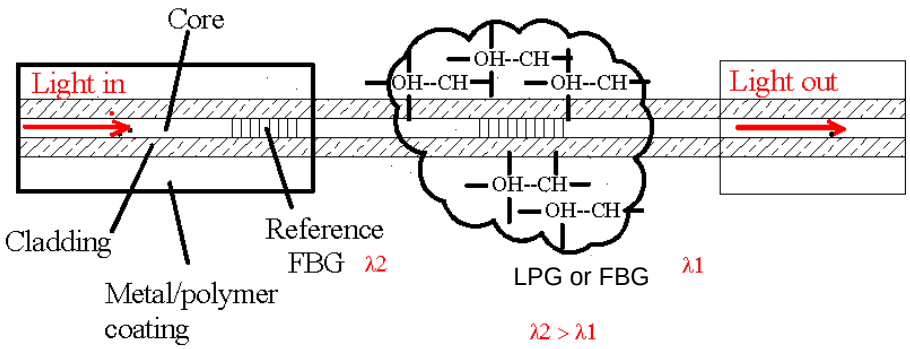

Figure 5.3. Fiber LPG or Bragg-grating-based sensing method with wavelength-division-multiplexing technology, where the reference FBG is for temperature correction.

Figure 5.4 shows the typical fiber gas sensor spectra from such a two-fiber-grating-based sensing modulus. The two-FBG-based sensing modulus can be setup in a reflection mode so that only two Bragg resonant peaks are detected, as shown in Figure 5.4 (a). The first FBG_1 is used for reference, and FBG_2 should be coated with sensing material so that it can respond to external gas interactions. Although it is very difficult to functionalize a FBG and make it highly sensitive to any combustible gas according to external medium refractive index change, it is possible to realize gas sensing by using the strain effect of some sensing materials. The typical example is that of Palladium, which interacts with hydrogen to form hydrides by accompanying a lattice expansion up to 3.5%. Such a lattice expansion induced strain effect could introduce FBG_2 wavelength shift.

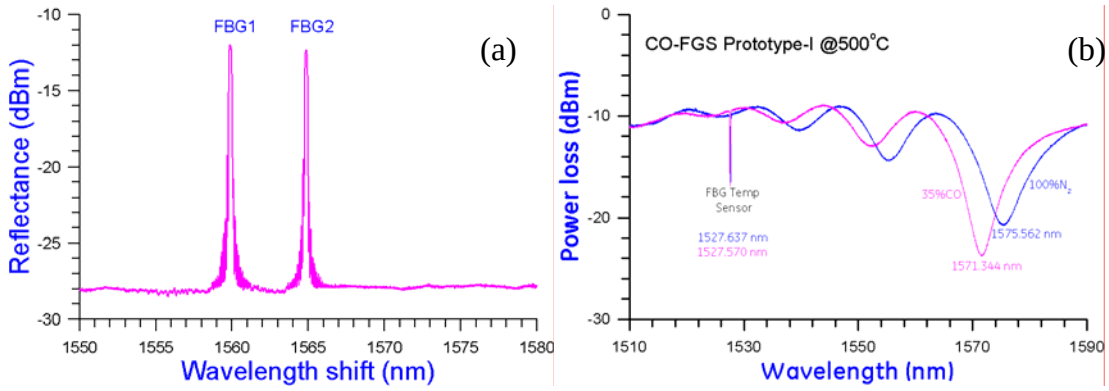

Figure 5.4. The typical fiber gas sensor spectra from (a) a sensing modulus of two FBGs, and from (b) a sensing modulus with a hybrid FBG/LPG.

Figure 5.4 (b) corresponds to a sensing modulus or fiber gas sensor (FGS) with a hybrid FBG/LPG. The sensing-material-functionalized LPG provides a gas selective response for refractive index change. If the sensing material also induces a strain effect on the LPG wavelength, the reference FBG should be also coated with the same sensing material. As shown in this sensing modulus, the FBG wavelength can differ from the LPG LP_{01} mode wavelength. The data corresponds to a test with 35% carbon monoxide at 500ºC.

5.2.2. Three-fiber-gratings-based sensing modulus

Compared with a two-fiber-gratings-based sensing modulus, the following three fiber-grating-based sensing modulus could provide more benefits for constructing distributed sensing instrumentation. The design of the three fiber-gratings is explained in Figure 5.5.

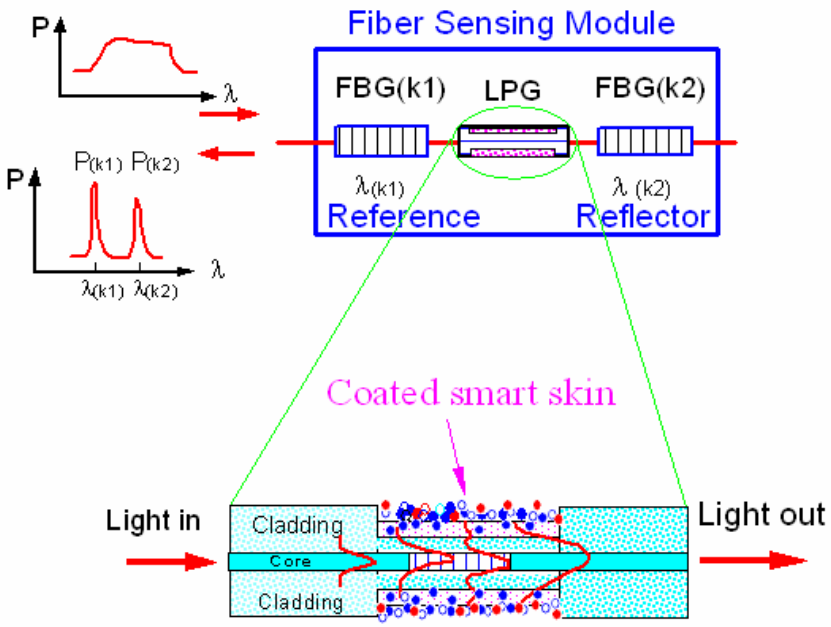

Figure 5.5 Three fiber-gratings based sensing modulus for fossil fuel gas sensing. The sensing element is based on a LPG with coated sensing material or "smart skin" around the fiber grating cladding. The first FBG provide temperature reference, and second FBG provide a broadband reflection for reflectance based sensing.

The sensing element is based on a LPG with coated sensing material or smart skin around the fiber-grating cladding. The first FBG provides the initial signal power reference and the second FBG provides a broadband reflection for reflectance-based sensing.

When the sensing light source is sent from FBG_1 to FBG_2, the reflected signal will pass the LPG twice. The transmission loss from the LPG will effectively reduce the reflected power so that the reflected power loss ratio from two FBGs can be used for combustible gas sensing. The central wavelength of the FBG_1 should be far away from the transmission LP_{01} mode wavelength, while that of FBG_2 could be at the same wavelength as LPG's LP_{01} mode for maximum sensitivity or response amplitude. Figure 5.6 shows the test results from one of the fiber hydrogen gas sensors or sensing module, where the first FBG_1 is represented by the color green, FBG_2 by blue, and the LPG by pink. The reflected power from FBG_2 at either N_2 or H_2 status shows at least 2.5 dB difference.

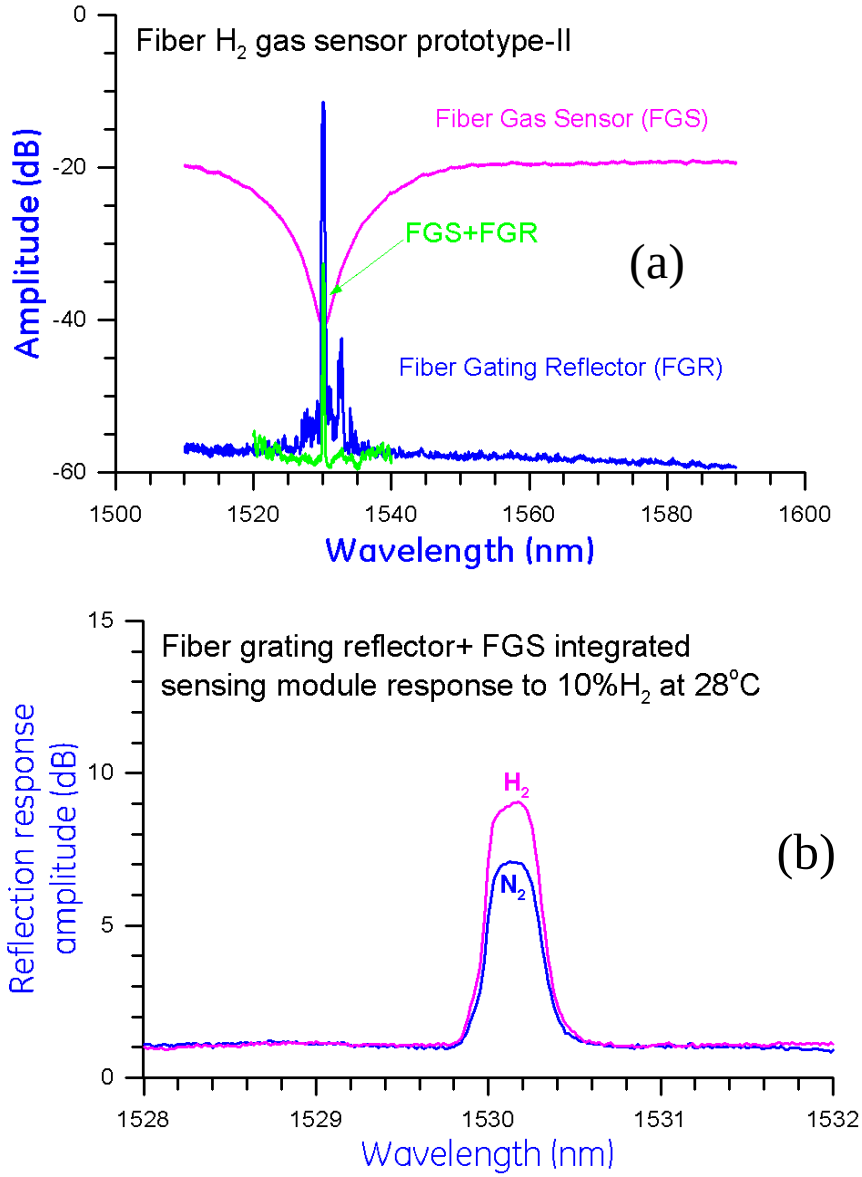

Figure 5.6 (a) The central wavelengths of the LPG, FBG1 and FBG2 in one of three-fiber-grating based sensing module, where the "Green" corresponds to FBG1, "Blue" to FBG_2, and "Pink" to LPG; and (b) the reflected power variation to N_2 and 10%H_2 gas at 28°C.

The advantage of this sensing modulus lies in the convenience of sensing in either a transmission mode configuration or in a reflection mode configuration. In the transmission mode configuration, the two FBGs are used as references for temperature correction and the sensing-material-functionalized LPG will detect fossil fuel gases by its LP_{01} mode wavelength shift and transmission loss. Obviously, the transmission-mode-based sensing configuration is similar to the two-fiber-grating-based sensing modulus and there is no advantage to using one more FBG. However, this sensing modulus shows great benefit when it is operated in the reflection mode configuration. In this case, the reflected power ratio, $P_2(FGB_2)/P_1(FBG_1)$ of two FBGs, is used

for gas analysis. Since two FBGs are not necessary in a harsh environment, it will be of less concern on the FBG thermal stabilization and its thermal induced reflected power variation.

Figures 5.7 and 5.8 show an example of reflection and transmission-based hydrogen gas sensing at 27ºC. The transmission loss is induced by LPG cladding modes to radiation coupling in the sensing material and the reflected power of the FBG_2 is modulated by alternative N_2/H_2 gas cycling. The observed power loss amplitude is about 2.5 dB to 10% hydrogen, blended with N_2 gas. In the transmission mode, the LPG wavelength response has also been recorded during these tests, as shown in Figure 5.8, where the wavelength shift is over 300 pm. It was also found that these responses are consistent with each other during H_2/N_2 cycling.

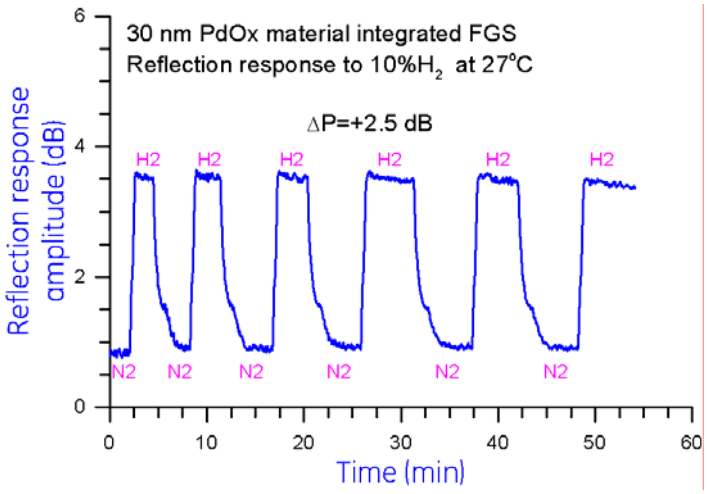

Figure 5.7. Measured reflectance variation from a FBG_2's reflectance during a cycling test with 10% H_2 gas, blended with N_2 gas at 27ºC.

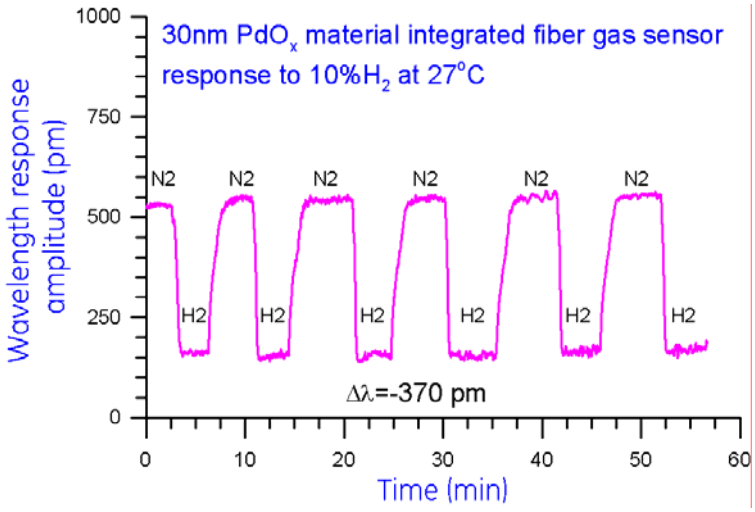

Figure 5.8. Measured wavelength response from LPG in the transmission mode configuration during a cycling test with 10% H_2 gas, blended with N_2 gas at 27°C.

The sensing modulus presented in Figure 5.5 could overcome conventional limitations found when using a LPG as a distributed-fiber-sensing instrument because several fiber-gas-sensing modulus can be multiplexed or cascaded in one fiber cable. If each LP_{01} mode linewidth is less than 10 nm, every fiber cable can carry at least six FGS for the distributed sensing application. With the current 4-channel Micron Optics sm125 optical interrogator unit, 24 fiber gas sensors can be easily deployed within its 80 nm tunable range.

An additional advantage of this sensing modulus design lies in the moderate requirement for LPG sensor quality. As a clear design, the central wavelength of the LPG should be 5-8 nm greater than 1510 nm, or should be 5-10 nm smaller than 1590 nm. In this design strategy, a LPG can have large dynamic range of operation. Furthermore, the requirement for the LPG linewidth seems to be of less concern, typically for single fossil fuel gas sensing. When designed for multiple fiber gas sensors in one fiber cable, all LPGs should be separated by at least 10 nm to avoid any interference and to achieve better transmission peaks tracking.

5.2.3. Fiber grating modulation profile engineering

To make a fossil-fuel-gas-sensitive fiber-gas sensor or sensing modulus, except for its device design with different grating combination, a fiber grating modulation profile engineering is needed. Such an engineering process actually maximizes the guiding mode energy coupling to the cladding mode and thereby enhances the evanescent field at the cladding and sensing material interface. Apodization is a conventional process to eliminate side lobes, but it also enhances the guiding mode coupling with cladding modes. The fiber-grating refractive index modulation profile could be uniform type, blazed type, Gaussian or cosine apodized type, or a combination of each type. Figure 5.9 is a schematic illustration on an apodized fiber Bragg grating structure that could effectively shed guiding modes energy into cladding regions. Such a grating profile can be apodized multiple times so that more guiding modes can be coupled into cladding.

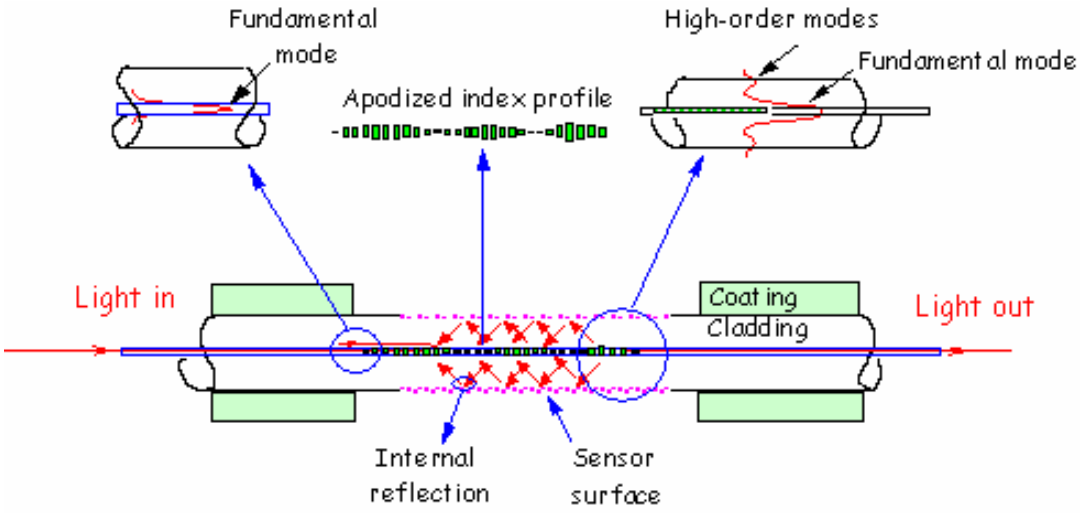

Figure 5.9. Schematic illustration of apodized fiber Bragg grating structure.

The grating-modulation profile can be realized by using a fabrication method with two titled laser beams to get a grating apodized either with a Gaussian or cosine profile. Figure 5.10 shows four types of grating structures that can be used to enhance the LPG evanescent field energy distribution at the fiber grating cladding and sensing material interface. Type I is a commercially-available uniform LPG and the remainder of the types are customized grating structures that can greatly enhance the guiding mode to cladding modes coupling.

Figure 5.10. Four types of fiber long period grating structures.

Based on the engineered-fiber-grating structures, one can construct six types of fiber gas sensing modules or FGS that combine both FBG and LPG as combustible gas sensing devices. The uniform LPG is a conventional LPG, which is used mainly in telecom devices. Its sensitivity is limited because a telecom device does not need to shed the guiding mode to cladding that causes transmission loss. Three additional engineered gratings require customized design and

fabrication processes and it has been verified that they have relatively higher sensitivities than uniform LPGs.

Figure 5.11 further summarizes the six types of fiber gas sensors and sensing modules that are a combination of FBGs and LPGs, each with different refractive index modulation profiles. The LPG has been functionalized with a layer of sensing material. The sensing material around the LPG could be sensitive and selective to either hydrogen or carbon monoxide. A detailed discussion of the sensing materials can be found in Chapters 4 and 6.

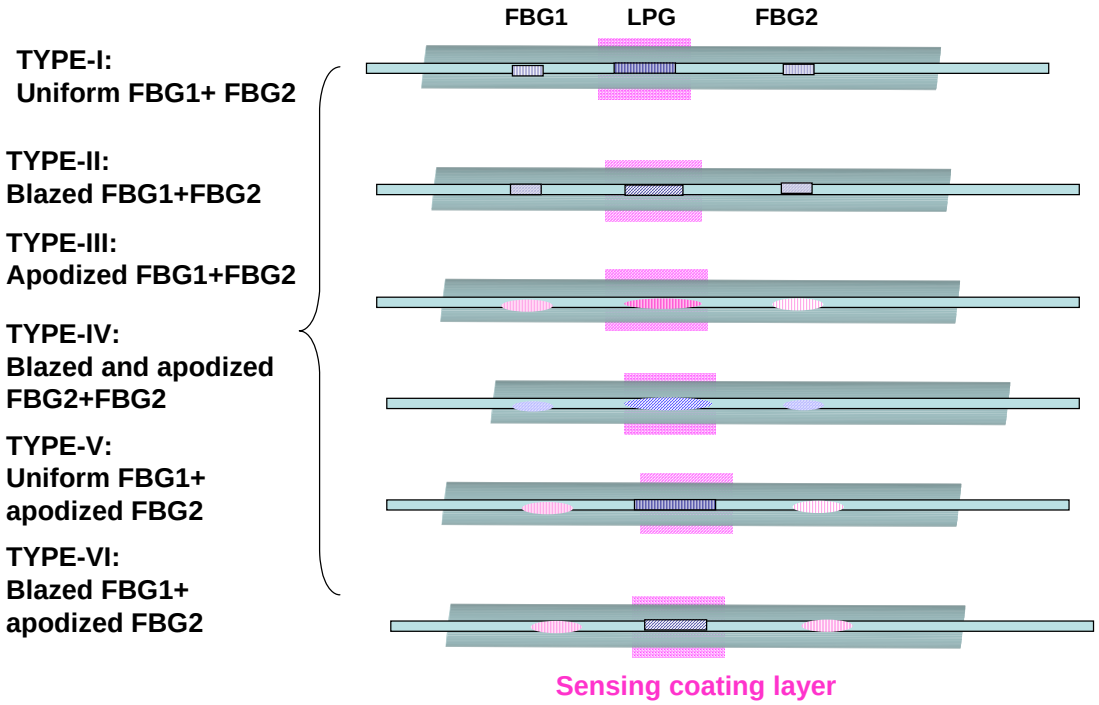

Figure 5.11. Six types of fiber gas sensing modulus or fiber gas sensors.

5.3. Fiber-gas-sensing instrumentation

5.3.1. Transmission-based distributed sensing system

Figure 5.12 illustrates the wavelength-division-multiplexing-based fiber-gas sensor interrogation technique. As discussed in previous sections, a sensing device can be made of FBGs, LPGs, or a combination of FBGs and LPGs. Figure 5.12 shows that the fiber-gas-sensing modulus designed during this program can be integrated with lasers, and a signal detection system as a fiber gas sensing instrument that consists of interrogating system, gas mixing system, testing chamber, and fiber sensor. The fiber sensing cable, which contains the LPG for gas sensing and the FBG for temperature monitoring, is located in the gas chamber.

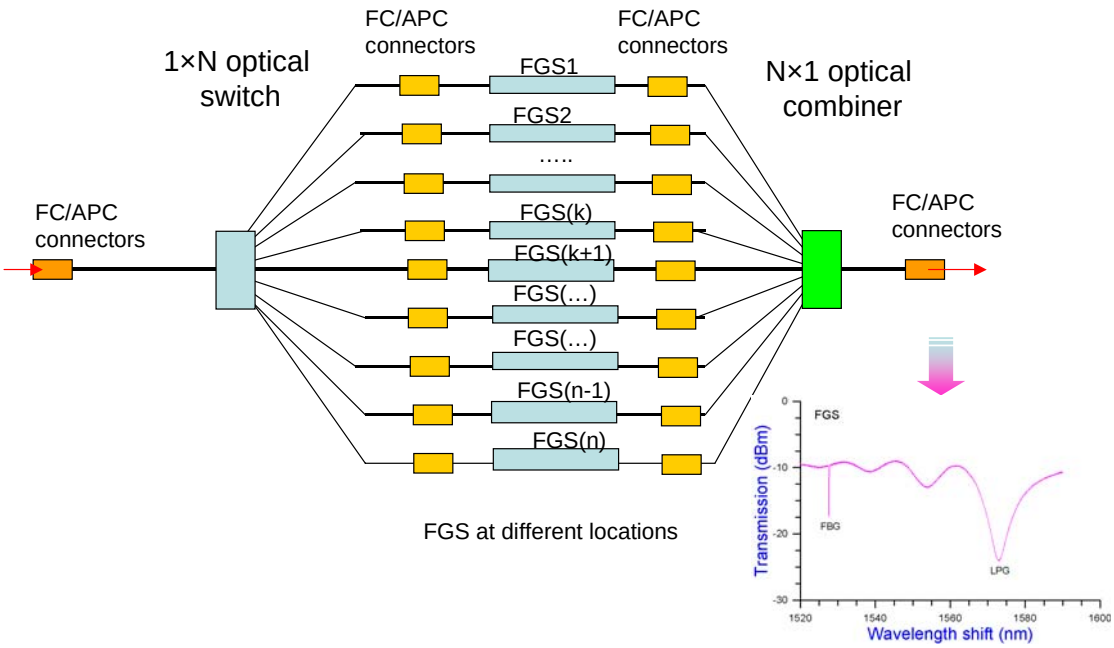

Figure 5.12 The transmission configuration based fiber gas sensing instrumentation for multiple gases or multiple location gas detection. Each fiber gas sensor (FGS) could be one of sensing modulus designed from Figure 5.9.

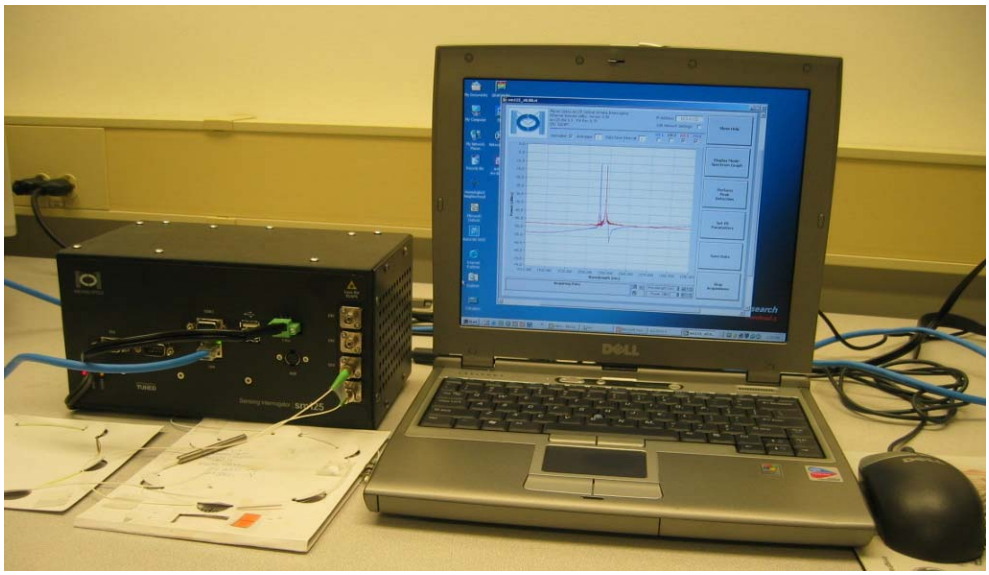

Figure 5.13 Four channel optical interrogator unit from Micron Optics that has 80-nm bandwidth, ±1pm accuracy for wavelength shift, and 0.5pm repeatability.

Figure 5.12 shows further integrated multiple fiber-gas sensors for distributed sensing applications. Each sensing module can be coupled with an optical switch to optical interrogator. The fiber is connected to the optical interrogator through an optical circulator, therefore, a tunable laser beam from the laser source can go through the fiber and return to the photodetector. Gas species are controlled by the multi-gas mixing system when they enter the testing chamber.

The optical interrogator unit is a real fiber-gas-sensing instrument that can carry a few tens of gas sensors, as shown in Figure 5.13. This 4-channel interrogator unit has 80 nm bandwidth, ±1 pm accuracy for wavelength shift, and 0.5 pm repeatability. Customized software with peak detection algorithm was developed for fiber gas sensor signal detection and analysis.

If four 1×16 optical switches are used, the above interrogator can handle 64 fiber gas sensors, which would form a distributed fiber gas sensing system for multi-parameter sensing or multi-location sensing applications.

5.3.2. Reflection-based distributed sensing system

A transmission-based fiber sensing system is often limited by either the LPG linewidth, the interrogator bandwidth, or both. To overcome this issue, Figure 5.14 shows a refection-based fiber-gas sensing system design that uses optical splitter or coupler to deliver laser light to each fiber-gas-sensing module or FGS. The sensing signal is analyzed by tracking the reflectance ratio of Bragg resonant peaks from each FGS.

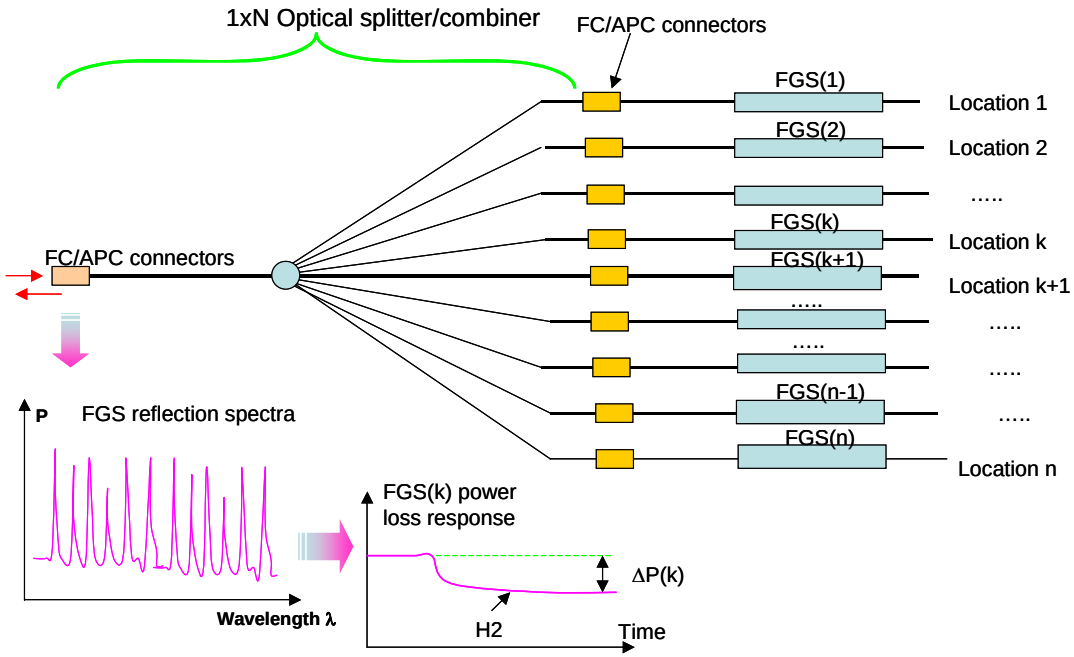

Figure 5.14. Reflection configuration based fiber gas sensing instrumentation for multiple gases or multiple location gas detections. Each FGS could be one of sensing modulus designed from Figure 5.9.

The advantage of this distributed sensing instrumentation lies in its simple multiplexing capability. Any number of the fiber gas sensors can be added or dropped out of the sensing system. Moreover, any number of FGS can be replaced without interrupting the sensing system's operation. In addition, if each FGS is functionalized with different sensing materials, the individual sensing module could be configured separately as gas sensors, temperature sensors, strain sensors, or different gas sensors.

Summary: This chapter has given a detailed description of the gas-sensing module, the sensing system design, and preliminary results from these fiber-gas sensors. A fiber-optic distributed fossil fuel gas sensing instrumentation system is comprised of three sub-systems, namely: the sensing module, laser and signal interrogation system, and software. The distributed sensing system can be configured either in transmission mode or in a reflection mode. The designed sensing instrumentation was demonstrated by the data presented in this chapter and in next chapter.

CHAPTER 6: FIBER GAS SENSOR PROTOTYPE EVALUATIONS

A fiber-gas sensor is an integration of fiber grating and sensing material using either a sol-gel-based dipping/spin coating or magnetron sputtering method. The merit of a sol-gel produced material is that it contains a porous microstructure so that gas molecules can easily diffuse into the sensing film. This porous microstructure also provides the flexibility to allow for other material doping and co-doping in order to form a porous dielectric structure with selective response characteristics for a specific chemical or gas. At the same time, the sol-gel film's refractive index can be easily modified to match that of the fiber cladding for high-sensitivity performance. Magnetron sputtering is a conventional thin film deposition technique that is used mainly for metal oxide sensing materials. The low deposition rate of the sensing material makes it much easier to control the thickness of the sensing layer during depositing on a fiber-grating cladding surface. The sensing material compositions can be controlled either with a target that has certain alloy constituents or an alternative co-sputtering method of 1-3 target materials.

Sensing materials developed from both deposition techniques were evaluated in this program. The first evaluation was carried out by optical reflectance measurement (Figure 6.1(a)). Since such a reflectance measurement can be conducted easily from a thin film that is deposited on a quartz or silicon substrate. Experiments have demonstrated that this is a quick screening method that can be used on an as-grown or post-thermal-treated material to measure its response

to certain gases, such as hydrogen and carbon monoxide. After conducting this material property screening, the best sensing material was selected in order to fabricate FGS prototypes. Next, the FGS prototypes were evaluated at elevated temperatures and a gas concentration from 1-75% for hydrogen and 1-35% carbon monoxide. The FGS instrumentation had a transmission-based configuration (Figure 6.1(b)). The FGS prototype was composed of several elements: a gas sensing device, which is an integration of an apodized LPG and a thin layer of sensing material; and a short-period Bragg grating, which could be coated with the same sensing material or without coating. The second fiber-grating element was used for simultaneous temperature and/or strain monitoring, which can be used as a correction factor for the first fiber sensing element. As shown in Figure 6.1(b), the Bragg grating can be inscribed either on the same LPG fiber or on another fiber closed to the first.

6.1. Fiber gas sensor based on sol-gel sensing film

The initial tests were conducted on the sol-gel thin films coated on glass substrates, instead of LPG fiber sensors. A fiber-optic reflection probe was utilized during these tests as indicated in Figure 6.1(a).

6.1.1. Temperature response of TEOS-based sensing film

An H_2 test was conducted on one of the TEOS-based sensing films (Film ID: K335-6, 10.545% Pd nano-particle doped TEOS, thickness ~100 μm) made from a sol-gel process on a glass substrate over a wide range of temperatures (25ºC to 525ºC). The relative responses to 5% H_2 gases are summarized in the plots in Figure 6.2 and 6.3.

Relative reflectance response vs. temperature—The relative reflectance response, which is the quotient of the change of signal to the signal level, is plotted in Figure 6.2. The signal was evaluated by averaging the faster change signals. Results show that within the temperature range where the film is capable of sensing, hydrogen sensitivity increases with temperature. This indicates that the reflectance or refractive index of this film increases with temperature.

Response time vs. temperature—When the TEOS-sensing material was exposed to H_2 at different temperatures, the reflectance signal took to stabilize. The response time is plotted in Figure 6.3. Results show that within the temperature where the film is capable of sensing, the higher the temperature, the shorter the response time. This is consistent with the increasing chemical reaction rate at elevated temperatures.

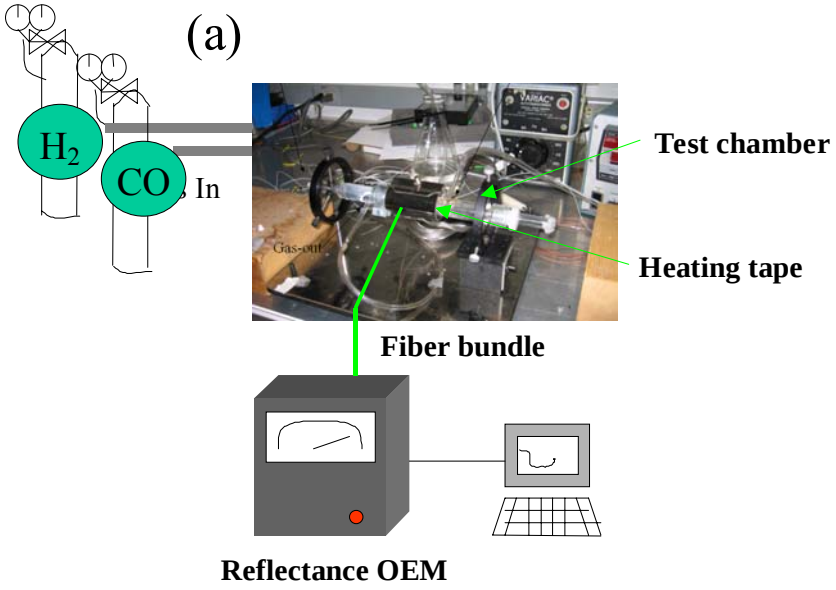

Figure 6.1(a). Optical reflectance based setup for sensing film material quick screening tests.

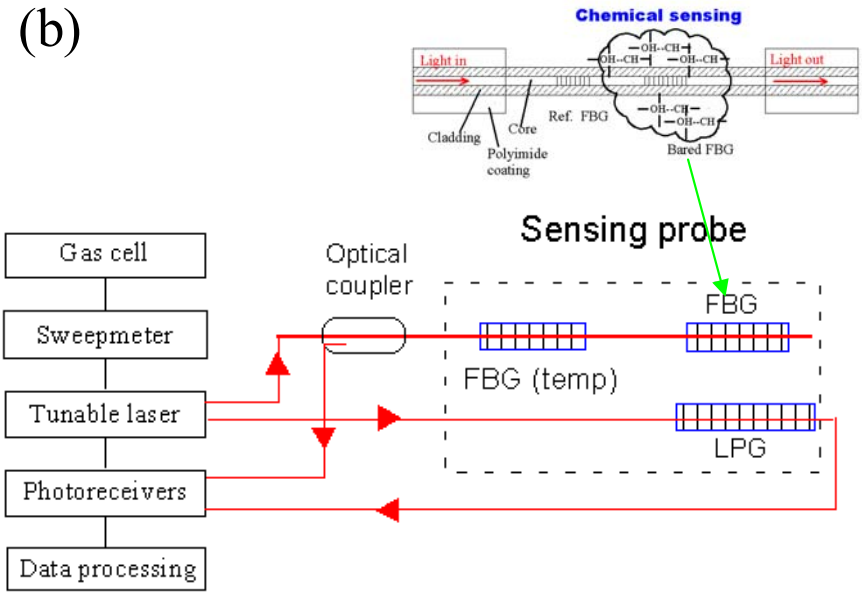

Figure 6.1(b). The diagram of wavelength-division-multiplexing (WDM) technology based fiber gas sensor evaluation setup.

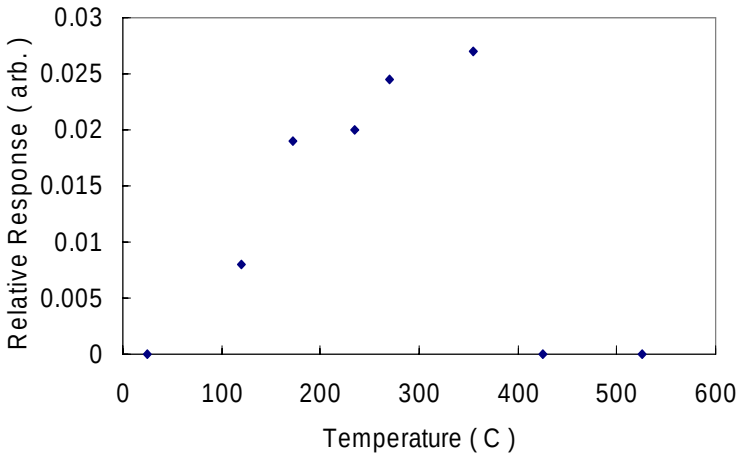

Figure 6.2. Film relative refractive index change-induced reflectance variation as a function of temperature, measured with optical reflectance setup from Film ID#K335-6, 10.545% Pd nano-particle doped TEOS film with a thickness of ~100 μm.

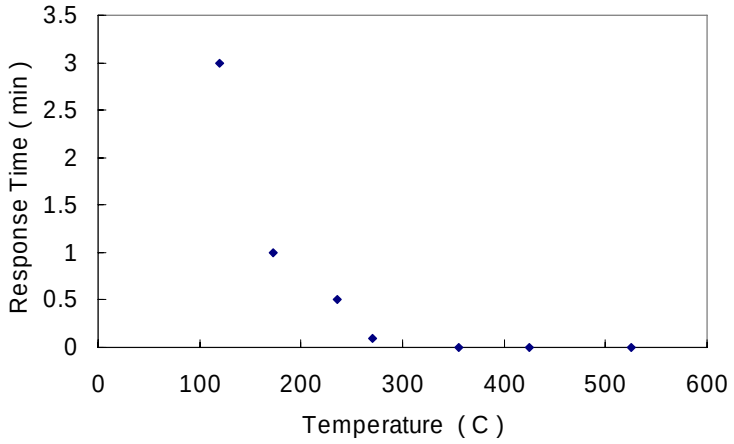

Figure 6.3. Response time to H_2 at different temperatures, from Film ID# K335-6, 10.545% Pd nano-particle doped TEOS film with a thickness of ~100 μm.

6.1.2. H2 responses of Pd-SiO2 sensing material

Figure 6.4 illustrates the reflectance response of the Pd-SiO_2 based sensing film, fabricated with the TEOS based sol-gel process at elevated temperatures ranging from ambient temperature to 525ºC. During the tests, N_2 and 5% H_2 (blended with 95% N_2) were introduced to the test chamber alternatively.

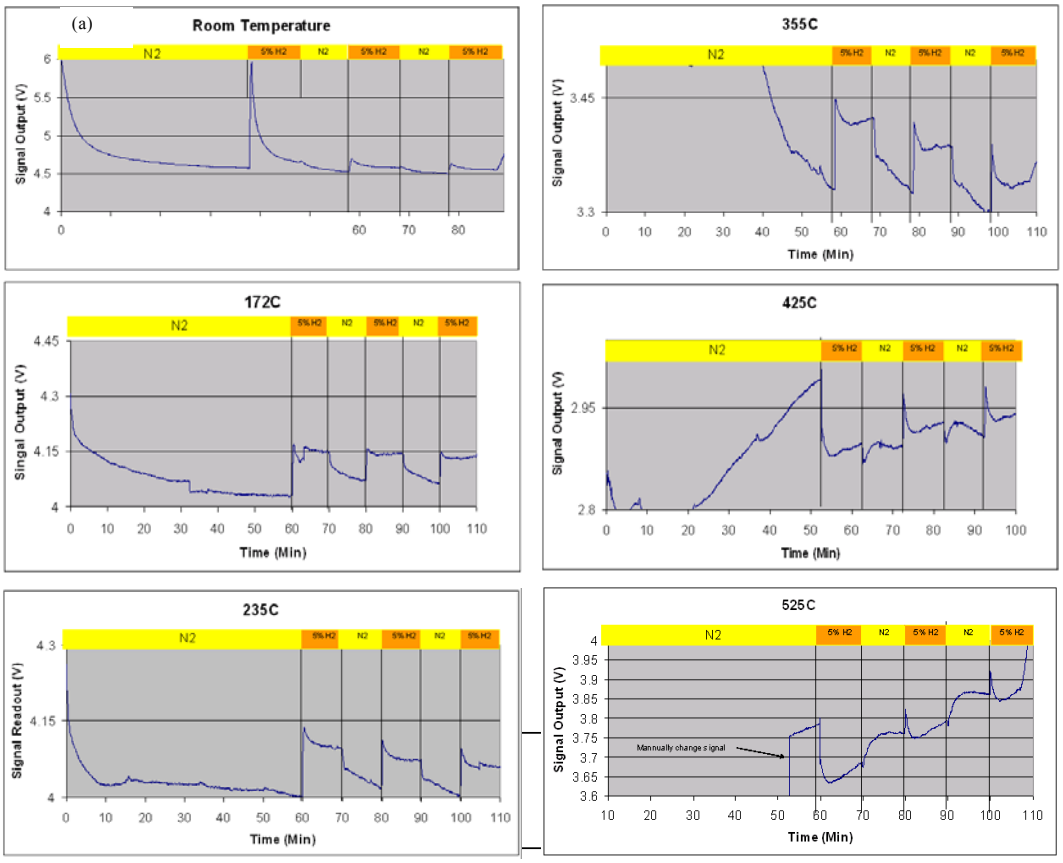

Figure 6.4. Measured optical reflectance response at 5% H_2 at different temperatures, from Film ID:#K335-6, 10.545% Pd nano-particle doped TEOS film with a thickness of ~100μm.

At low temperature, a weak response was found in the optical reflection test. There was a spike at low temperature when the H_2 was introduced to the system for the first time. This can be explained by the different effects that H_2 and H induce on the sensing film's surface. H_2 has a more dominant effect on the reflectivity of the sensing film than H. As H_2 was first introduced to the film, a large signal response was produced by the index difference at lower temperature. The adsorbed H_2 gradually disassembled into H, which reduced the sensing film's response to H_2. Later, the adsorbed H occupied the surface with sufficient bonding so that it could not be easily washed out by N_2. As a result, less H_2 was absorbed to the film.

For medium temperatures from 170 to 355ºC, the sample demonstrated a good response to H_2. As temperature increased, the response time began to decrease, but the signal had a larger drift over time. The faster change at higher temperature could come from the chemsorption process, while the slower signal drifting could come from the diffusion process in the porous structure of the film. For elevated temperatures from 400~525ºC, no sufficient optical reflection response was observed.

6.1.3. CO responses of low-Pd doped SnO_2 sensing material

A CO gas test was performed on one of the TEOS-based sensing films made from a sol-gel process on glass substrate over a wide range of temperatures (25-525ºC). First, a blank film with glass only was tested to baseline the optical reflection probe in the high-temperature gas chamber. The baseline was used to calibrate any variation in the test condition, such as mechanical, local temperature gradient, and vibration, that might be caused by temperature changes. After the baseline data was obtained, tests were conducted on alloy-based and sol-gel based films both with similar contents (SiO_2 80% SnO_2 15% Pd 5%) over a wide temperature range (25~525ºC). An optical probe was placed inside the gas chamber. Optical reflection was observed with TEOS-based Pd-doped films at elevated temperatures from 280ºC ~ 525ºC. The measured optical reflectance responses are shown in Figure 6.5.

Although the sputtered film with the same material composition (80% SiO_2, 15% SnO_2, and 5% Pd) shows reflection at room temperature, no optical reflection was observed for the TEOS-based sol-gel film with a similar composition. The test results at room temperature of a sol-gel film (SiO_2, SnO_2, Pd) are shown in Figure 6.5(a). While temperature increased to above 325ºC, we started to see significant responses to CO gases. The following two plots (Figures 6.5(b) and Figure 6.5(c)) show the test results at 425ºC and 525ºC, respectively.

At 525ºC, a series of much more detailed experiments were conducted for this sol-gel film. Different concentrations of CO were introduced to the gas chamber to examine the responsiveness of the sol-gel thin film. The concentration of the CO was changed from 1% to 5%, and the responsiveness of the sol-gel sensing film did change accordingly. At first, three cycles of N_2 and 5% CO were introduced to the chamber. For the first two cycles, the sensing film demonstrated similar responses, with a sharp drop and rise in the magnitude of 0.25 V. However, for the third cycle, a rather slow response from the thin film was observed, which indicated that saturation occurred within the sol-gel film. A closer look showed that even in the second cycle some slow response was observed during the time frame of 130~140 min. Later, when the concentration of H_2 was reduced, the reflection signal came back. For the last two cycles (1%, 2%, and 3%), the sol-gel film showed a non-linear response; the largest response was observed when the CO concentration exceeded 1%.

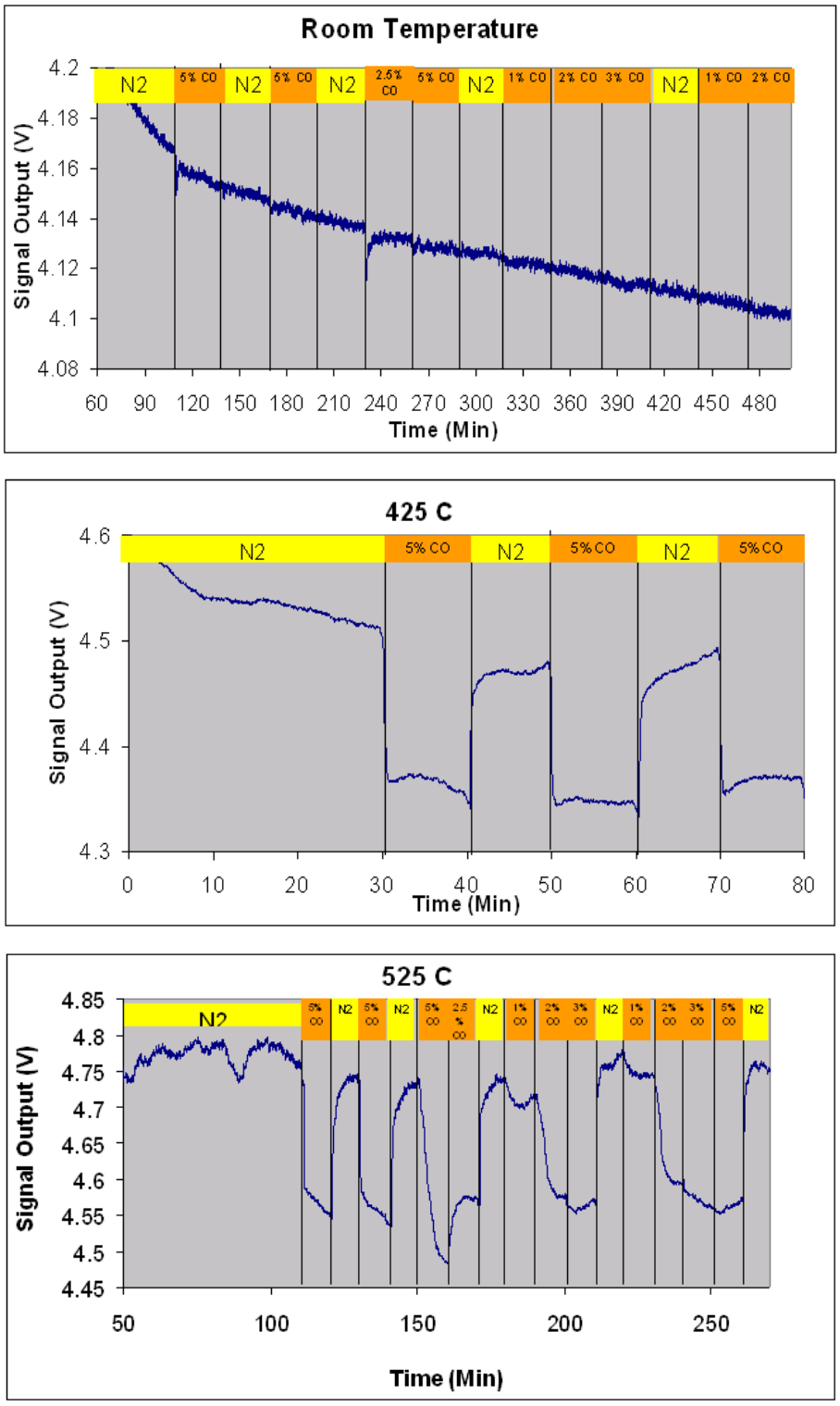

Figure 6.5. Optical reflectance measured from Pd doped SnO_2 TEOS film at elevated temperatures.

6.1.4. CO responses of high-Pd doped SnO2 sensing material

In another sample, TEOS with 10.5% Pd was tested for CO detection. Even at 280ºC, as is shown in Figure 6.6(a), there was no obvious response from this sensing film. However, at 525ºC, distinct and consistent responses were observed, as shown in Figure 6.6(b).

Comparing this film with the previous sol-gel film ((80% SiO_2, 15 SnO_2, and 5% Pd), it was seen that by changing the sensing component within the sol gel, the temperature range where the sensing film had better performance could be shifted.

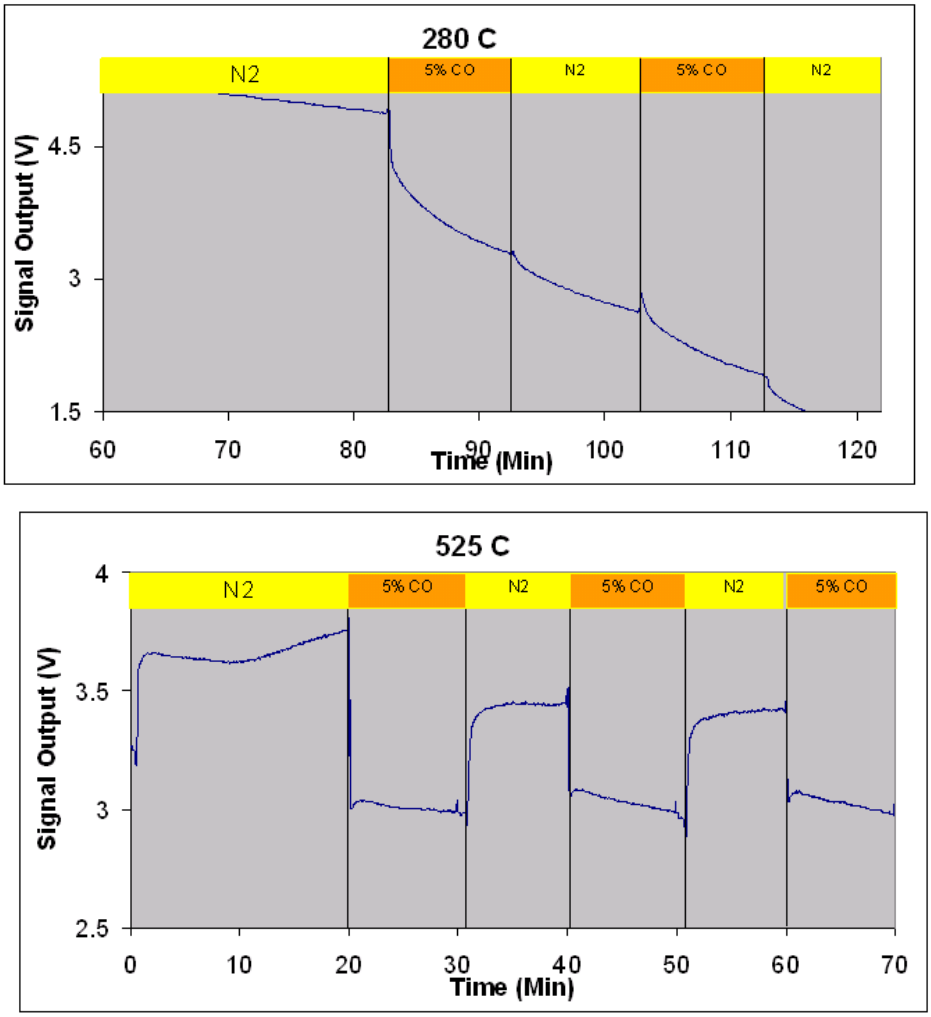

Figure 6.6. Optical reflectance measured from a sol-gel film (10.5% Pd) with alternative nitrogen and 5% carbon monoxide at a) 280°C, and b) 525°C.

6.1.5. Discussion: temperature response of sol-gel sensing film

When a sol-gel porous thin film was used for gas sensing, two types of adsorption were recognized to contribute to its response to gases, namely physical adsorption and chemical adsorption, or chemisorption. The physical adsorption takes place if the gas molecules are attached to the sol-gel porous surface by Van Der Waals forces; the chemisorption by forces similar to those involved in chemical combination.

Physical adsorption takes place very rapidly at all temperatures and the process is reversible. Adsorption is an exothermic process and the heat released per mole of adsorption is called the heat of adsorption. The adsorbate is removed in a chemically unchanged condition when the pressure is low. The relatively small heat of adsorption, about 5 kcal per mole of adsorbate or less, is on the same order as heat from vaporization. The gases that can be easily liquefied are more readily adsorbed, and the forces involved in adsorption are the same as those in condensation, which are van der Waalse forces.

Chemisorption, on the other hand, is characterized by a release of much more heat than than with physical adsorption, on the order of 20~100 kcal/mole. The rate of adsorption often increases rapidly with temperature, indicating a process that involves activation energy. At low temperatures, chemisorption may be so slow that only physical adsorption is observed experimentally. As the temperature increases, chemisorption will begin to accelerate when the adsorbed molecules acquire sufficient energy to chemically interact with the surface. This behavior is observed with hydrogen on nickel powder. Chemisorption is often irreversible and the adsorbed molecules are difficult to remove merely by reducing pressure. When decorporation does take place it may be accompanied by chemical changes. For example, when oxygen is adsorbed on charcoal, carbon monoxide and carbon dioxide will come out with a strong release of heat.

Figure 6.7 shows the energy barrier of the physical adsorption and chemisorption processes. In physical adsorption, multi-molecular layers of adsorbed gas occur at temperatures below the critical temperature and at pressures approaching the liquid saturation vapor pressure. Both physical adsorption and chemisorption could change the sensing film's surface reflectivity. The plot in Figure 6.8 shows a diagram for general physical adsorption, chemisorption, and the diffusion rate. It illustrates that as the activation energy increases, the reaction rate increases dramatically with the temperature. At low temperatures, physical adsorption is the dominant process for the change of reflectivity, while at higher temperatures, chemical adsorption and the diffusion process will dominate with different energy barriers between chemical bonds. By carefully choosing a material with different bond energy with CO/H_2 and the help from mass diffusion, it is possible to engineer material properties, such as surface porosity, to increase CO and H_2 interaction at high temperatures.

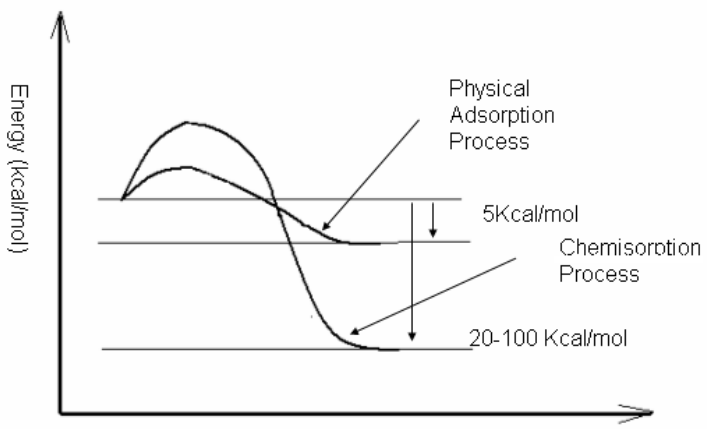

Figure 6.7. Energy barriers of physical adsorption and chemisorption processes.

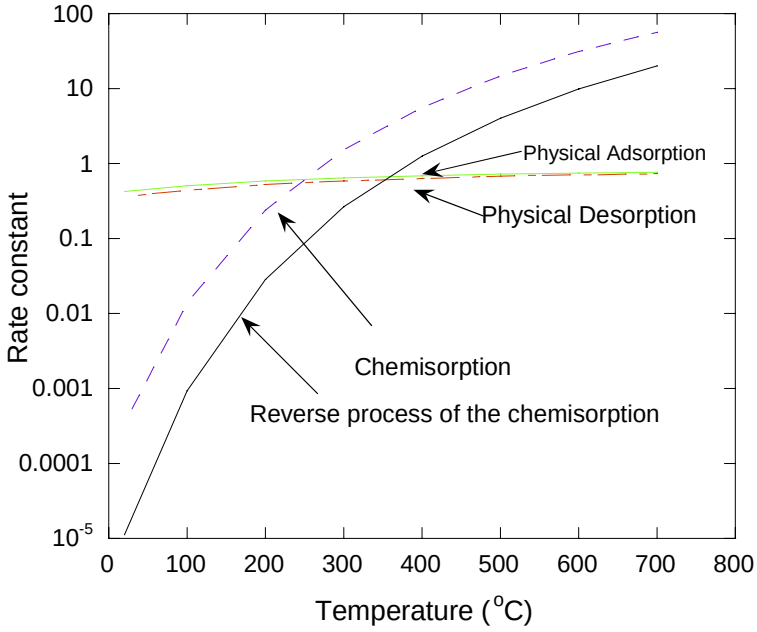

Figure 6.8. Two major processes contributing to temperature-dependent reaction rate of gases with sensing material.

6.2. Fiber gas sensor prototype post-thermal treatment

6.2.1. Sol-gel-based sensing material condensation

Unlike the optical-reflectance-based sensing material and sensor prototype evaluation, the LPG-based sensing prototype is an integration of an LPG and a sensing material. The mode coupling between the fundamental mode and high-order cladding modes make a LPG highly sensitive to external refractive index variation, since an LPG can allow the evanescent wave field to leak out of the fiber core and cladding boundary, and reach the cladding surface by guided cladding modes. When a LPG's cladding is modified or integrated with a polymeric, metallic, and semiconducting thin film material, the sensing device can be a chemical and biochemical sensor after sensing material activation and functionalization processes.

However, a FGS' functionality, especially at elevated temperatures, requires a constant wavelength response. Normally, internal thermal strain exists either between the sensing material and the fiber grating cladding, or in the sensing material. A post-thermal treatment is a crucial process that could convert the dilute TEOS film into a condensed structure. During the annealing process, both the LPG and the sensing material were subjected to thermal treatment. When the fiber-gas sensor was placed in an elevated temperature, a shift of resonant wavelength ws observed, as shown in Figure 6.9. From time 1 (beginning) to time 3 (4.5hr@250ºC), the LPG shifted 2-3 nm. This blue shift continued and eventually slowed down throughout the high-temperature test. This was mainly due to the residue TEOS material, as the original annealing process had not completed the densification of the sol-gel film. As the fiber went through high temperatures, the continuing densification introduced extra stress on the LPG, which in turn caused the LPG spectrum to blue shift in wavelength toward the shorter wavelength.

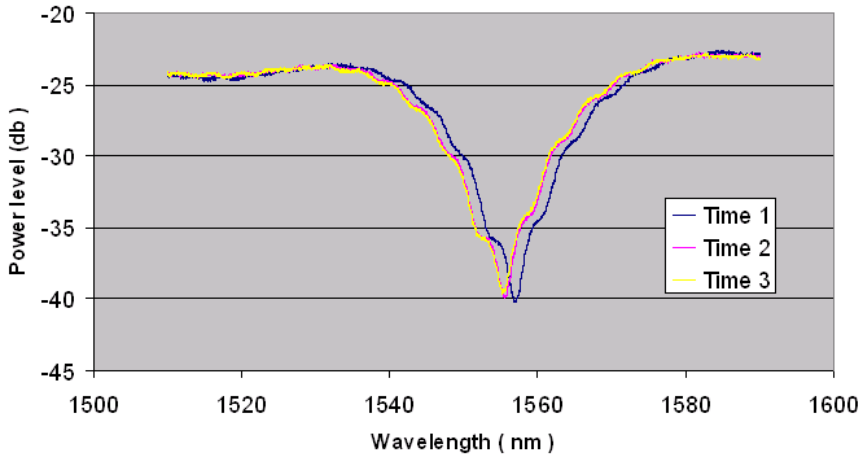

Figure 6.9. LPG spectra measured before, during and after sol-gel film annealing process. Notice the continue shift of spectrum toward shorter wavelength (blue shift) as discussed in the text.

6.2.2. Strain relief and thermal response calibration

A fiber grating may contain internal strain that would induce a wavelength down shift. A FGS response will be affected by any strain and temperature if the sensor prototype is not in a stabilized condition. A practical criterion for obtaining a strain-free and thermal-stabilized FGS is to anneal the sensor prototype with a temperature ~10% higher than its operating temperature. Figure 6.10 shows the transmission spectra difference before and after the sensing material deposition. The fiber cladding modification with palladium oxides was performed with a sputtering technique. After film deposition, the transmission loss of the sensor prototype increased about 5.7 dB with a central wavelength shift of -5.61 m full linewidth increase, as indicated in Figure 6.10(a). Figure 6.10(b) also shows the temperature response characteristics of the FGS prototype from 84ºF to 257ºF.

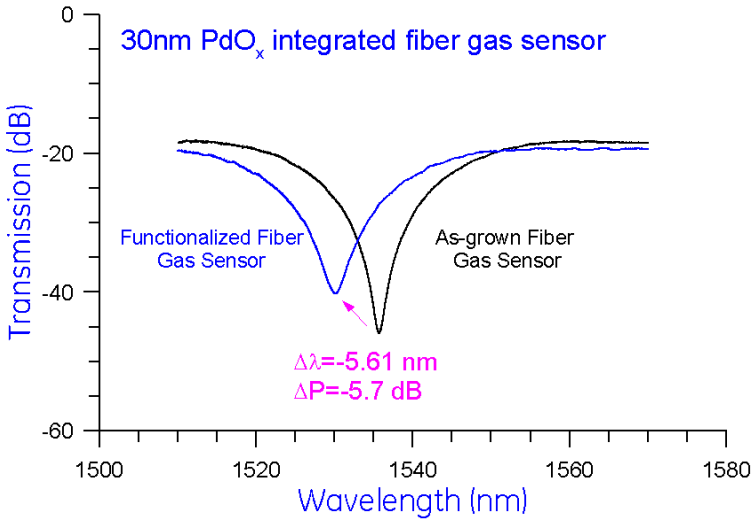

Figure 6.10(a). Transmission a fiber gas sensor prototype before and after sensing material deposition.

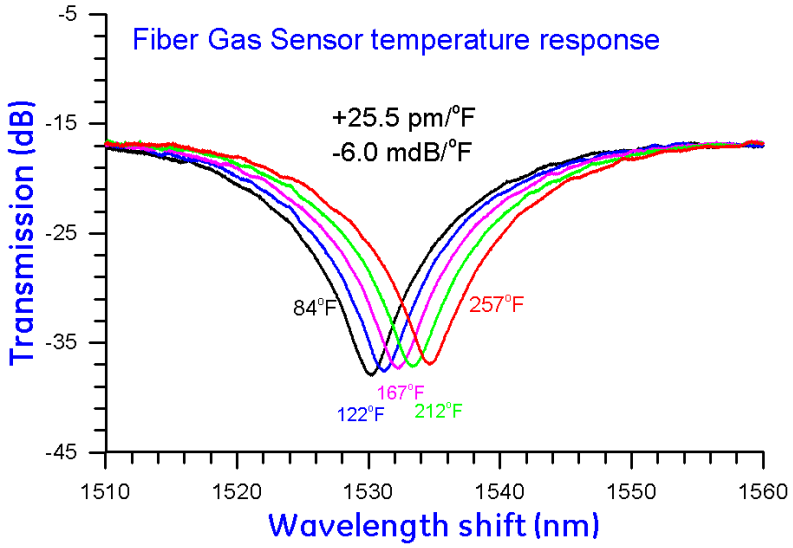

Figure 6.10(b). The temperature sensitivity of the fiber gas sensor prototype.

Figure 6.11 further plots the temperature sensitivity of a H_2 FGS prototype that is a 30nm nanocrystalline integrated LPG. Two sensitivities can be seen: 53pm/ºC and 88pm/ºC at elevated temperature. It will be pointed out later that the temperature sensitivity of the fiber-gas sensor prototype is strongly dependent upon the sensing material thickness and intrinsic stress.

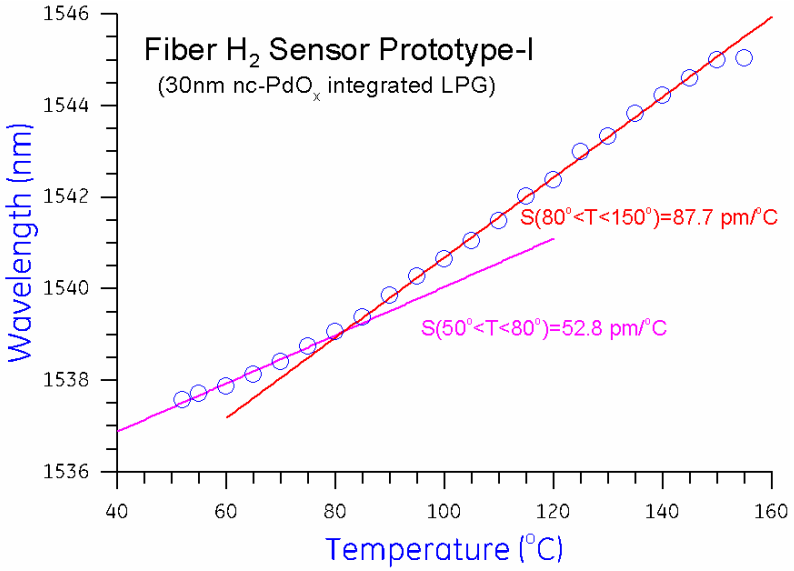

Figure 6.11 Fiber gas sensor temperature sensitivity from a prototype H_2 sensor.

6.3. Fiber-gas-sensor based on metal oxides sensing films

6.3.1. Fiber-gas-sensing method

In this section, data from the prototype FGS, which was based on metal oxides sensing material integrated into a fiber LPG, is presented. The prototype sensor is based on a fiber cladding modification by a magnetron sputtering technique. A LPG was mounted onto a frame surface and rotated 180 degrees after one side deposition was completed. The sensing film was meniscus-like shape on each side. The particle morphology of the sputtered thin films was examined by atomic force microscope, as shown in Figure 6.12, on a PdOx sensing film.

Figure 6.12 demonstrates an image from a 30 nm thick nc-PdOx sensing material surface of 1×1 μm^2. The PdOx-Au alloy sensing material shows large clusters, while the PdOx film is more or less like fine grains. The image color indicates that the size of the Pd oxide particles are about 2-5 nm for as-grown material and up to 10 nm for PdOx-Au alloy sensing materials. With these nanostructural materials, a sputtering process could be used to fabricate FGS. Figure 6.13 describes the steps from the sensing material to FGS integration.

Figure 6.14 shows how a FGS was used to perform the gas sensing process. A FGS module, consisting of a FBG and a sensing material integrated LPG, is the sensing element that must be packaged with pre-strain. The transmission peak is measured when the N_2 and H_2 is alternatively cycled. The measured wavelength shift could give such an alternative cycling characteristic as shown in Figure 6.14, bottom left. The fiber-gas response time, a time interval used for the FGS from one steady state to next steady state, can be varied by either gas concentration or temperature.

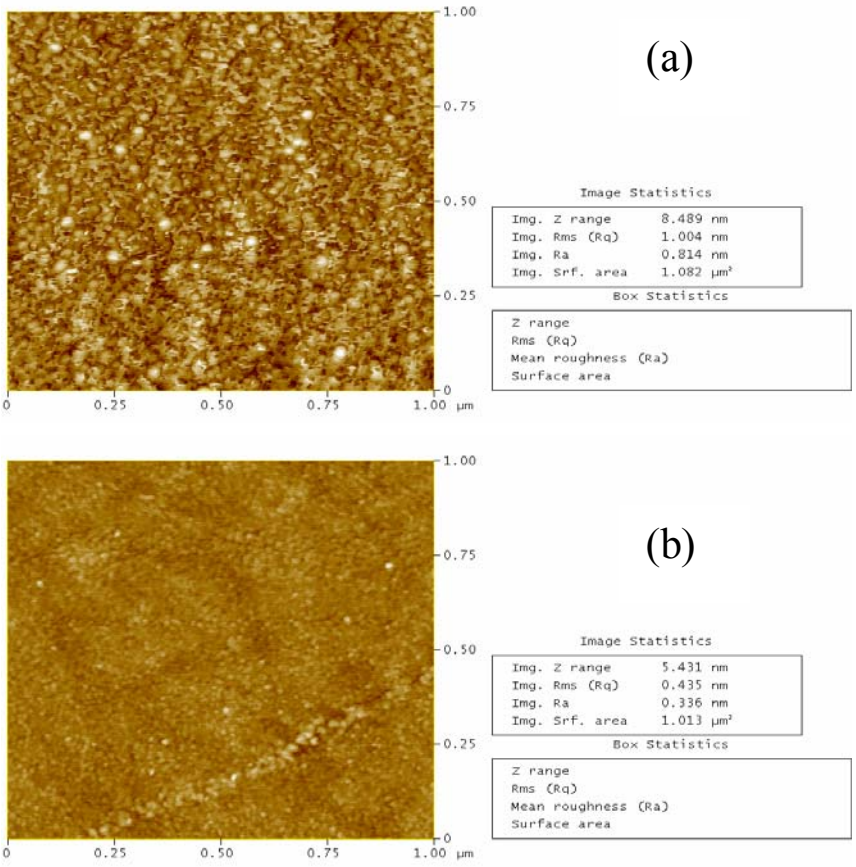

Figure 6.12. AFM images of 30nm-thick sensing materials that were used for modifying fiber-cladding surface. (a) PdOx-Au alloy film, (b) as-grown PdOx film.

FGS= Fiber grating + Gas sensitive material

AFM micrograph of H2 sensing material

Nanoparticle sensing material integration with fiber gas sensor prepared by sputtering process

Integration of sensing material and fiber long-period grating

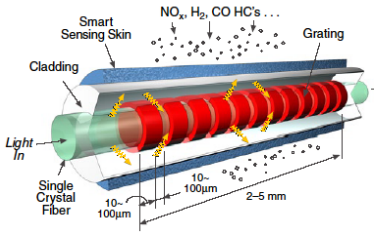

Fiber gas sensor

Figure 6.13. Fiber gas sensor integration process with a sputtering fabrication method.

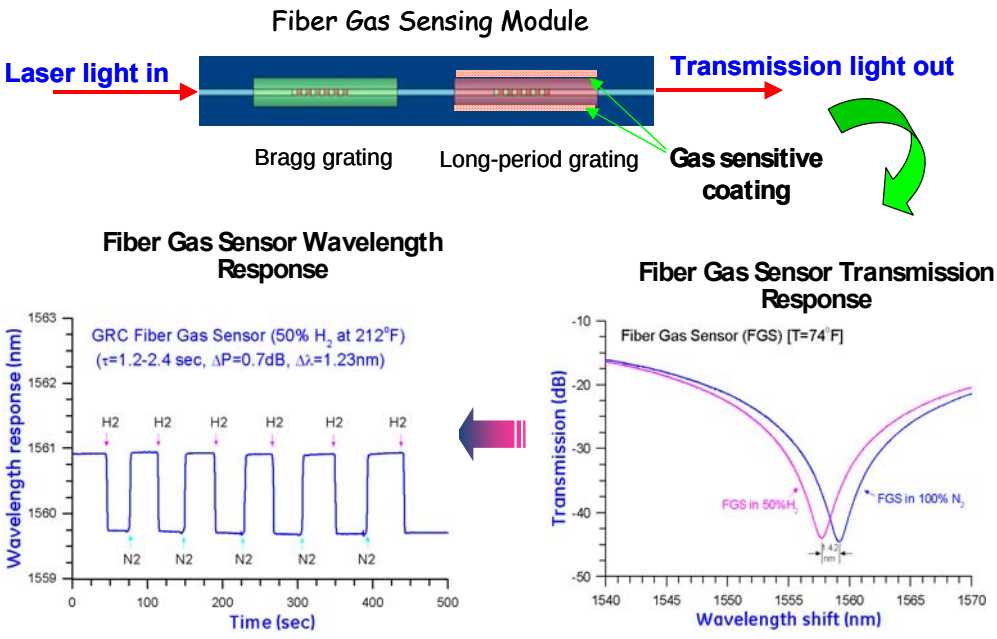

Figure 6.14 Fiber gas sensor working diagram. A fiber gas-sensing module consists of a FBG and a sensing material integrated LPG. The transmission is measured during alternative N_2 and H_2 cycling.

6.3.2. Wavelength response of prototype hydrogen fiber gas sensor

The FGS prototype was evaluated from ambient temperature to several elevated temperatures. The sensor response was first measured at different hydrogen concentrations from 1-75% H_2 blended with nitrogen gas. Figure 6.15 shows one of the hydrogen gas sensor prototypes response to different hydrogen gas concentration at both ambient and elevated temperatures. On the left panel, the hydrogen gas concentration varies from 1% to 10%, 35%, 50% and 75%, the FGS' wavelength shifted from 22 pm to 1740 pm. While the measurements were at elevated temperature, the wavelength response amplitude was reduced. The observed wavelength response amplitude was from 6 pm to 1250 pm. Such a reduction in wavelength shift means the change of the refractive index of the sensing material was reduced by temperature, in another words, the solubility of the hydrogen atoms in the sensing material was reduced by temperature. This is consistent with other published results regarding the temperature dependent hydrogen solubility and its influence on hydrogen gas sensing response.

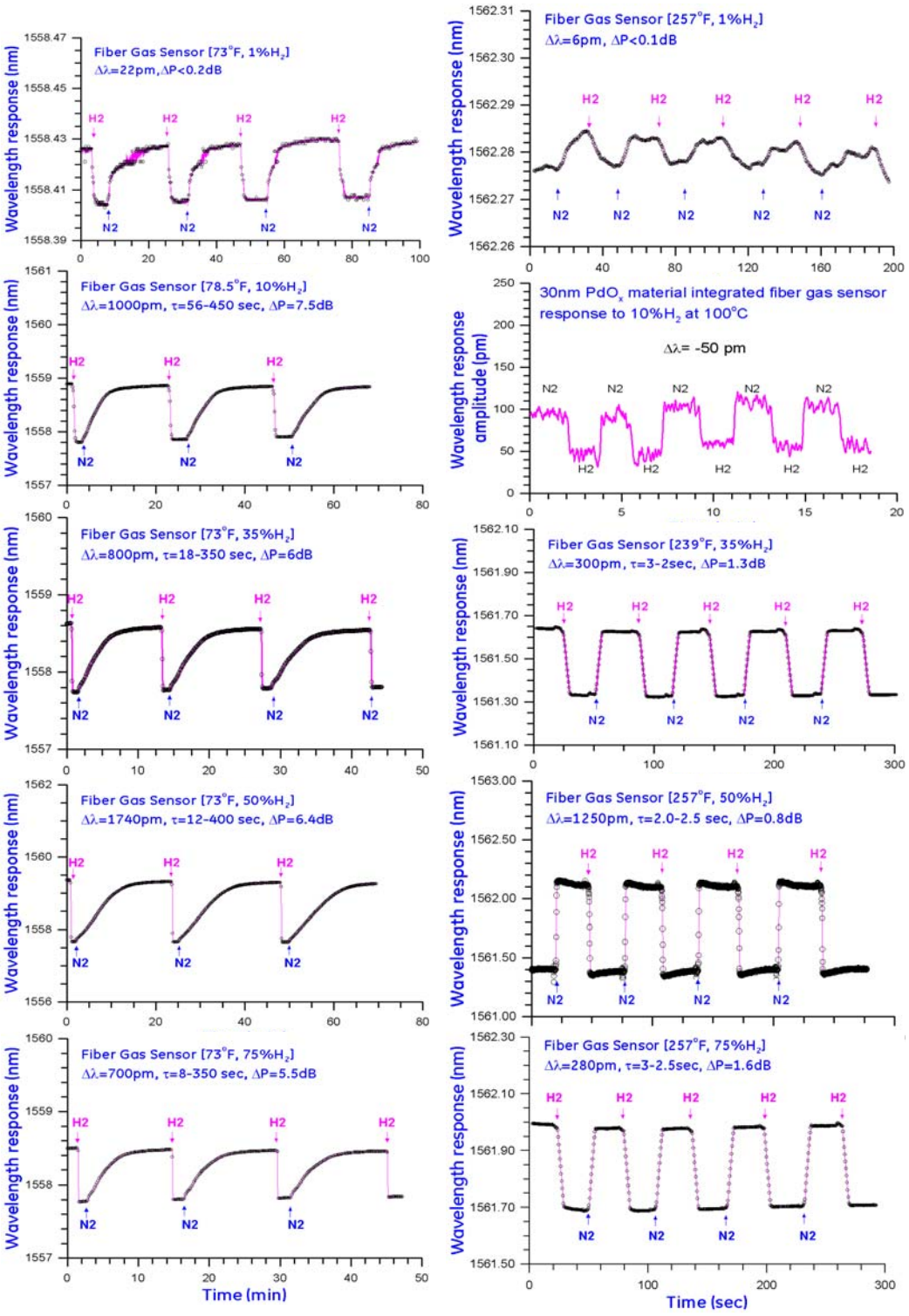

Figure 6.15. The fiber hydrogen gas sensor prototype wavelength response amplitude from ambient (left panel) to elevated temperatures (right panel). The relative changes in wavelength and transmission loss are indicated in each measurement.

6.3.3. Transmission response of H_2 fiber gas sensor prototype

Another interesting feature of the fiber hydrogen gas sensor prototype's response is its transmission variation during hydrogen gas cycling tests. Figure 6.16 displays both wavelength and transmission responses from 10% H_2 at 104ºF, and 75% H_2 at 257ºF, respectively. The comparison between wavelength and transmission response clearly demonstrates a close correlation. Hydride formation in the sensing material could increase cladding mode dissipation into the sensing material or cladding modes and radiation modes coupling so that the transmission losses increase. The recovery of the sensing status by nitrogen gas seems to clearly have decoupled the cladding modes to radiation modes.

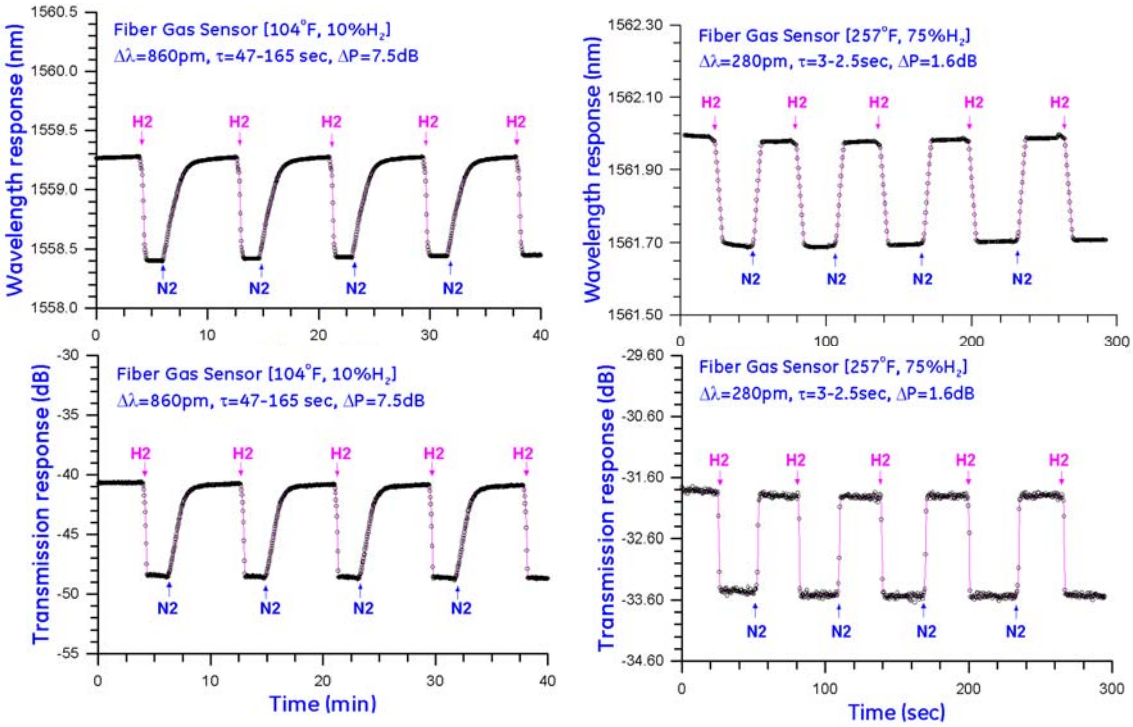

Figure 6.16 Wavelength and transmission loss response characteristics from a fiber hydrogen gas sensor prototype, measured at 10%H_2@104°F, and at 75%H_2@257°F.

The correlation between transmission response and wavelength response, observed from this study, suggests that both of the response features can be used for hydrogen gas sensing. Combining two response characteristics could help mitigate any special events that may be due to unexpected temperature surges or other uncertain factors. Experiments further verified that the transmission response has no dependence upon the temperature, but the temperature will affect the wavelength response of a FGS.

6.4. High-temperature fiber gas sensor and responses

6.4.1. Responses of fiber CO gas sensor prototype

As seen in the previous sections, the FGS prototypes could provide response signatures from both wavelength shift and transmission loss from ambient to elevated temperatures, but lower than 200ºC. In this section, the FGS prototype tests and evaluations are described.

The XPS measurements, as shown in Figure 6.17, were performed on a Kratos Axis Ultra DLD XPS system using monochromatic Al Ka radiation (1486.6 eV) at 225 W. XPS probing depth is typically 0.5-5 nm. The analysis area employed for this study was ~700×300 mm from a SnO_2 sensing material. To minimize the charging effects on the sample, a low energy electron gun was used for charge neutralization. Survey scans were performed to obtain the overall compositions, which are reported in atomic percent. The quantitative compositions of the surface species taken from survey scans were determined from the integrated intensities corrected by atomic sensitivity factors provided by the vendor. High-resolution spectra were also collected for chemical bonding information.

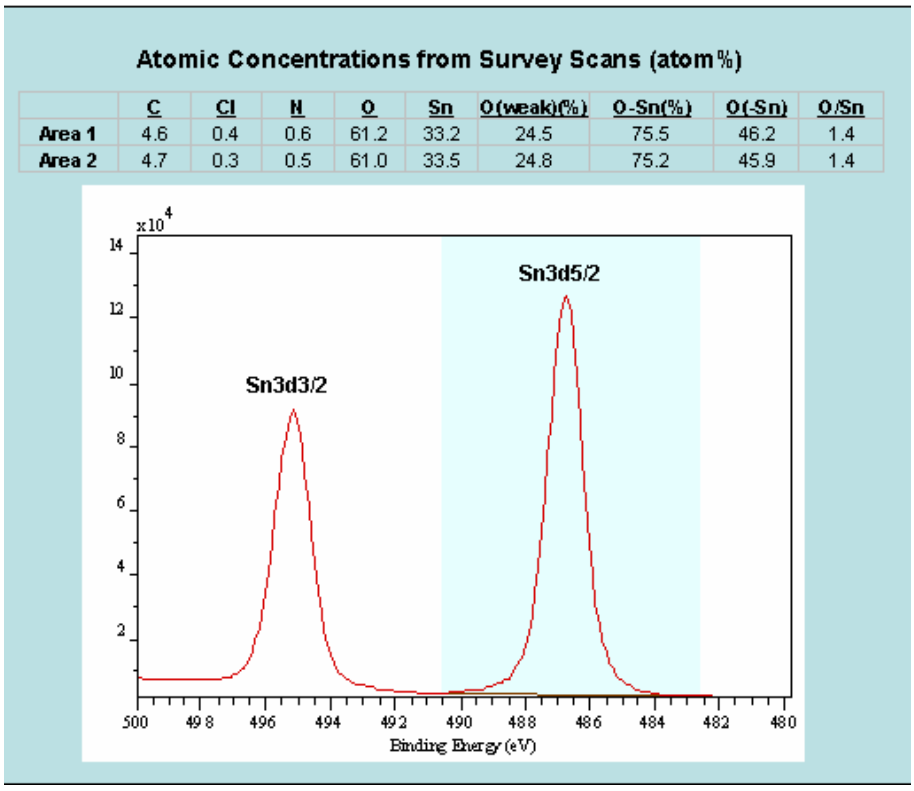

Figure 6.17. XPS measurements from a SnO_2 based carbon monoxide sensing material to analyze the O/Sn ratio from the composition table. The binding energy scales of all the core-level spectra have been charge-corrected to C(1s) signal for the hydrocarbon at 284.6 eV.

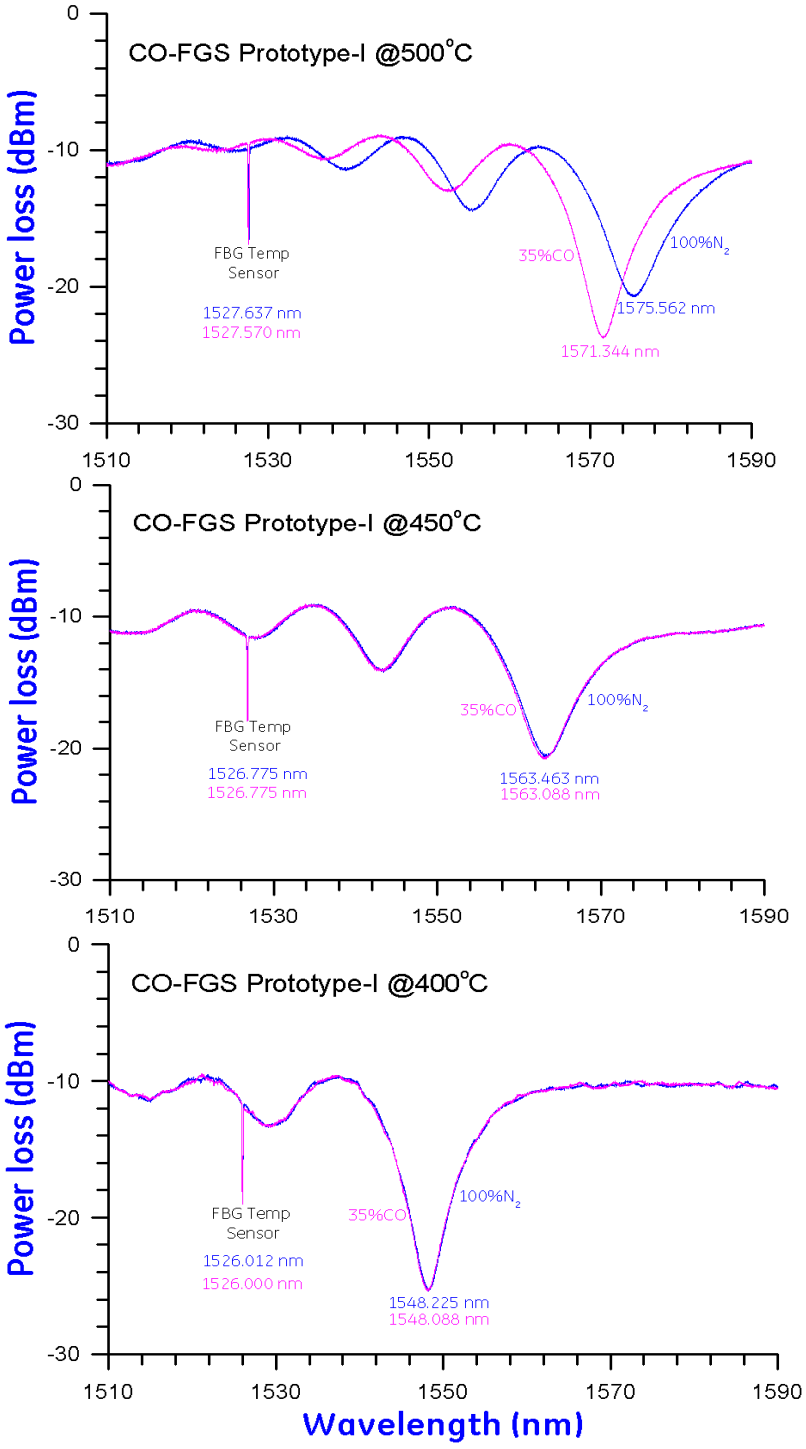

Figure 6.18 Transmission spectrum of fiber gas sensor where a FBG temperature sensor is used for temperature monitoring, and LP01 mode is used to measure CO gas response.

SnO_2 was sputtered on the LPG as the CO sensing film. In the meantime, a FBG was inscribed in the same fiber, about 5 cm away from where the LPG was located.

No coating was on the FBG. Both the LPG and FBG went through the thermal annealling process and could sustain high temperatures. Figure 6.18 shows the transmission spectrum of the entire fiber sensor measured at several temperatures. On the left-hand side, the sharp spike represents the FBG spectrum, which has a bandwidth of about 0.2 nm. The LPG has a much broader spectrum shape and several modes of the LPG exist on this figure. The highest-level mode, the 5^{th} order on the right-hand side, has a spectrum bandwidth of 8 nm, and its peak wavelength is tracked for the response for CO. When 35% CO was introduced into the gas chamber, illustrated by the pink color curve, the LPG resonant peak wavelength shifted to a shorter wavelength. The FBG peak, on the other hand, showed no change, which indicated that the temperature within the chamber was not affected by switching gases.

Figure 6.19 shows a fiber CO gas sensor prototype with nc-SnO_2 as the sensing material response to 35% CO at 400, 450, and 500ºC. The FBG sensor indicated that there is no temperature variation during CO/N_2 cycling tests, but the CO obviously caused wavelength shift. The test chamber temperature was kept constant as was done in alternative CO/N_2 cycling tests. Before the test, fiber sensor was placed in the chamber under 500ºC for 2 hours and was flushed with 100% N_2. Once the system temperature reached steady state, 35% CO was introduced into the gas chamber, and within a 15 min interval, 100% N_2 was switched back into the chamber. Four such cycles were repeated in turn. The wavelength shifted downward about 300 pm during the 15 min interval when 35% CO was introduced. When the N_2 was flushed in, the peak wavelength went back very quickly to its original location, around 1570.55 nm in this case.

Overall, the responses from the fiber sensor were quite consistent from cycle to cycle. However, a detailed observation revealed that differences from cycle to cycle do exist. The peak wavelength dropped very quickly at the beginning when the CO was introduced, then the drop slowed down. Compared with the four cycles, it was found that the slopes at the end became more and more flat. Correspondingly, when the N_2 gets back to the chamber, the responses showed some fluctuation at the beginning portion, which may indicate that the thin sensing film structure changed when the CO diffuses in and it takes some time to recover when the CO diffuses out.

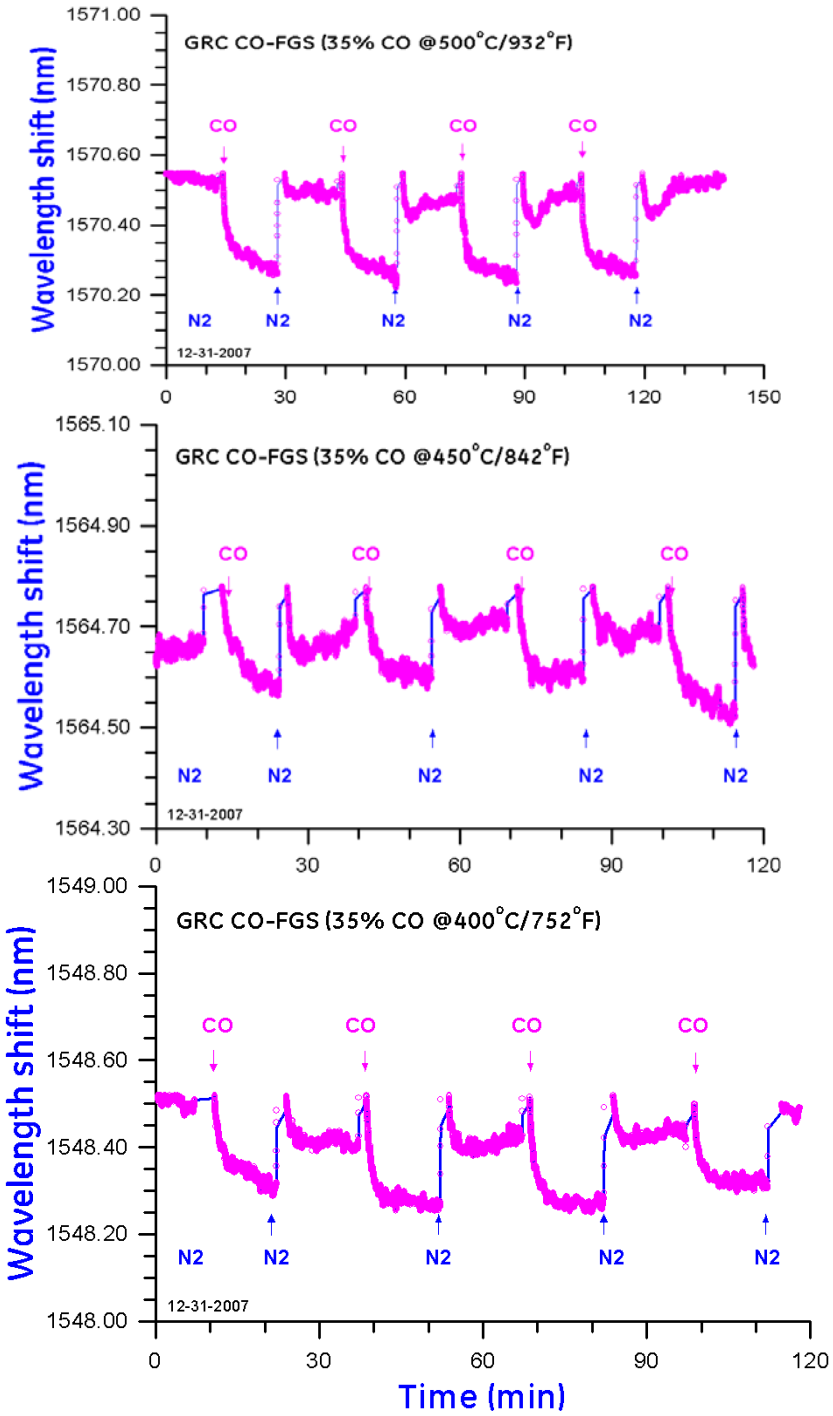

Figure 6. 19. Fiber CO gas sensor prototype responses at elevated temperatures with a nanocrystalline Tin oxide sensing material (nc-SnO_2).

6.4.2. Response of fiber H_2 gas sensor prototype

To overcome the low hydrogen solution issue with a Pd-alloy based sensing material, the following results are from wide-band-gap nanocrystalline tungsten oxide (nc-WOx). Figure 6.20 shows the response of the nc-WOx LPG-based FGS prototype at 35% H_2 and 500ºC. Similar to the CO test, the fiber sensor was placed in the chamber under 500ºC for 2 hours before the test and was then flushed with 100% N_2. When the system temperature reached steady state, 35% H_2 was introduced into the gas chamber. Since the response of nc-WO_x sensing film to 35% H_2 was much faster than that of the nc-SnO_2 sensing film to 35% CO, instead of waiting for 15 minutes, the gas was manually switched back to N_2 after 4 minutes. Four such cycles were conducted.

Compared to the CO test, as shown in Figure 6.20, the response of nc-WOx to H_2 was much faster and more consistent. The magnitude of the wavelength shift also doubled. This was mainly attributed to the smaller size of H_2 molecule compared to CO, which made H_2 easy to diffuse in and out of the sensing film. During the switching of gases between N_2 and H_2, some sharp overshooting of wavelength shift was observed. This was caused by the pressure wave from the gas flow control valve when the valve was opened.

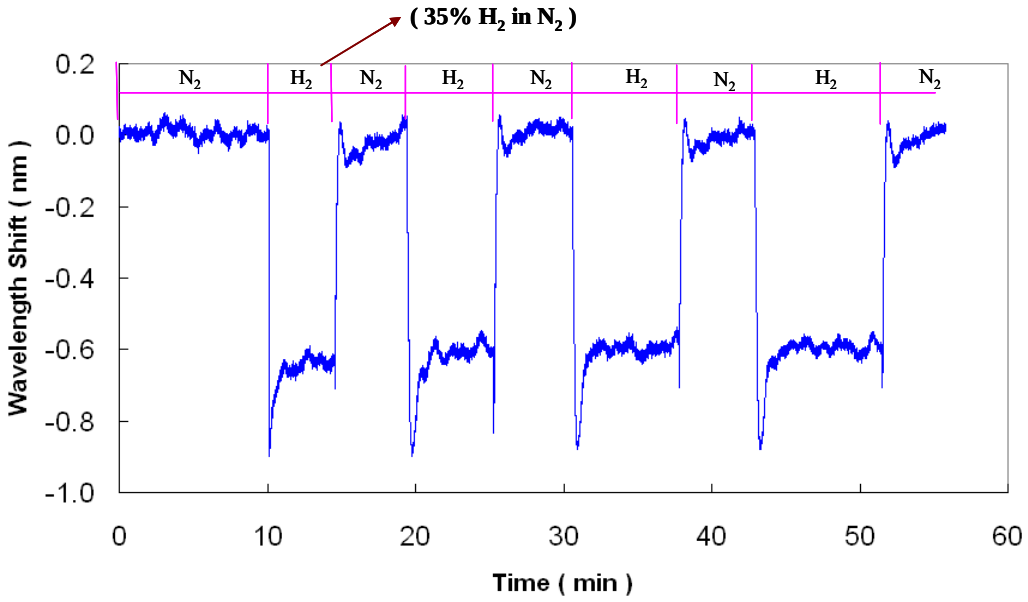

Figure 6.20. nc-WOx-based H_2 fiber gas sensor response on 35% H_2 (blended with N_2) at 500ºC.

6.4.3. Responses of fiber gas sensing array

The above-described tests demonstrated that LPGs coated with nc-SnO_2 respond to CO, and LPGs coated with nc-WOx respond to H_2. These tests used the individual FGS prototype. The following results show how two combined FGS array prototypes respond to both 35% H_2 and CO at elevated temperatures. It is very interesting to find out what occurs when the nc-SnO_2 coated LPG is exposed to H_2, and nc-WO_x coated LPG is exposed to CO. To evaluate the selectivity of these sensing films, both LPGs with different coatings were placed in the same gas chamber.

One fiber with two LPGs can be simply realized by splicing these two fibers together. Since the interrogator has four channels, two channels were occupied, instead of performing splicing. Another concern regarding splicing is that both of the LPGs have very broad bandwidth, and the interrogator has only 80 nm bandwidth. When these two LPGs went through the same channel, spectrum overlapping would occur and would cause trouble for peak detection. Though this can be solved using a smart software algorithm, for the purpose of these proof-of-concept experiments, two separate fiber LPGs with two channels were adopted.

Some clarification must be made before going through the results. After 10 hours of continuous testing under 500ºC, the resonant peak wavelength of the LPG shifted to a longer wavelength, and it was out of the rang of the interrogator (1500 ~ 1580 nm). Therefore, the gas chamber had to be set to a lower temperature, 300ºC, when the resonant peak returns to the interrogator window. It is safe to say that the LPG does survive 500ºC temperature, however, its stability must be further improved.

As shown in Figure 6.21, at 300ºC, the nc-WOx sensing film shows different responses between H_2 and CO. When the sensing film is exposed to H_2, the resonant peak wavelength decreases; when the CO is introduced, the LPG moved back to its original peak wavelength. The magnitude of wavelength shift was around 100 pm, which is smaller than those shown in Figure 6.20. This difference is mainly due to the temperature difference. The S/N ratio was also lower than those shown in Figure 6.20. These results indicate that the nc-WOx sensing film has better sensitivity under higher temperature.

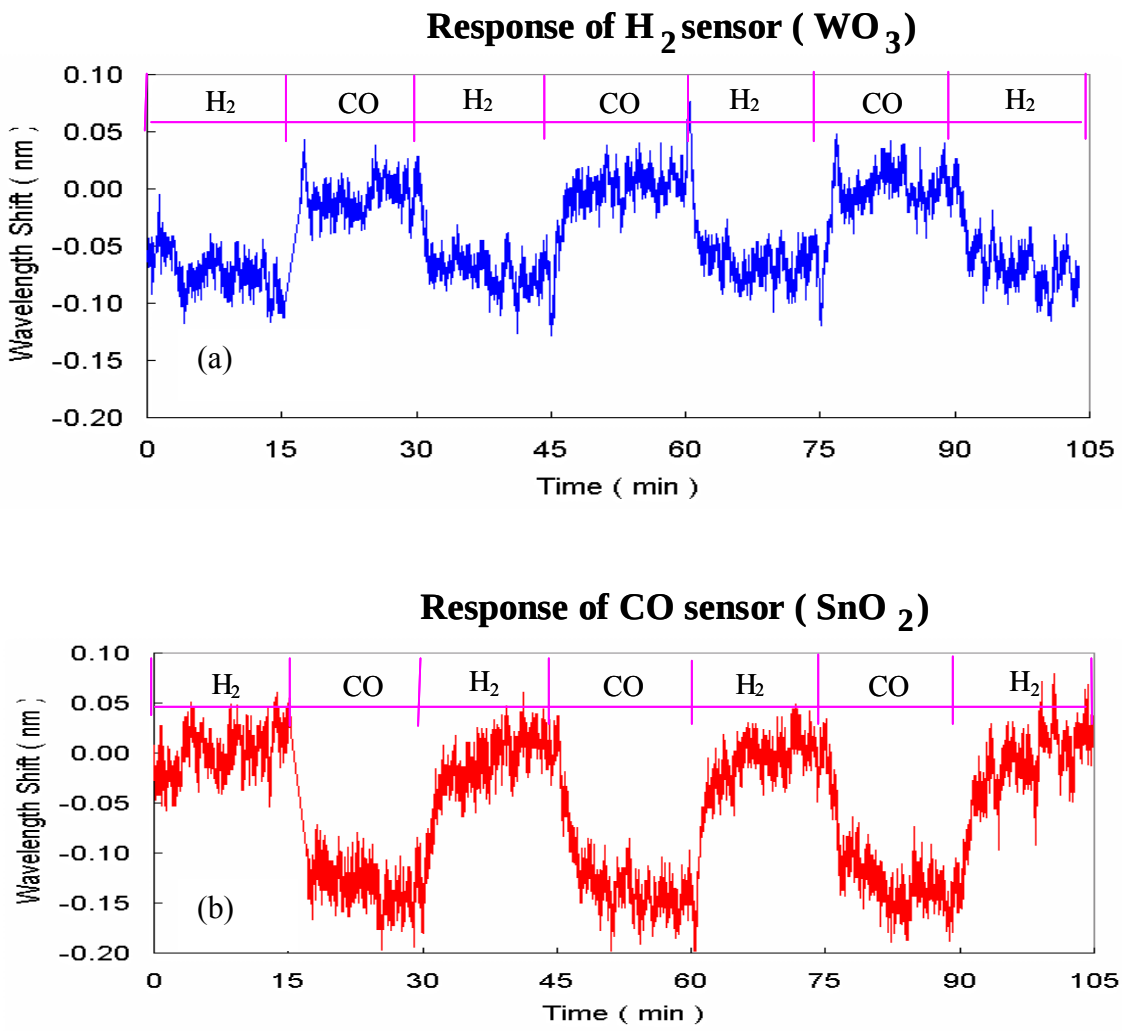

Figure 6.21. Response of fiber gas sensor prototypes to 35% H_2 and 35% CO at 300°C.

The Nc-SnO_2 sensing film also demonstrated good selectivity compared to CO. The change of wavelength is relatively larger, about 150 pm, which is still far less than its response to CO at 500ºC, as seen in Figure 6.21(b).

To further verify the sensitivity of these sensing films coated on LPG sensors, gases with reduced concentration were introduced into the gas chamber. Following similar test procedures, 20% H_2 and 20% CO were introduced into the test chamber alternatively, and the temperature was kept constant at 300°C, as shown in Figure 6.22. Both nc-WOx and nc-SnO_2 still showed responses to H_2 and CO, respectively, and the response magnitudes were reduced accordingly, due to the reduced gases concentration. The wavelength shift of nc-WOx film on 20% H_2 was about 50 pm, and that of nc-SnO_2 film on 20% CO was about 10 pm. Compared to the 100 pm wavelength shift for 35% H_2 and 150 pm wavelength shift for 35% CO, the responses of these sensing films were not linear to their corresponding gases.

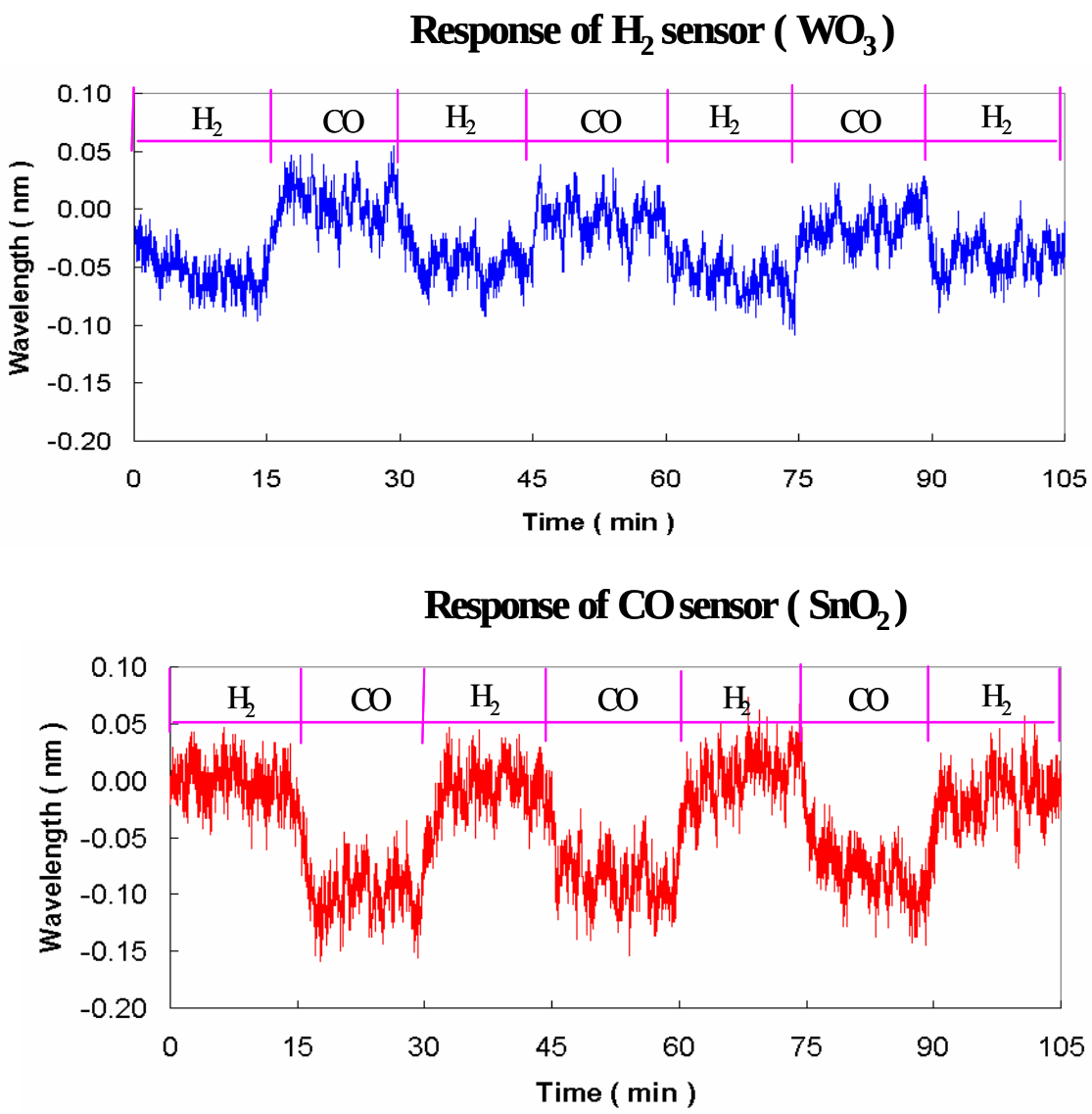

Figure 6.22. Response of a fiber gas sensing array to 20%H_2 and 20% CO at 300°C.

Another set of tests were performed with the simultaneous introduction of H_2 and CO. As indicated in Figure 6.23, after switching from 35% H_2 to 35% CO, 17.5% CO and 17.5% H_2 were introduced to the gas chamber simultaneously and then the gas was switched back to 35% CO. Nc-WOx sensing film showed responses to H_2, and its wavelength shift was reduced from ~100 pm to ~25pm when the H_2 concentration was reduced in half, from 35% to 17.5% at 300ºC.

The response of the nc-SnO_2 sensing film is shown in the plot in Figure 6.23(b). Compared to nc-WOx film, the nc-SnO_2 sensing films seemed to have better performance in terms of a larger wavelength shift and better stability. Its wavelength shift was reduced from ~150 pm to ~50pm when the CO concentration was reduced in half, from 35% to 17.5%.

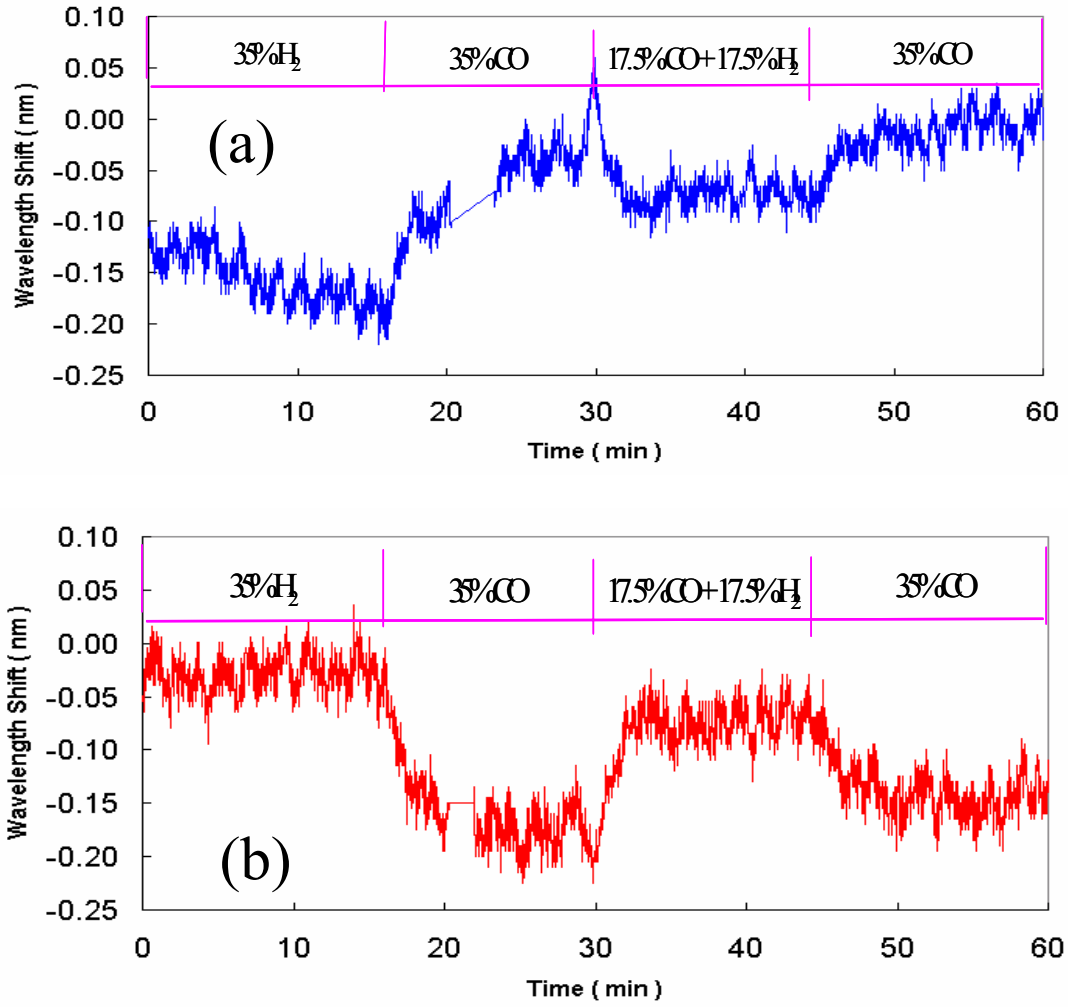

Figure 6.23. (a) Response of the nc-WOx based fiber gas sensor prototype to different H_2 and CO alternative cycling tests; (b) Response of nc-SnO_2 based fiber gas sensor prototype to different H_2 and CO alternative cycling tests at 300°C.

Summary: This chapter presented laboratory evaluation data for both H and CO FGS prototypes, as well as their combined sensing array prototypes. These gas sensor prototypes were tested from ambient to elevated temperatures up to approximately 500ºC. Two response characteristics were found: wavelength shift and transmission amplitude loss. Both were correlated and can be used to mitigate special gas sensing events that could be triggered by temperature surges or pressure fluctuation. The sensing array of H_2 and CO sensor prototypes further demonstrated its functionality for simultaneous syngas sensing for harsh environments.

CHAPTER 7: PROGRAM SUMMARY

The advancements in fiber-optic-based fossil fuel gas sensing technology developed during this program have addressed for the first time sensing device design, system and sub-system design, engineering, and prototyping. These efforts included transforming a fundamental fiber grating into a functionalized gas sensor; effectively enhancing a fundamental guide mode to couple to cladding modes and evanescent field distribution at the fiber grating cladding and sensing material interface; modifying a sensing material's refractive index to enhance the coupling strength from cladding modes in the fiber cladding to radiation modes in the sensing material; developing nanostructural sensing materials and associated material process engineering and downselection; and constructing distributed sensing instruments with the capacity for multi-parameter and multi-point simultaneous sensing. The progress in fundamental physics, materials, and sensing technology have enabled smart-skin fiber gas sensors to be designed and fabricated. The sensitivity and selectivity of these sensors to H_2 and CO was successfully demonstrated. These fiber gas sensors were evaluated from ambient temperature up to 500ºC.

High-temperature LPG sensors were fabricated by electric arc in silica fiber. Long-term thermal test demonstrated that the LPG performance was quite stable at 500ºC. Smart-skin sensing films were developed by sensitized chemical/gas active agents or by modifying the fiber cladding through an atom doping process. As this cladding modification wa on the nanometer scale, its influence on the material thermal strain effect can be ignored, which improves the device reliability. Combining a LPG and FBG in one fiber provides the capability to simultaneously monitor the surrounding gas and temperature. Harsh environment sensing systems based on fiber-optic technology offers a feasible path to develop a distributed sensor network to be used for plant-wide monitoring and diagnosis. These light-weight, small-size, all-passive fiber sensors have the potential to measure a large number of data points with minimum intrusiveness on the gas or heat flow. These characteristics make these sensors an ideal candidate for collecting valuable data in large-scale harsh environments, such as in an IGCC power plant. Also, the fiber sensor array allows for multi-parameter sensing in harsh environments including temperature, strain/stress, vibration, and gas composites.

The developed fiber-optic, harsh-environment fossil fuel gas sensing method is a cost-effective, versatile, plug-and-play platform that can be used to detect and measure a large number of targeted combustible gases, including hydrogen-rich syngas, hydrogen and carbon monoxide balanced syngas, hydrocarbons, chemical agents and solvents. This platform can also potentially measure heavy metals, such as mercury, lead, and actinides, by using different functionalized sensing materials integrated with fiber grating. The distributed fiber-optic fossil fuel gas sensing instrumentation was designed to accommodate ready deployment in harsh

environment applications with its plug-and-play fiber gas sensing module; therefore, the fiber gas sensing instrument developed in this program is modular, ruggedized, and field deployable technology. The unique fiber gas sensing module design and its demonstrated performance provide a shortcut to allow a new sensing method to be built from a matured telecom technology.

This fossil fuel gas sensing technology—perhaps more so than with any other technology—provides DOE a significant advantage that can be used to improve the efficiency, process control, and optimization of power industrial production. Unlike existing chematography, mass spectrometers, Raman spectroscopes, and ring-down spectrometer-based offline devices, which are bulky and dedicate, GE's fiber-sensing device and sensing system can be used in a gas turbine, coal boiler, coal gasification, or at an exhaust section and interface. The fiber-grating-based gas sensor uses commercially-available grating fabrication technology and integrated sensing material prepared by sol-gel and magnetron sputtering technologies, thereby significantly reducing the costs to procure the sensing instrument.

Additionally, the modular sensor is capable of supporting a variety of fiber-optic sensing mechanisms including index of refraction, absorption, and fluorescence. All of these optical properties can be embedded into the sensing design and the functionalization of the grating skin. Moreover, this fiber-optic distributed fossil fuel gas sensing technology can potentially be used for diagnostics and prognostics of a power generation system, such as f gas turbine, coal gasification vessel, engine and combustor operation status, specious event monitoring, and environment emission monitoring. Also, as a distributed sensing technology and multi-point sensing capability, it could be used to detect large-scale gas leaks from pipelines, gas/oil tanks, or chemical storage facilities. Furthermore, it can be naturally used for homeland security applications such as for the detection and identification chemical and biochemical threats in any large-scale infrastructure, such as a train station, airport, or government building.

The fiber-optic sensing platform and plug-and-play sensing module developed in this program are designed to be capable of continuous operation in a harsh environment where the temperatures could range from ambient temperature to 500ºC and beyond and pressure could be as high as 200 psi. The prototyped sensing module is capable of working where high concentrations of the target fossil fuel gases, such as hydrogen and carbon monoxide, are present. For example, in measuring hydrogen blended with CH_4 and other heavy hydrocarbons, the system is capable of operating continuously in a gas turbine exhaust section. Currently, the only reliable sampling technique requires an individual to physically collect a sample at the testing site and then forward the sample to a laboratory for analysis. The fiber-optic distributed sensing method developed in this program can be operated remotely and continuously, therefore eliminating the need for human interaction and sampling. This design and prototype were completed and demonstrated successfully.

The critical program deliverables include:

- By multiplexing the fiber-gas sensing module, simultaneous multi-point or multi-gas detections can be readily obtained, which is based on matured wavelength-division-multiplexing technology. These quasi-distributed sensors have demonstrated their sensitivities to hydrogen (1-75%H_2) and carbon monoxide (1-35%) from ambient conditions up to 500ºC, individual sensing modulus structures and their sensing performances.
- Demonstrated electric arc method, for fused silica fiber. We have demonstrated that the grating can sustain long-term stability at 500ºC, and femto second laser inscribed Bragg grating in sapphire fiber can extend the operating temperature up to 1350ºC.
- Based on the robust fiber grating fabrication technologies, we successfully fabricated highly-thermal stabilized fiber long-period gratings and further found that different apodization methods and different grating modulation profiles can effectively enhance the evanescent field energy around the fiber grating cladding so that sensing nanomaterial modified fiber cladding have chemical and fossil fuel gas sensitivity.
- The gas-sensing device is based on refractive index profile modulated long-period grating structure that enhances coupling between the guide and the cladding modes. The sensing material further enhances the coupling between the cladding modes to radiation modes with a higher refractive index close to fiber cladding. The two-step mode coupling enhancement significantly increases interaction of evanescent fields with the sensitized film and thereby forms a smart skin.
- Demonstrated multi-parameter sensing using distributed arrays–chemical/gas sensor arrays based on wavelength division multiplexing allows multiple sensors to be integrated on a fiber to sense temperature, strain/stress, pressure and gas compositions.

APPENDIX

Publications:

1. Juntao Wu, Kung-li Deng, Boon Lee, Renato Guida, "Fiber-Optic Photo-Acoustic Spectroscopy Sensor for Harsh Environment Gas Detection", *Proceedings of SPIE,* San Diego, CA, Aug., 2007.
2. Juntao Wu, Kung-li Deng, Boon Lee, Zhe Wang, "Advanced In-line Laser Induced Breakdown Spectroscopy (LIBS) and Fiber-Optic CO Sensor for Model-based Control in the Integrated Gasification Combined Cycle (IGCC) Power Plant", Coal Utilization Conference, Clearwarer, FL, 2007
3. Juntao Wu, Kung-li Deng, Zhe Wang, Boon Lee, and Renato Guida, "Sapphire-fiber-based pyrometer for harsh environment applications," *Proceedings of SPIE,* 6314-35, San Diego, CA, Aug., 2006.
4. Kung-li Deng, Juntao Wu, Zhe Wang, Boon Lee, and Renato Guida, "On-line compositional analysis in coal gasification environment using laser-induced plasma technology," *Proceedings of SPIE,* 6314-36, 2006.
5. Hua Xia, Kung-li Deng, Ken Bousman, Juntao Wu, Boon Lee, Renato Guida and Kevin McCarthy, "Temeprature dependent fiberoptic gas sensor response characteristics," *Proceedings of SPIE,* 6314-37, 2006.
6. Kung-li Deng, Juntao Wu, Boon Lee, Stuart Yin and Aaron Avagliano, "Harsh environment fiber-optic sensor and sensor fusion for applications in integrated gasification combined cycle power plant", Coal Utilization Conference, Clearwarer, FL, 2006